This is to certify that the

dissertation entitled

SOL GEL SYNTHESIS AND PILLARING REACTIONS OF BEIDELLITE AND RELATED SMECTITE LAYERED SILICATE

presented by

Danyun Li

has been accepted towards fulfillment of the requirements for

Ph.D. degree in chemistry

Thomas J. Pinnavaia
Major professor

Date Dec. 28, 1994

SOL GEL SYNTHESIS AND PILLARING REACTIONS OF BEIDELLITE AND RELATED SMECTITE LAYERED SILICATES

By

Danyun Li

A DISSERTATION

Submitted to
Michigan State University
in partial fulfillment of the requirements
for the degree of

DOCTOR OF PHILOSOPHY

Department of Chemistry

1994

ABSTRACT

SOL GEL SYNTHESIS AND PILLARING REACTIONS OF BEIDELLITE AND RELATED SMECTITE LAYERED SILICATES

By

Danyun Li

The 2:1 relation between the tetrahedral and octahedral sheets of smectite clays allows these minerals to be classified as a 2:1 phyllosilicate. Smectites are readily pillared owing to the combination of swelling ability, low charge density and transverse layer rigidity. Beidellite is a member of the smectite family of 2:1 layered silicate clays, in which the net negative charges on oxygen framework arise mainly from the substitution of Al^{3+} for Si^{4+} in the tetrahedral sites. This structural analogy to zeolite makes this clay and its aluminum pillared derivatives more attractive for acid catalytic application relative to montmorillonite and other smectites in which the layer charge arises from metal ion substitution on the octahedral sheet. In the present work well-crystallized beidellite is synthesized at 200 ^{o}C, whereas conventional synthesis temperature is over 300 ^{o}C. In order to enhance the reactivity of the reactants, the hydrated gel rather than a calcined gel is used for hydrothermal synthesis. The factors that influence the reactivity of the gel are investigated. Also, the properties of synthetic and natural beidellites are characterized.

The disadvantages of pillared clays use as acid catalysts, especially as cracking catalysts, are their limited thermal and hydrothermal stability. This work reports a synthesis procedure for the preparation of alumina pillared montmorillonites that reliably affords products with exceptional performance properties, in particular, high BET surface area, microporosity, and Brönsted/Lewis acidity, when calcined at elevated temperatures. The approach utilizes a common pillaring agent (base-hydrolyzed $AlCl_3$) and typical montmorillonite compositions. However, certain synthesis and

processing conditions that afford pillared products superior in structural thermal stability to those reported previously have been optimized. Also, the study focuses on the hydrolytic chemistry of the alumina pillar, which is a crucial factor in determining the thermal stability of the final product.

Alumina pillared beidellites, in addition to their thermal stability of up to 800 ^{o}C, exhibit high catalytic reactivity for the alkylation of biphenyl by propene. Furthermore, the pillared beidellites obtained from the H^{+}-exchanged form offer compatible thermal stability as well as catalytic activities that are superior to those of the corresponding pillared beidellites prepared from the Na^{+}-exchanged form.

New tubular silicate-layered silicate (TSLS) are obtained by the pillaring of imogolite (a tubular silicate) into a beidellite layer host. The TSLS is a pillared species in which the pillars themselves are microporous. The interests in this are the unique features of the TSLS complex which are different from the conventional pillared clays. Due to the hydrophilic structure of the imogolite tube, the swelling of the clay galleries by imogolite is reversible. The weak interaction between the pillar and clay host and miroporous structure provide the possibility of building desired microporous pillared clays by simply adjusting the amount of microporous pillars intercalated during pillaring.

To my family,

To Yishi

ACKNOWLEDGMENTS

I sincerely appreciate the guidance and support of Dr. T. J. Pinnavaia throughout this work. I am grateful for his patience and inspiration during the experimental work and shaping this thesis.

I would like to thank Dr. H. Eick for all the help he has given to me. My gratitude also to the member of my committee, Dr. J. Ledford and Dr. W. Reusch.

I would like to express my true appreciation to my former and present group members. The help and friendship from my "international" group have been a very important part of my graduate experiences. Especially, I would like to thank Prof. J. Wang for his assistance for the catalysis study, Prof. Z. Ge for his cooperation, and Dr. M. Chibwe for revising this thesis.

My deepest gratitude goes to my family - my parents, my parents-in-law, brother, sister, brother-in-law and their lovely daughter. From distance I always feel and receive their unconditional love and support.

Finally, the tribute must be given to my husband, Yishi. His consistent encouragement and help is deeply appreciated. I really thank him for his accurate assistance with the figures for this thesis.

TABLE OF CONTENTS

CHAPTER THREE
PREPARATION OF ALUMINA PILLARED MONTMORILLONITE WITH HIGH THERMAL STABILITY, REGULAR MICROPOROSITY AND LEWIS/BRÖNSTED ACIDITY

CHAPTER FIVE

IMOGOLITE PILLARED BEIDELLITES

APPENDIX

LIST OF TABLES

LIST OF FIGURES

ABBREVIATIONS

BET:	Brunauer, Emmett and Teller
CEC:	Cation Exchange Capacity
FTIR:	Fourier Transformed Infra Red
GC:	Gas Chromatography
ICP:	Inductively Coupled Plasma
MAS:	Magic Angle Spinning
NMR:	Nuclear Magnetic Resonance
SEM:	Scanning Electron Microscopy
TEM:	Transmission Electron Microscopy
TPD:	Temperature Programmed Desorption
XRD:	X-ray Diffraction

CHAPTER ONE
INTRODUCTION

A. SYNTHESIS AND CHARACTERIZATION OF BEIDELLITE

1. SMECTITE CLAYS

a) Structural Classification

Clay minerals comprise a large family of fine-grained crystalline sheet silicates. There are four main classes, namely the 1:1, 2:1, 2:1:1 and 2:1 'inverted ribbon' clay minerals. Each class has a different arrangement of tetrahedral and octahedral layers as shown in Figure 1.1.

The structure of 2:1 clay minerals consists of parallel stacked sheets, each composed of two tetrahedral and one octahedral layers (TOT layer). They can be either trioctahedral or dioctahedral, having octahedral layers based on brucite or gibbsite, respectively.

The 2:1 relation between the tetrahedral and octahedral sheets allows the smectite clay to be classified as a 2:1 phyllosilicate.[1-3] The octahedral sheet generally contains metal ions suitable for octahedral coordination, i.e. Al^{3+} or Fe^{3+} and Mg^{2+}. The tetrahedral sheet usually contains Si^{4+} and occasionally, Al^{3+}. Figure 1.2 illustrates the structure of smectite based on octahedral and tetrahedral sheets. In a unit cell, there are eight tetrahedral sites and six octahedral sites formed from 20 oxygens and four hydroxyl groups.

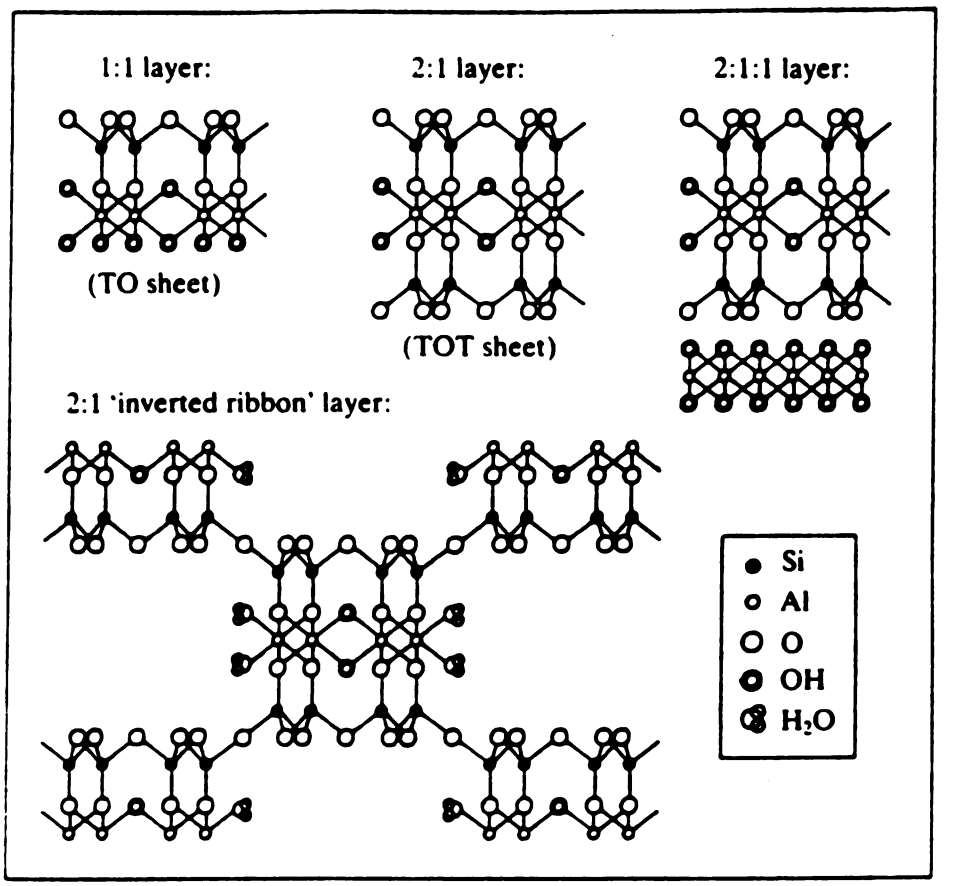

Figure 1.1 Layer structures of the clay minerals.

Smectites are distinguished from other 2:1 phyllosilicate minerals by the layer charge. In talc, all the tetrahedral and octahedral sites in the oxygen framework are filled by Si^{4+} and Mg^{2+}, respectively. For pyrophyllite, Si^{4+} occupies all eight tetrahedral holes and Al^{3+} fills two-thirds of the octahedral holes, so their layers are electrically neutral. In contrast to talc and pyrophyllite, the layers in muscovite and phlogopite bear a net charge of $2e^-$ per Si_8O_{20} unit due to a positive charge deficiency which results from the substitution of Si^{4+} by Al^{3+} in tetrahedral positions. The charge on the layers of smectites is intermediate between talc/pyrophyllite and the micas. Typically the positive charge deficiency on smectite layers ranges from 0.4 to $1.2e^-$ per Si_8O_{20}. Layered hydrated cations (Na^+, Mg^{2+}, Ca^{2+}, etc.) are intercalated between silicate layers to balance the layer charge. In montmorillonite, the layer charge originates from the substitution of octahedral Al^{3+} by Mg^{2+}. Hectorite also is octahedrally charged with Li^+ substituting for Mg^{2+} in the octahedral sheet. Beidellite and saponite are tetrahedrally charged smectites with Al^{3+} replacing Si^{4+}. Nontronite can be regarded as a ferruginous analogue of beidellite. The idealized structural formulae are listed in Table 1 for three dioctahedral smectites and two trioctahedral smectites.

Given the above classification scheme, a rapid test called Green-Kelly test is used to distinguish a beidellite-type smectite from a montmorillonite-type smectite.[4-5] This can be achieved by first saturating the exchange sites with Li^+, and then heating to 200 ^oC. For Li^+-montmorillonite, the net charge is permanently decreased and the clay subsequently cannot be swelled with glycerol. Li^+-beidellite with only tetrahedral charge is unaffected by heating, and the clay layer can still be swelled with glycerol. The reason for the difference in layer charge reduction is that the unhydrated

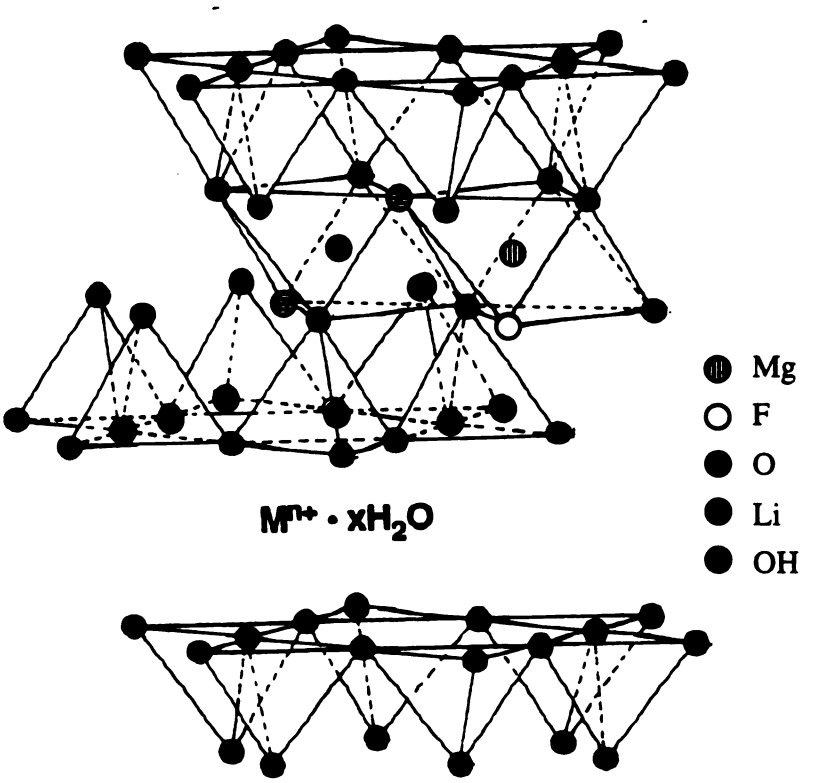

Figure 1.2 Structure of a typical smectite clay such as hectorite.

Li^+ is a rather small cation (r = 0.82 Å) that can migrate into the vacant sites in the octahedral sheet of montmorillonite and so neutralizes some of the net octahedral charge on the layers. On the other hand, Li^+ is strongly electrostatically bonded to the charged tetrahedral sites in beidellite and the charge on the octahedral sheet is unchanged upon heating.

Table 1.1. Idealized Structural Formulas for Some 2:1 Phyllosilicates

Mineral group	Dioctahedral	Trioctahedral
Pyrophyllite-talc	Pyrophyllite:$[Al_4][Si_8]O_{20}(OH)_4$	Talc: $[Mg_6][Si_8]O_{20}(OH)_4$
Smectite	Montmorillonite: $M^{n+}{}_{x/n} \cdot yH_2O[Al_{4-x}Mg_x][Si_8]O_{20}(OH)_4$	Hectorite: $M^{n+}{}_{x/n} \cdot yH_2O[Mg_{6-x}Li_x][Si_8]O_{20}(OH)_4$
	Beidellite: $M^{n+}{}_{x/n} \cdot yH_2O[Al_4][Si_{8-x}Al_x]O_{20}(OH)_4$	Saponite: $M^{n+}{}_{x/n} \cdot yH_2O[Mg_6][Si_{8-x}Al_x]O_{20}(OH)_4$
	Nontronite: $M^{n+}{}_{x/n} \cdot yH_2O[Fe_4][Si_{8-x}Al_x]O_{20}(OH)_4$	
Micas	Muscovite: $K_2[Al_4][Si_6Al_2]O_{20}(OH)_4$	Phlogopite: $K_2[Mg_6][Si_6Al_2]O_{20}(OH)_4$

b) Properties of Smectite Clays

The negative layer charge of a clay mineral is manifested as a cation exchange capacity. Since smectites have the lowest densities amongst the phyllosilicate group, the galleries are hydrated and most cations will penetrate between the lamellae and so participate in ion exchange. However for other high charge density phyllosilicate clay, the lamellae are held together by dehydrated cations and only the cations on the outside surfaces

of the crystallites stacks participate in ion exchange. Neither the N_2 used for surface area determination nor the exchange cation used to measure charge can penetrate between the lamellae.[6]

Surface areas of clay minerals can be measured by the classical BET method, usually using N_2 as the adsorbate. The adsorption isotherms are almost invariably of Type IV of the conventional BDDT classification showing hysteresis at partial pressure above about 0.5. Despite the limit of applicability of the simple BET equation, the results are reproducible and are of value in comparing one sample with another. The BET N_2 method involves complete initial degassing of the surface and this removal of surface water pulls the lamellae together and the lamellae are not subsequently intercalated by N_2. It is for this reason that the surface area of smectites should usually be measured by adsorption of a species that can be intercalated from aqueous solution. Cetyl pyridinium bromide has been used frequently.[7] If water vapor is applied as the adsorbate in the BET approach to surface area determination, the amount of water adsorbed at the 'monolayer' is strongly influenced by the identity of the exchange cation and great care has to be taken in interpreting the results.

Acidity plays an important role in the use of clays and pillared clays as catalysts and catalyst matrices. The origin and enhancement of acidity of pillared clay will be discussed later. Brönsted (or protonic) sites and Lewis (or aprotonic) acid sites can coexist in a swelling clay and its pillared analogue. The presence of several types of protonic acid sites can be viewed in the following ways:[8-11]

(1) One type of Brönsted acidity is associated with the initial sites of ion exchange. Hydrated cations are more acidic in clay interlayers than in homogenous aqueous solution because the water molecules in the hydration

shell of the exchangeable cations are subjected to the strong polarized field of the cation.

(2) A second type of acidity can be associated with the Si-O-Al linkage. When the negative charge arises from Si^{4+} substitution by Al^{3+} in the tetrahedral layer, as in the beidellite, opening of Si-O-Al bridge results in a structure similar to that known to exist in acidic zeolites. This type of Brönsted acidity is represented in the equation given below. Such acidity is believed to exist in acid-leached beidellite or in thermally treated NH_4^+-beidellite and pillared beidellite. Also, the aluminum atoms exposed at the crystal edge may become either Brönsted acid sites or Lewis acid sites. However, their contributions are limited by site density.

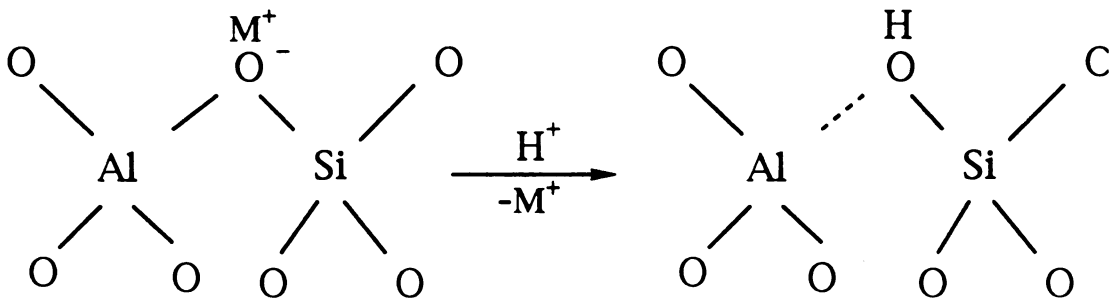

The members of the smectite group have the greatest ability to swell, which allow for cation exchange and access to active sites between adjacent TOT layers by reactants. Also, smectite clays have low layer charge density and high transverse layer rigidity. Smectites are readily pillared owing to the combination of swelling ability, low charge density and transverse rigidity of the layer. Therefore, smectite clays are the most important 2:1 clay minerals for catalytic applications.

2. SOL-GEL PROCESS

Sol-gel chemistry is based on the polymerization of molecular precursors, such as metal oxides of the type $M(OR)_n$. Hydrolysis and condensation of these alkoxides leads to the formation of oxo-polymers which are then transformed into an oxide network.

Early interest in sol-gel processing with silica gels for inorganic ceramic and glass materials began in the mid-1800s.[12,13] These early investigator observed that hydrolysis of tetraethyl orthosilicate (TEOS), $Si(C_2H_5)_4$, under acidic conditions yielded SiO_2 in the form of a "Glass-like" material. However, extremely long drying times were necessary to avoid the silica gels fracturing into fine powder. The potential for achieving very high levels of chemical homogeneity in colloidal gel was recognized and hence the method was used in the 1950s and 1960s to synthesize a large number of novel ceramic oxide compositions, involving Al, Si, Ti, Zr, etc. that could not be made by traditional ceramic powder methods.[14,15] The commercial development of colloidal silica powder in the same period began and ammonia was used as a catalyst for a TEOS hydrolysis reaction that could control both the morphology and the size of powders.[16,17]

New analytical and computational technology is one reason for the increased scientific understanding of sol-gel chemistry. The use of nuclear magnetic resonance (NMR), x-ray small-angle scattering (XSAS), Raman spectroscopy, x-ray photoelectron spectroscopy (XPS), differential scanning calorimetry (DSC), dielectric relaxation spectroscopy (DRS) provide the availability of investigating on a nanometer scale the chemical process of hydrolysis, polycondensation, gelation, dehydration and densification of materials.

The advantages of the sol-gel process are primarily the potentially higher purity and homogeneity of the product and the lower processing temperature.[18,19] Sol-gel chemistry offers the possibility to design molecular precursors and to control the polymerization process so that, in principle, material of the required porosity and surface area can be prepared.

Sols are dispersions of colloidal particles in a liquid. Colloids are solid particles with diameters of 1-100 nm. A gel is an interconnected, rigid network with pores of submicrometer dimensions and polymeric chains whose average length is greater than a micrometer. Inorganic gels exhibit high surface areas and small pore sizes. These unique properties have been exploited in applications such as filtration, catalysis, coating, film, and fibers in the past decade. Sol-gel processing is approached by (i) hydrolysis and polycondensation of alkoxide or metal salts and (ii) gelation of a solution of colloidal particles. The processing steps generally include hydrolysis and polycondensation, gelation, aging and drying.[20]

The design of molecular precursors and the control of processing parameters such as hydrolysis ratio, solvent or catalyst allow the production of tailored microstructures. If sol-gel chemistry is described in terms of hydrolysis and condensation of metal alkoxide, these reactions can be written as follows:[21]

hydrolysis: $\text{-M-OR} + H_2O \rightarrow \text{-M-OH} + \text{ROH}$ (1)

condensation: $\text{-M-OH} + \text{RO-M-} \rightarrow \text{-M-O-M} + \text{ROH}$ (2)

Condensed species are then progressively formed giving rise to oligomers, oxopolymers, colloids and gels or precipitates. At the end of the process, a hydrous oxide or hydroxide is obtained. Actually, these reactions correspond to the nucleophilic substitution of alkoxyl ligands by hydroxylated species XOH as follows:

$$M(OR)_z + zXOH \rightarrow [M(OR)_{z-x}(OX)_x] + ROH \quad (3)$$

They can be described by a S_N2 mechanism. OR groups are replaced by OX ligands. The chemical reactivity of metal alkoxides toward hydrolysis and condensation depends mainly on the positive charge of the metal atom and its ability to increase its coordination number. Generally, as the electronegativity of metal atoms decreases, their size increases and the chemical reactivity of the corresponding alkoxides increases when going down a group in the periodic table. Silicon alkoxides are not very reactive. Gelation occurs within several days after water has been added. Hydrolysis and condensation rates have to be increased via acid or base catalysis.[22]

Acid and base catalysis of silicon alkoxides $Si(OR)_4$ not only increase gelation rates, they also lead to completely different silica materials.[23] Inorganic acids reversibly protonate negatively charged alkoxide ligands and increase the reaction kinetics by producing better leaving groups. Acid-catalyzed condensation is directed preferentially toward the ends of oligomeric species and results in chain polymers. Base catalysis provides better nucleophilic OH^- groups for hydrolysis while deprotonated silanol groups ($Si\text{-}O^-$) enhance condensation rates. The positive partial charge on silicon increases with its connectivity, so that nucleophilic addition of $Si\text{-}O^-$ is directed preferentially toward the middle parts of oligomers leading to more compact, highly branched species. Hydrolysis and condensation rates also can be increased via nucleophilic activation by using highly nucleophilic species such as fluoride. The choice of solvent is also very important. Coordination expansion via solvate formation occurs when alkoxides are dissolved in their parent alcohol. Coordination expansion occurs via alkoxide bridging or solvation. The molecular complexity of

metal alkoxides can then be controlled by an appropriate choice of the solvent.[24]

3. SYNTHESIS OF BEIDELLITE

Clay minerals can be synthesized from oxide and hydroxides at moderate temperature by using hydrothermal methods.[25-27] Generally, the formation for clay formation under basic conditions involves stabilization of alumina tetrahedra, which allows for 2:1 condensation of a layer. Acidic conditions favor formation of gibbsite, a layered, octahedrally coordinated aluminum hydroxide and the condensation of silica tetrahedra in a two dimensional array. Minerals with 2:1 layered structure like smectite and mica are synthesized at high pH and 1:1 structures like kaolinite and serpenite are formed at low pH. Also, the reaction temperature for synthesis of smectites should be below 400 ^{o}C, since pyrophyllite is formed preferentially at temperatures higher than 400 ^{o}C. In the case of beidellite, reaction is usually carried out around 340 ^{o}C for 7 days.[28,29] For instance, beidellite is conventionally prepared by mixing the sources of exchangeable cations, like Na^{+}, Ca^{2+}, Mg^{2+}, aluminum e.g. $Al(NO_3)_3 \cdot 9H_2O$ and silica e.g. TEOS. The gel was formed by adding NH_4OH into the mixture. The gel obtained was dried and calcined to convert the nitrates to oxides. The hydrothermal reaction was then performed for the resulting mixture at 300 ^{o}C to 340 ^{o}C, preferably at 340 ^{o}C for 5 to 7 days in an autoclave.[29-31] However, the high reaction temperature limited the practical application, and the products thus obtained are not as well-crystallized as the natural beidellite as is evidenced by the XRD and MAS NMR results.

B. Thermal and Hydrothermal Stability of Pillared Clays

1. Alumina Pillared Clays

The conversion of heavy oil fractions is a problem of lasting economic significance.[32-34] The conversion of heavy feedstocks requires pre-cracking matrices which possess the following properties: (1) > 8 Å pore size; (2) high selectivity with a low coke production; (3) numerous and strong acid sites; (4) catalyst stability in the thermal and hydrothermal conditions required for regeneration. Zeolites are traditional fluid cracking catalysts (FCC) that convert heavy oil fractions in the processing of heavy crude oils. However, the relatively small pore openings of zeolites limit the approach of large residue molecules. Additionally, zeolites hardly resist the poisoning effect of V and Ni that are present in crude oil. However, the recent discovery of mesoporous materials (MCM-41) by Mobil workers [35-36] has opened up the potential for large pore zeolites. But it is yet to be seen whether these mesopore catalysts will possess the acidity and structural stability required for FCC catalysts.

Pillared clays were developed in 1970's in the search for materials having larger pores than zeolites. Pillared clays are an attractive class of acidic microporous solids owing to their facile synthesis and structural adaptability. Pillared lamellar solids should possess two structural characteristics. Firstly, the gallery species should be sufficiently robust to prevent gallery collapse upon dehydration. Secondly, the pillars should be laterally spaced so as to allow for interpillar access by molecules at least as large as nitrogen.[37]

Pillared clays are prepared by direct ion-exchange oligomer cations presumably containing intercalated polyoxycations of the same nuclearity as the related cations in aqueous solutions. These large cations function as pillars and prevent the collapse of the structure during outgassing. At elevated temperatures, dehydration and dehydroxylation occur, resulting in the oxide aggregates forming stable pillared clays. This process is illustrated in Figure 1.3.

The first step in a pillared clay synthesis is preparation of the pillaring agent. The most frequently used pillaring reagent is an Al_{13} species because it is clean and reproducible. Two types of aluminum pillaring reagents have been used. One type is a base-hydrolyzed $AlCl_3$ solution prepared at OH^-/Al^{3+} ratio in the range 1.0 - 2.5. The second type, known as aluminum chlorohydrate (ACH) is a commercial product prepared by the reaction of aqueous $AlCl_3$ with Al metal. ^{27}Al NMR spectra in Figure 1.4 showed that both types of pillaring reagents exhibited a sharp resonance near 63 ppm, which was consistent with the presence of the tetrahedral site in the $Al_{13}O_4(OH)_{24}^{7+}$ as shown in Figure 1.4. In addition, the ACH solutions exhibited broad tetrahedral and octahedral resonances indicative of higher polymers. The resonance near 0 ppm is from monomer ($Al(H_2O)_6^{3+}$) and dimer ($(Al_2(OH)_2(H_2O)_8)^{4+}$ at certain pH ranges.[38-39] Due to the properties of a quadrupolar nucleus in a strong electric field gradient, the octahedral resonances are too broad to observe in solution. These two types of pillaring reagents afford very similar pillared products in terms of d-spacings, composition, and surface areas. On the basis of these similarities it was suggested that the Al_{13} species is preferentially bound to the intracrystal surfaces and that it is this species which acts as the initial pillaring agent.[39-40]

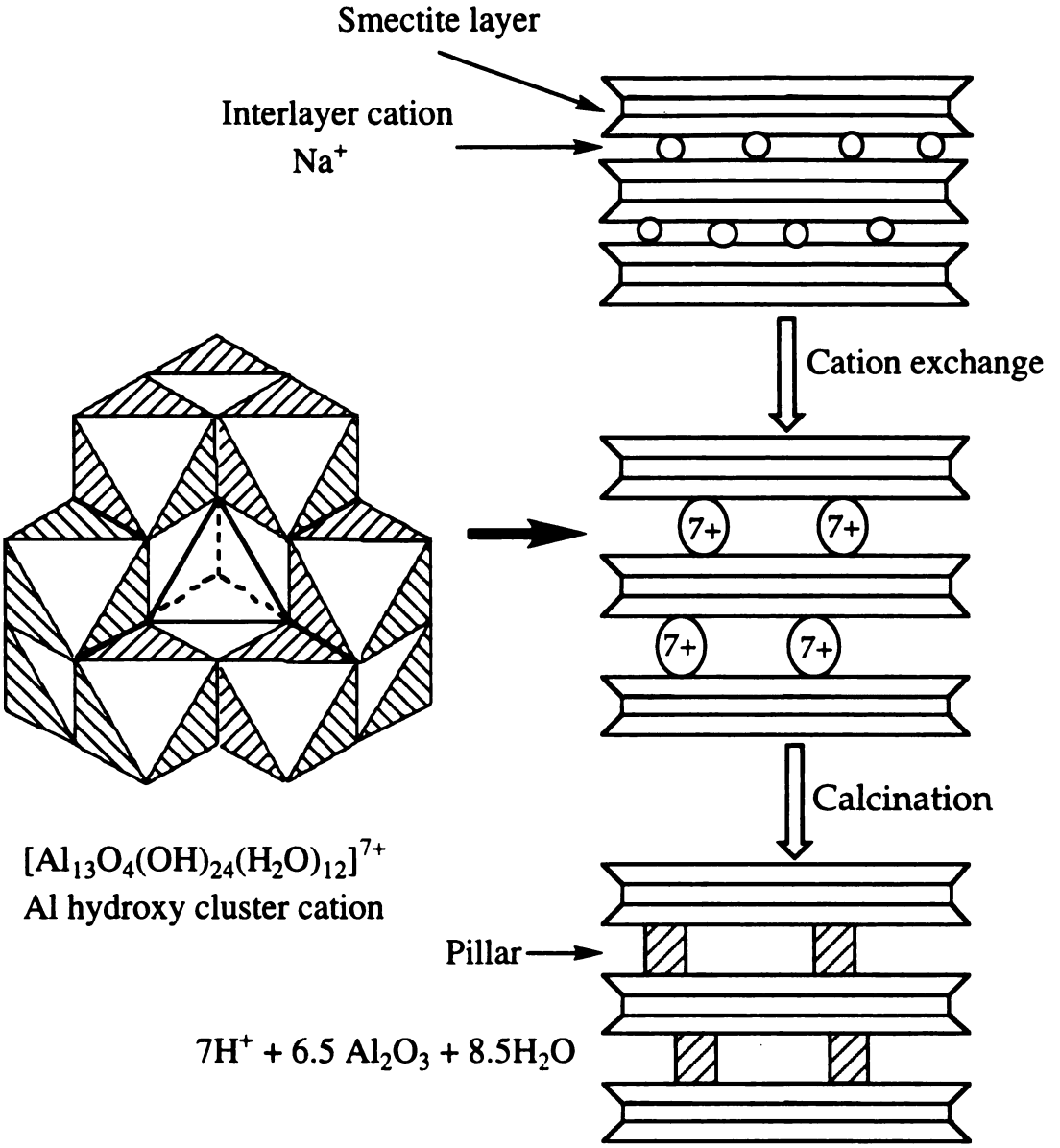

Figure 1.3 Schematic diagram for the preparation of pillared clay.

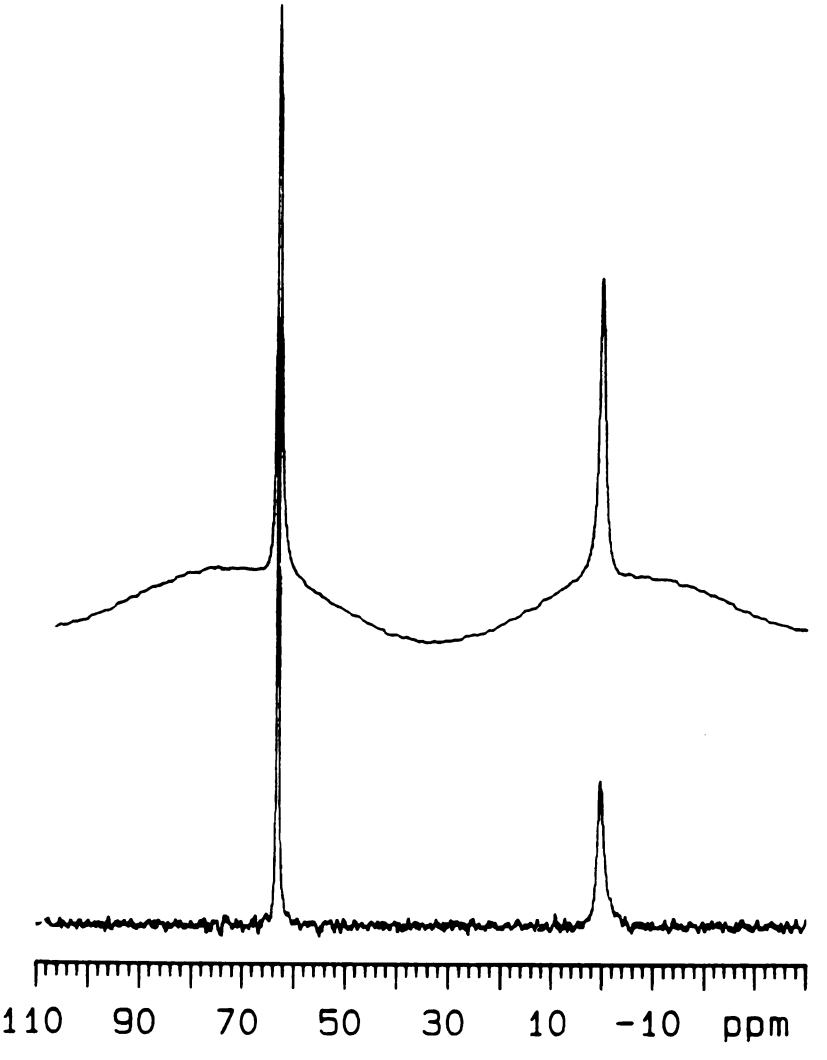

Figure 1.4 ^{27}Al NMR spectra of (A) $[Al_{13}O_4(OH)_{24}(H_2O)_{12}]^{7+}$ oligomer; (B) ACH.

The next step is the exchange of the swelled clay suspension with the oligomer cation, for example, by adding dropwise the clay suspension to the pillaring agent. The pillaring agent in solution is usually used in excess of the actual CEC of the clay.

The washing process removes extraneous ions, such as chloride, and results in the flocculation of clay layers. The product can then be either freeze-dried or air-dried. Finally, the dried product is stabilized by calcining at high temperature to dehydrate pillars into stable oxides usually done at least at 350 ^{o}C.[41]

The preparation and properties of smectite clays pillared with Al-hydroxy oligomer (PILC) have been extensively investigated.[42-49] The thermal stabilities characterized in terms of the d-spacing, porosity and acidity, depend on the properties of the layer host, the properties of the pillar, and processing variables. It appears that for pillared clays thermal stability, especially hydrothermal stability and coke formation are limiting factors. Consequently, they have not yet been used commercially as cracking catalysts.

2. Thermal Stability and Hydrothermal Stability

One useful area to explore in an effort to improve thermal stability of pillared clays may relate to the sheet - pillar connectivity as well as pillar reactivity. Hydrothermal studies posed two important questions:

i) What was the cause of variable behavior - clay, pillar or the connectivity between the two.

ii) Could the stability be improved by choice of clay or by building larger and more stable pillars?

In the last two decades a lot of work has been done in order to understand the first of these problems. Early structural studies of clay intercalate materials were evaluated by Brindley.[50] Chemical bonding between sheet and pillar were established by using electron and x-ray density mapping by Adams.[51] ^{27}Al and ^{29}Si-MAS NMR studies of Plee[52] addressed the connectivity of sheet and pillar.

a) Sheet Stabilization

That the clay layer is less stable for a pillared clays is suggested by sintering studies of of alumina pillared clay.[46,53] The mechanism would seem to be that the protons released migrated to the octahedral layer during the "setting" of the pillar, and further hydrolyzed the octahedral cations. Thermogravimetric analysis showed that dehydroxylation occurred at lower temperatures in PILC than in the non-pillared clay, suggestive that protons attacked octahedral cations. In addition NMR provided evidence that protons migrated into the clay layers.[54] Further evidence was provided by a series of cation exchange reactions on heated and steamed PILC, which showed progressive loss of exchange capacity with time and temperature.[55] If the assumption of protonic attack is true, blocking the proton migration should enhance the clay stability and maximize the cation exchange capacity of PILC. To arrest the migrating proton at the earliest possible time, $(Al_{13})^{x+}$ exchanged clay was calcined in an atmosphere containing ammonia gas, so that the reaction described below could take place in the interlayer during the Al_{13} decomposition to "Al_2O_3". This resulted in maximum cation exchange capacity for the PILC.

$$NH_3 + (Al_{13})^{x+} \text{ - clay} \xrightarrow{\text{heat}} NH_4^+ (Al_2O_3) \text{ - clay}$$

The nature of the clay layer is also an important factor affecting pillared clay thermal stability. Rectorite, an interstratified clay, has two 2:1 layers (one mica and one beidellite layer). Alumina pillared rectorite which retained 75% of its surface area even after 17 hours of steaming at 800 °C, exhibited significantly enhanced thermal and hydrothermal stability.[55-57] The relatively more rigid layer structure of rectorite is suggested to be responsible for it being more stable than pillared smectite.[56] However, pillared illites exhibited poor high thermal performance relative to pillared rectorites.[58] Illites exhibit a thickness similar to that of rectorite, but the smectite layer has less beidellite character. The suitable clay structure would thus appear a combination of increased layer thickness and beidellite character.

b) Pillar Stabilization

The collapsed pillared products had 9.3 Å basal spacings after being used as cracking catalysts, showing that the pillaring species migrated from between the sheets to the external clay surface.[59] In occasional cases evidence was observed for chlorite- like degradation products that would indicate in situ conversion of the "chlorohydrol" pillar into sheet $Al(OH)_3$ polymers.[59]

The first attempt to stabilize the pillar was to increase the molecular weight of the pillaring species by hydrothermal treatment of the pillaring species. Due to further polymerization of the pillaring cation, the pillared

products using pre-hydrothermal treated aluminum chlorohydrate (ACH)[60] and base hydrolyzed aluminum chloride solution[61] exhibited improved the thermal statility.

The second approach was to form co-polymers by reacting or co-polymerizing the Al_{13} species with compounds or salts like Mg, Si, B, Ti or Zr, producing large or more stable polymers. Figure 1.5 is a scheme showing more details of PILC types with enhanced stability. Rare earth elements have been used to modify the pillared clay. For example, the pillared clay treated by K_2CO_3[62] or NH_3[63] regenerated partially the clay cationic exchange capacity and allowed for a cationic exchange with a rare earth. The modified pillared clays exhibited a surface of 150 m^2/g, but no observable d_{001} x-ray diffraction line after thermal treatment at 800 °C. Competitive ion exchange between Al_{13} and NH_4^+ during pillaring reactions also increased the thermal stability of alumina pillared clays.[64]

Many elements have been used successfully as pillaring agents, here we focus ourselves on alumina pillaring species. Hydrothermal treatment of aluminum chlorohydrate yields positively charged bohemite particles. Interaction of these particles with montmorillonite yielded significant cracking activity and thermal stability.[65-66] Aluminum chrorohydrate and a cerium salt co-pillared clay exhibits a large basal spacing typically between 25 and 28 Å and a high cracking activity even after steam deactivation at 760 °C.[63] Similar results were obtained with lanthanum.[68] The Ga/Al pillar has been well characterized by NMR.[69] This Keggin-like ion ($GaAl_{12}^{7+}$) cation in which Ga^{3+} occupied athe tetrahedral position is more stable than the Al_{13}^{7+} cation.[66-67] The surface area obtained after calcining at 700 °C was about 200 m^2/g for $GaAl_{12}^{7+}$ pillared clay compared to 110 m^2/g for alumina pillared clay under similar conditions.[70]

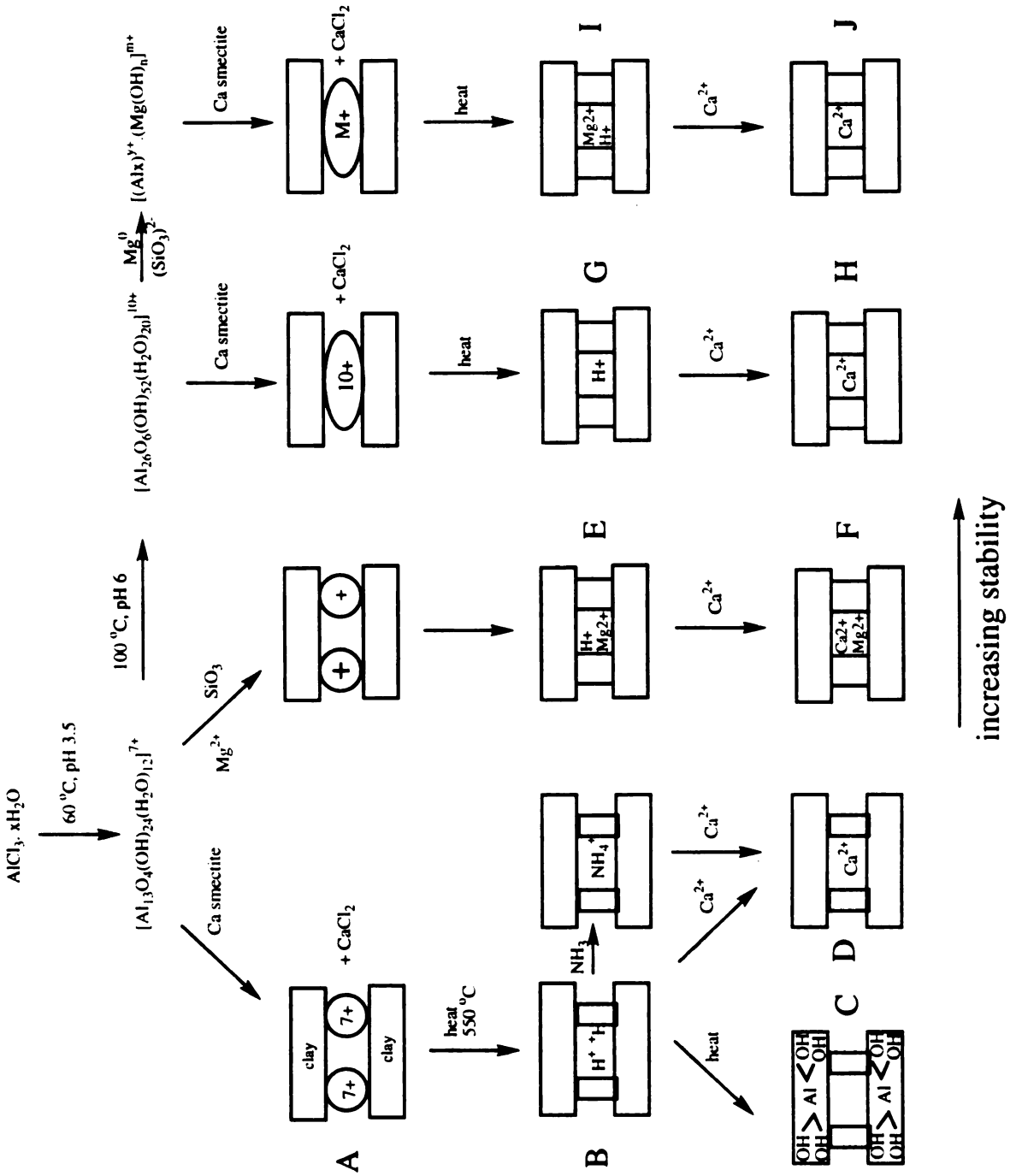

Figure 1.5 Schematic of various Al-PILC modifications made by manipulation of pre- and post- pillaring reactions of the Al polymer intercalating species. (The scheme illustrated by Vaughan, D. E. W.[59]).

c) Thermal Stability of Pillared Montmorillonites

Pillared montmorillonites are the most well-studied pillared clays. There are abundant natural montmorillonites from different geological locations with various charge densities and structural compositions. Different charge densities are expected to influence the properties of pillared products, such as pillar density, pore structures etc. Due to delocalization of the main charge in the octahedral layer, maximum swelling of montmorillonites is easier to achieve compared that obtained with localization of the charge in the tetrahedral layer. It seems that a basal spacing of 18 - 20 Å resulted pillared analogues were obtained by all types of the montmorillonites with various charge densities and under various pillaring variables, for example, the OH^-/Al ratio of the pillaring solution, concentration of Al, and Al/clay ratios. Montmorillonite has the layer rigidity of smectites clay which is less rigid than that of interstratified clay, e. g., rectorite and illite. Also, interaction between the pillar and clay layer is less pronounced than pillared beidellite, therefore, pillared montmorillonites are often used to study the pillaring mechanism. Their thermal stabilities are more dependent on the pillaring conditions.

Several factors have been proposed to control the stability of pillared montmorillonites. Tichit[72] , Tokart and Shabtain[61] correlated the stability of Al-montmorillonites to the pillar density. Bukka and Miller[73] correlated the thermal stability to the charge density of clay layers. The strength of the bond linking the pillars to the clay sheet was emphasized by Plee.[52] For montmorillonites pillared by hydroxy - Al species bonding was supposed to be ionic, with resulting weaker bonds.[74-75] Tichit et al [72] concluded that the thermal stability of the PILC was controlled by the sintering of the pillars at

< 750 °C. At > 750 °C, the clay structure itself appeared to be unstable. Several details of preparations, such as the size of the particle of the original clay were found to influence the stability of the resulting PILC.[76] Clay particles 0.2 μm in size fixed more Al than particles in the range 2 - 10 μm, which suggests that diffusion controlled the distribution of the pillar within the particles. These authors[61,72,76] postulated that the homogeneity of the distribution of the pillar controlled thermal stability.

d) The Thermal Stability of Pillared Beidellites

Compared to montmorillonite, beidellites represent another type of smectite clay with charge in the tetrahedral layer. The effects of the tetrahedral charge site such as swelling ability, bonding of water molecules and surface acidity have been investigated. Cationic (isomorphous) substitution in the tetrahedral (e.g. beidellite, nontronite, saponite) sheet exerts a greater influence on the above reaction than those located in octahedral sheet (e. g. montmorillonite, hectorite). This is due to the differences in ionic attraction for tetrahedral or octahedral charge sites as imposed by their distance from the interlayer positions. Consequently, the tetrahedral charge of clay sheet influences both structure and properties of pillared clays.

The main weakness of pillared montmorillonites is the poor thermal stability of the acid sites. Pillared beidellite, in contrast, retains acid properties after calcining at higher temperature (> 500 °C). Plee, Schutz and Poncelet[77-79,49] claimed that the acidity of pillared beidellites was much stronger, than that of pillared montmorillonites prepared under similar conditions. The Brönsted acidity was accounted for by the proton attack of

Si-O-Al bonds of the tetrahedral layer and formation of silanol groups responsible for the O-H stretch band at 3440 cm^{-1}. This behavior is similar to that of NH_4^+-Y zeolite, whereas the Lewis acidity was associated with the alumina pillars.[47,76] Also, catalytic properties were studied by comparison of pillared beidellite with pillared montmorillonite and zeolite.[78] The aim was to achieve similar catalytic activity as observed for H-Y zeolite.[78,81]

Structural information for pillared beidellites has been obtained from MAS NMR. Plee[52] et al. observed a decrease form tetrahedral aluminum (Q^3(1Al)) upon calcining pillared beidellite, and attributed it to a change of the tetrahedral sites into a three dimensional-like structure. Recent MAS NMR studies of pillared saponites[82-83] suggested the splitting of Si-O-Al bonds. Additionally, the cross-linking between SiO_4 (clay sheet) with alumina pillars could be achieved by inverting some silica tetrahedra into the interlayer.

C. IMOGOLITE PILLARED BEIDELLITE

1. Structure of Imogolite

Imogolite is a natural aluminosilicate mineral found in weathered volcanic ash and pumice beds. It was named by Yoshinga and Aomine in 1962. Instead of an end member of allophane[84] or layered structure[85] Gradwick, Armer and Russel[86] in 1972 proposed that imogolite had a hydrated tubular structure. The basis for their structure was the combination of following evidence. The chemical composition of imogolite was $SiO_2 \cdot Al_2O_3 \cdot nH_2O$. Deuterium exchange showed the presence of surface hydroxyl groups. The infrared spectrum had adsorption bands near 930 cm^{-1} and 950 cm^{-1} which could result from orthosilicate units. After converting the silicate anion to its corresponding trimethylsilyl ether,[87-89] the examination of the different degrees of polymerization showed that about 95% of the silicate derived from orthosilicate units. The electron diffraction pattern consisted of fibers with 8.4 Å repeat units parallel to the fiber axis and 23 Å perpendicular to the axis.[86]

The basic structure of an imogolite tube is a single gibbsite sheet bent round in the form of a cylinder with orthosilicate groups attached to the inside of the cylinder, each group replacing three OH groups above an empty octahedral site as shown in Figure 1.6 (A). Natural imogolite tubes contain eleven repeat units with an outside diameter of 21 Å and synthetic tubes have twelve repeat unit with an outside diameter of 23 Å. The internal diameter is 9-11 Å, and the lengths of the tubes vary from hundreds of angstroms to several microns. The empirical formula for the tubular aluminosilicate imogolite is $(OH)_3Al_2O_3SiOH$. The formula is

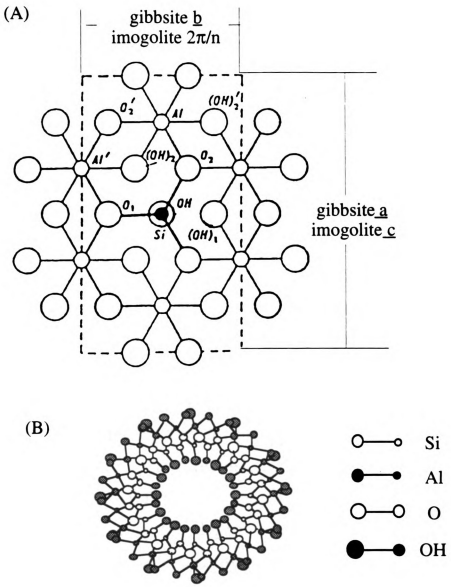

Figure 1.6 Structure of imogolite (A) mode in which the orthosilicates group is attached to the face of a gibbsite sheet; (B) cross sectional view of the imogolite structure.

written so that it corresponds to the ordering of atoms along a path from the outside to the inside of the tube as shown in Figure 1.6(B).

2. Properties of Imogolite

Associated with its unique structure, imogolite has unique physical properties. What is of interest to us here are its solution flocculation, cation exchange capacity, anion exchange capacity, acidity and microporosity.

The colloid behavior of imogolite formed in aqueous solution depends upon the pH and imogolite concentration. In acidic solution and low concentration (30 mM Al or less), imogolite is completely soluble, forming a crystal clear solution. When the pH increases up 7, aggregation of the tubes begins and the solution turns cloudy. As the pH increases gelation begins. This behavior is due to charge on the surface with changing pH. Below pH 5.5 the surface aluminum hydroxides are all protonated and the tubes remain separate due to electrostatic repulsions.[90] When the pH is increased, deprotonation on the surface results in the aggregation of the tubes. The other factor influencing the degree of aggregation is the imogolite concentration. An imogolite suspension containing more than 30 mM Al begins to flocculate. The aggregation process is never completely reversible by means of either pH or by concentration variation.

The CEC and AEC of imogolite are also pH dependent and affected both by temperature and by ions being measured. At pH 7, the CEC for an oven-dried sample, as determined by Na^+ adsorption from 0.05 N $NaCH_3COO$, is found to be 30 meq/100g.[90] CEC values increase in the order $Na^+ < K^+ < Mg^{2+} < Ba^{2+}$. The ACE, measured by adsorption of Cl^-

from 0.05M NaCl, is 15 meq/100g at pH 7. The AEC values increase as $NO_3^- < Cl^- < CH_3COO^- << SO_4^{2-}$.

Since hydroxyls groups on both external and internal surfaces are responsible for the acidity, the state of these highly hydrophilic hydroxyls determines the acidity. Using sulfuric acid as the reference, under very dry conditions, <5% relative humidity, imogolite is a strong acid, comparable to 71% H_2SO_4 acidity. Below 20% relative humidity its acidity corresponds to that of 2 x 10^{-2}% H_2SO_4. Above 20% relative humidity the acidity is only equivalent to an acid concentration of 8 x 10^{-8}% H_2SO_4. The structure of the acid sites under different relative humidity is as follows:[90]

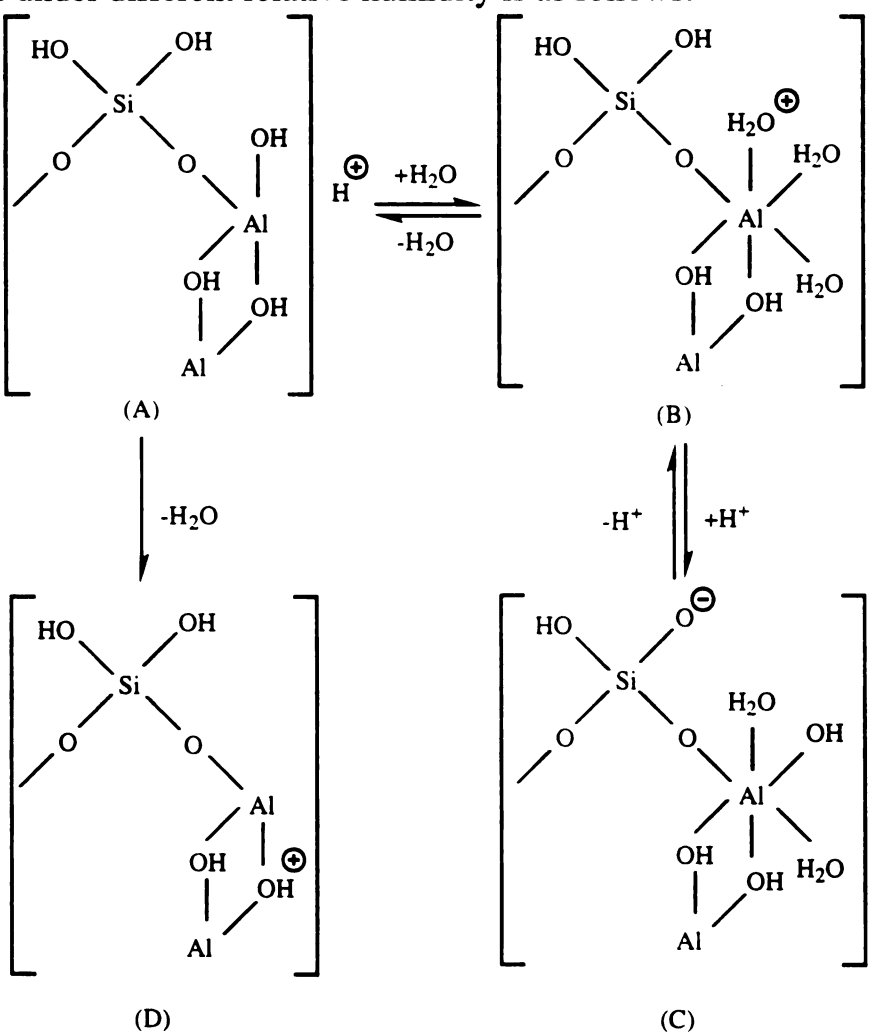

In the presence of water a proton is very weakly donated from SiOH and $AlOH_2^+$, as shown from species (B) to species (C). The species (B) shifts first to (A) and then to (D) by removing water. Species (A) represents a strong Brönsted acid site and species (D) a strong Lewis acid site.

The porosity of imogolite gives rise to spaces inside the tubes and to the pores formed between the tubes in packing solid state a arrangement. So factors like tube size, method used to dry the sample, and amount of water in various types of pores, influence the porosity. Natural imogolite tubes tend to pack more regularly than do synthetic tubes as evidenced by a higher order reflection obtained in electron diffraction patterns of the natural imogolite.[91] However, recent work[92] claimed that synthetic imogolite has longer range order than natural imogolite with little mesopore obtained by N_2 adsorption at 77K. Also, the model[92] shown in Figure 1.7 was proposed to represent the pores in imogolite. The water which filled in mesopores C could be removed at a low temperature, followed by tubular pores A. At a higher temperature of 275 ^oC, the process of removing water in B, e.g. intertubular water, might accompany dehydroxylation.

3. Imogolite Pillared Clay: TSLS Complex

Imogolite has been intercalated as a pillaring agent into smectite clays such Na^+-montmorillonite[93] in our lab. These new tubular silicate-layered silicate (TSLS) nanocomposites are viewed as a new type of pillared clay in which the pillars themselves are microporous.[94] Figure 1.8 is a schematic representation of a TSLS complex.

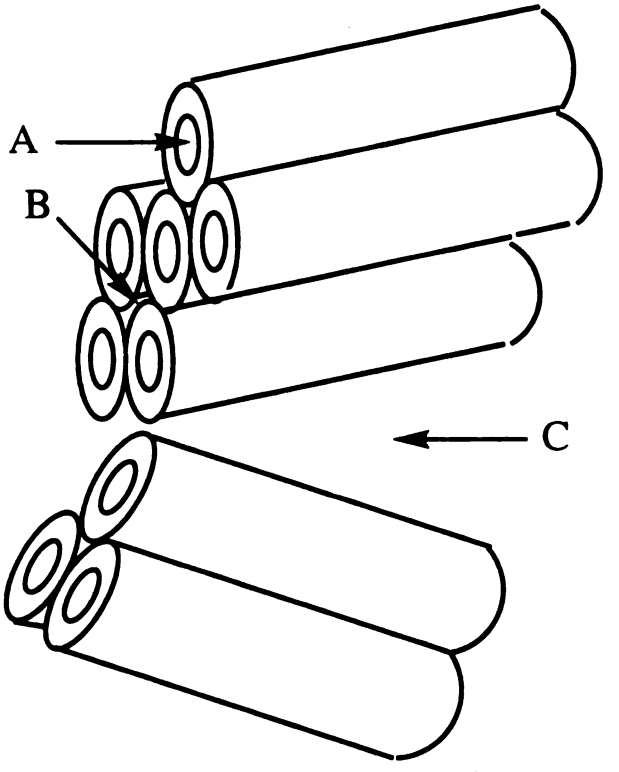

Figure 1.7 Conceptual diagram of the pores in imogolite. (Scheme as illustrated by Brinker C. J. et al.[92])

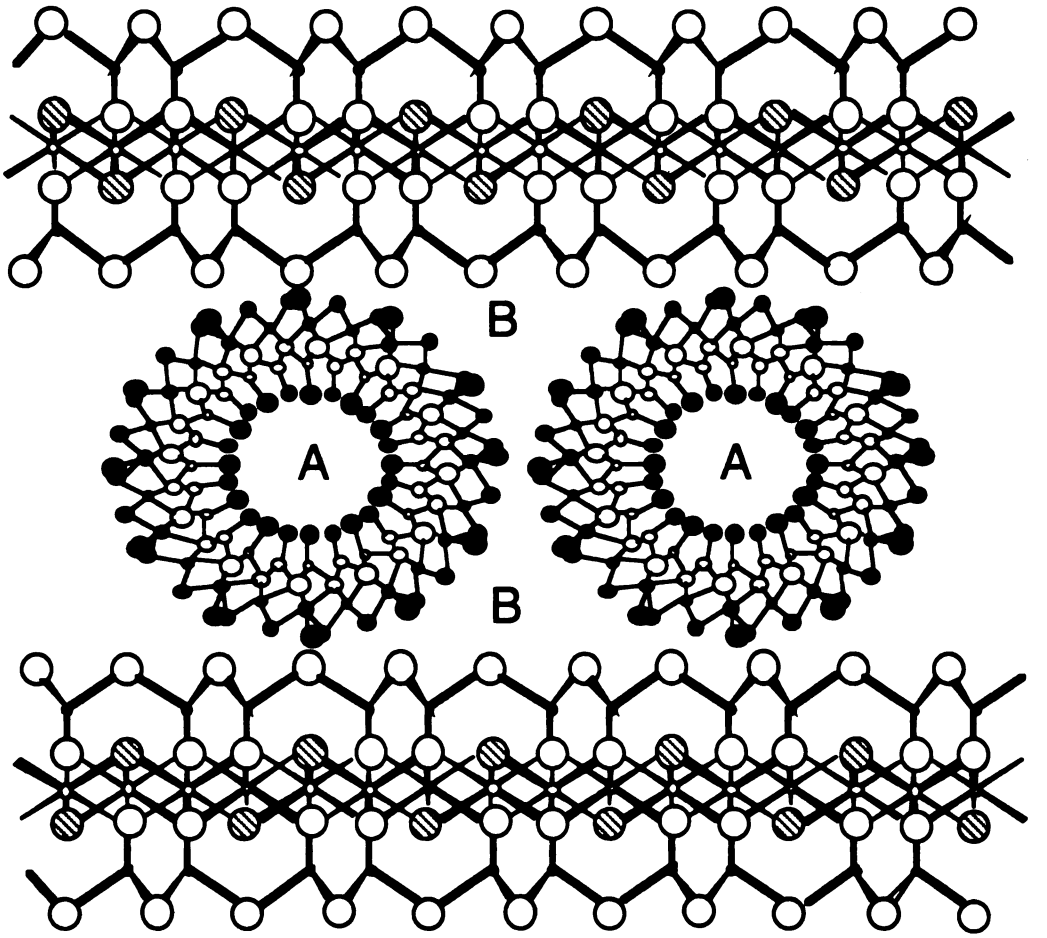

Figure 1.8 Diagram of imogolite pillared clays.

The structures of TSLS complex were determined from the observed d-spacing by XRD.[95] A d-spacing of > 44 Å was considered indicative of multilayers of imogolite tubes within the gallery. Single layers (<34 Å) were formed by washing away the excess imogolite tubes.

From of N_2 adsorption isotherm data,[96] TSLS complexes were found to be very microporous: the Langmuir surface area was 480 m^2/g, and the liquid microporous volume 0.205 cc/g. The surface area of 480 m^2/g derived from a t-plot was comparable to the value of 460 m^2/g obtained from BET treatment of the data. using the bimodel behavior of a t-plot, two adsorption environments designated the intra-tubular and inter-tubular pores were found as the model in Figure 1.8 shows.

Differential thermal analysis studies indicated that thermal stability of intercalated imogolite was enhanced dramatically compared with that of pristine tubes.[93] The intercalated tubes were thermally stable to 450 ^oC, whereas the pure imogolite tube began to collapse above 250 ^oC.

The FTIR spectrum of pyridine adsorbed on the TSLS complex presented both Brönsted and Lewis acid sites. TSLS complex was shown to be active for the acid-catalyzed dealkylation of cumene at 350 ^oC, but less reactive than a conventional alumina pillared montmorillonite.[96]

REFERENCE

1. Pinnavaia, T. J. *Science* **1983,** *220*, 365-371.
2. Pinnavaia, T. J. in " *Chemical Physics of Intercalation:"*, Legrand A. P. and Flandrois S. Ed.; NATO ASI Series B: Physics, New York, 1987, vol. 172, pp233-252.
3. Schulze, D. G. In *"Minerals in soil environment,"*, Dixon, J. B. and Weed, S. B. Ed.; Soil Science Soc. Amer.; Madison, 1977, Chapter 1.
4. Green-Kelly, R. *Mineral Mag.* **1955,** *30,* 604-615.
5. Malla, P. B.; Douglas, L. A. *Clays and Clay Miner.* **1987,** *35(3),* 232 236.
6. Mott, C. J. B. in *"Catalysis Today, 2"*, Bruch, R. Ed. Amsterdam, 1988, Chapter 2.
7. Greenland, D. J.; Quirk, J. P. *J. Soil Science,* **1964,** *15,* 178.
8. Fripiat, J. J. *In "Spectroscopic characterization of minerials and their surfaces"*, Coyne, L. M.; Mckeever, W. S.; Blake, D. F. Eds.; ACS Symposium Series, 415; American Chemical Society; Washington, DC; 1990; Chapter 18.
9. Parry, E. P. *J. Catal.* **1963,** *2*, 371-379.
10. Figueras, F. *Catal. Rev.-Sci. Eng.* **1988,** *30 (3),* 457- 499.
11. He, Ming-yun; Liu, Zhonghui; Min, Enze in "Catalysis Today,2", Ed. Burch, R. Ed. Amsterdam, 1988, Chapter 12.
12. Ebllmen, M. *Ann. Chimie Phys.* **1846,** *16,* 129.
13. Ebelmen, M. C. R. *Acad. Sci.* **1847,** *25,* 854.
14. Roy, D. M.; Roy, R. *Am. Minerral.* **1954,** *39,* 957.
15. Roy, R. *J. Am. Ceram. Soc.* **1956,** *39,* 145.
16. Iler, R. K. *Chemistry of Silica;* Wiley: New York, 1955.

17. Stober, W.; Fink, A.; Bohn, E. *J. Colloid Interface Sci.* **1968,** *26,* 62.

18. Sakka, S.; Kamiya, K. *J. Non-Cryst. Solids,* **1980,** *42,* 403.

19. Sakka, S.; Yoko, T. Structure and bonding, 1992, 77, 89.

20. Hench, L. L.; West, J. K. *Chem. Rev,* **1990,** *90,* 33-72.

21. Livage, J. J.; Sanchez, M. C. Progress in Solid State Chem., **1988,** *18,* 259.

22. Brinker, C. J.; Scherer, G. W. Sol-Gel Science, Academic Press, New York, 1989.

23. Brinker, C. J.; Scherer, G. W. *J. Non-Cryst. Solids,* **1985,** *70,* 301.

24. Sanchez, C.; Livage, J. *New J. Chem.,* **1990,** *14,* 513.

25. Harward, M. E.; Brinley, G. W. *Clays and Clay Miner.* **1965,** *6,* 209.

26. Iiyama, J. T.; Roy, R. *Clay Miner. Bull.* **1963,** *5,* 161.

27. Brindley, G. W.; Sempels, R. E. *Clay Miner.* **1977,** *12,* 229-237.

28. UK Patent GB 2,164 ,636 A, 1986.

29. Diadams, P. A.; Thomas, J. M.; Jones, W.; Ballantine, J. A.; Purnell, J. H. *J. Chem. Soc. Chem. Commun.* **1984,** 1340-1342.

30. Plee, D.; Gatineau, L.; Fripiat, J. J. *Clays and Clay Miner.* **1987,** *35 (2),* 81-88.

31. Theo Kloprogge, J.; Ben J.; Jansen, H.; John, W. Geus *Clays and Clay Miner. 38(4),* **1990,** 409-414.

32. *Pillared clays*; Burch, R. Ed.; Catalysis Today, 2; Elserier: Amsterdam, 1988.

33. Occelli, M. L. in *Keynote in Energy-Related Catalysis*; Kaliauine, S. Ed.; Stud. Surf. Sci. Catal.; Elserier: Amsterdam, 1988; pp 101-137.

34. Figure, F. *Catal. Rev. Sci. Eng.*, **1988**, *30(3)*, 457-459.

35. Kresge, C. T.; Leonowicz, M. E.; Roth, W. J.; Vartuli, J. C.; Beck, J. S. *Nature*, **1992**, *359*, 710.

36. Beck, J. S.; Vartuli, M. C.; Roth, W. J.; Leonowicz, M. E.; Kresge, C. T.; Schmitt, K. O.; Chu, C. T-W.; Olson, D. H.; Sheppard, E. W.; McCullen, S. B.; Higgins, J. B.; Schlenker, J. L. *J. Am. Chem. Soc.* **1992**, *114*, 10834.

37. Pinnavaia, T. J.; Kim, H. in *Zeolite Microporous Solids: Synthesis, Structure and Reactivity;* Derouane, E. G. Ed.; Kluwer , Belgium, p 79.

38. Bottero, J. Y.; Axelos, M.; Tchoubar, K. ; Cased, J. M.; Fripiat, J. J.; Fiessinger, F. *J. Coloid and Interface Sci.* **1987,** 47-57.

39. Pinnavaia, T. J. in *Chemical Reactions in Organic and Inorganic Constrained Systems;* Setton, R. Ed.; New York, 1986; pp151-164.

40. Pinnavaia, T. J.; Tzou, M. S.; Landau, S. D. Raythatha, H. R. *J. Mol. Catal.,* **1984,** *27,* 195-212.

41. Butruille, J. R. Ph. D thesis, Michigan State University, 1992.

42. Brindley, G. M.; Sempels, R. E. *Clay Miner.* **1977**, *12*, 229-237.

43. Lahav, N.; Shani, U.; Shabtai, J. *Clays and Clay Miner.* **1978**, *26*, 107-115.

44. Vaughan, D. E. W., Lussier, R. J.; Mcgee, J. S. U.S. Patent 4 248 739, 1979.

45. Jacobs, P. A.; Poncelet, G.; Schutz, A. Eur. Patent Appl. 0073 718, 1982.

46. Occelli, M. L.; Tinawa, R. M. *Clays and Clay Miner.* **1983**, *31*, 22-28.

47. Pinnavaia, T. J.; Tzou, M. S.; Landau, S. D. Raythatha, H. R. *J. Mol. Catal.,* **1984,** *27,* 195-212.

48. Plee, D.; Gatineau, L.; Fripiat, J. J. *Clays and Clay Miner.* **1987**, *35*, 81- 88.

49. Schutz, A.; Stone, W. E. E.; Poncelet, G.; Fripiat, J. J. *Clays and Clay Miner.* **1987**, *35*, 251-261.

50. Brindley, G. W.; Tsunashima, A. *Clays and Clay Miner.* **1973,** *21,* 233.

51. Adams, J. M. *J. Chem. Soc., Dalton,* **1974,** 2286.

52. Plee, D.; Borg, F. Gatineau, L.; Fripiat, J. J. *J. Amer. Chem. Soc.,* **1985,** *107*, 2362-2369.

53. Tichit, D.; Fajula, F.; Figueras, F.; Ducourant, B.; Mascherpa, G.; Gueguen, C.; Bousquet, J. *Clays and Clay Miner.* **1988,** *36*, 369-375.

54. Tennakoon, D. T. B.; Jones, W.; Thomas, J. M. *J. Chem. Soc., Faraday Trans I,* **1986,** *82*, 3081.

55. Vaughan, D. E. W.; Lussier, R. J.; Magee, J. S. U. S. Patent, 4 176 090, 1979.

56. Guan, J.; Min, E.; Yu, Z. in *Proceeding of International Congress, 9th.;* Philips, M. J.; Ternam, M. Eds. Chem. Inst. Can., Ottawa, Canada, 1988; p 104.

57. Brody, J. F.; Johnson, J. W. in *Proc. 1990 Fall Meet. Mat. Res. Soc.;* Materials Research Society, Pittsburgh, USA, p 65.

58. Sterte, J. in *Preparation of Catalysts V;* Stud. Surf. Sci. Catal., **1991**, *63*, 301.

59. Baughan, D. E. W. in *Pillared clays*; Burch, R. Ed.; Catalysis Today, 2; Elsevier: Amsterdam, 1988, Chapter 1.

60. Sterte, J; Otterstedt, J-E. Delmon, B; Grange, P. in *Preparation of Catalysts IV*, Jacobs, P.A.; Poncelet, G. Eds. Elsevier, Amsterdam, 1987, p 631.

61. Tokart, M.; Shabtai, J. *Clays and Clay Miner.* **1985,** *33*, 89-98.

62. Baughan, D. E. W.; Lussier, R. J.; Magee, J. S. US Patents 4 176 090, 1979,; 4 248 739, 1981,; 4 271 043, 1981.

63. Horio, M.; Suzuki, K.; Masuda, H.; Mori, T. *Appl. Catal.,* **1991,** *72,* 109.

64. Figueras, F.; Klapyta, Z.; Massiani, P. Mountassir, Z. Tichit, D.; Fajula, F.; Gueguen, C.; Bousquet, J.; Auroux, A. *Clays and Clay Miner.*, **1990**, *38*, 257.

65. Sterte, J.; Otterstedt, J.-E.; Thulin, H.; Massoth, F. E. *Appl. Catal.,* **1988,** *38,* 119.

66. Sterte, J.; Otterstedt, J.-E.; *Appl. Catal.,* **1988,** *38,* 131.

67. McCauley, J. R. Int. Pat. Appl. PCT/US88/00567 March 4, 1988.

68. Sterte, J. *Clays and Clay Miner.* **1991,** *39,* 167.

69. Thomas, B. Görz, H.; Schönherr, S. *Z. Chem.,* **1987,** *27,* 183.

70 Bradley, S. M.; Kydd, R. A.; Yamdagin, R.; Fyfe, C. A. in *Synthesis of Microporous Materials;* Occelli, M. L.; Robson, H. E. Eds, Van Nostrand Reinhold: New York, 1992; vol. II, p 13.

71. Gonzlez, F.; Pesquera, C.; Blanco, C. Benito, I.; Medioroz, S. *Inorg. Chem.,* **1992,** *31,* 727.

72. Tichit, D.; Fajula, F.; Figueras, F.; Bousquet, J.; Gueguen, C. in *Catalysis by Acids and Bases*; Imelik, B. C. et al. Eds.; Elserier, Amsterdam, 1985; 351-360.

73. Bukka, K.; Miller, J. D. *Clays and Clay Miner.* **1992,** *40(1)*, 92-102.

74. Pinnavaia, T. J.; Landau, S. D.; Tzou, M. S. Johnson, I. D. Lipsicas, M. *J. Amer. Chem. Soc.* **1985,** *107*, 7222-7224.

75. Sterte, J.; Shabtai, J. *Clays and Clay Miner.* **1987,** *35*, 429-439.

76. Tichit, D.; Fajula, F.; Figueras, F.; Guguen, C.; and Bousquet, J. in *Advances in Fluid Catalytic Cracking*; New Orleans, Occelli, M. L.

Ed.; ACS Symp. Series 375, Amer. Chem. Soc.: Washington, D. C., 1987; pp 237-252.

77. Plee, D.; Schutz A.; Poncelet, G.; Fiipiat, J. J. in *Catalysis by Acids and Bases*, Imelik, B., Naccache, C., Coudurier, G., Taarit, J. Gen, Vedrine, J. C., Eds.; Elsevier: Amsterdam, 1985;

78. Schutz, A.; Plee, D., Borg, F.; Jacobs, P., Poncelet, G.; Fripiat, J. J., in *Proc. Int. Clay Conf.*, Denver, 1987. Schultz, L. G., Olphen, H. van, Mumpton, F. A., Eds.; The Clay Minerals Society: Bloomington, Indiana, 1987; pp 305-310.

79. Poncelet, G.; Schutz, A. in *Chemical Reactions in Organic and Inorganic Constrained Systems*, Setton, R., Ed.; Reidel: Dorecht, 1986; pp 165-178.

80. Kojima, M.; Hartford, R.; O'Connor, C. T. *J. Catal.*, **1991**, *128*, 487-498.

81. Plee, D.; Schutz, A.; Poncelet, G.; Borg, F.; Jacobs, P.; Gatineau, L.; Fripiat, J. J. Fr. Patent 2 563 446, 1984.

82. Malla, P. B.; Komarneni, S. *Clays and Clay Miner.*, **1993**, *41(4)*, 472-483.

83. Li, L.; Liu, X.; Ge, Y.; Xu, R. *J. Phys. Chem.*, **1993**, *97*, 10389-10393.

84. Russel, J. D.; McHardy, W. J. and Freser, A. R. *Clay Miner.* **1969,** *8,* 87-88.

85. Weda, K. and Yoshinaga, N. *Am. Miner.* **1969,** *54,* 50.

86. Cradwick, P. D. G.; F, Armer, V. C. and Russell, J. D. *Natural Phys. Sci.* **1972,** *240,* 188.

87. Gotz, J.; Masson, C. R. *J. Chem. Soc. A* **1970,** 2683.

88. Gotz, J.; Masson, C. R. *J. Chem. Soc. A* **1971,** 686.

89. Inoue, T. and Wada, K. *Clay Sci.* **1971,** *4,* 61.

90. Henmi, T. and Wada, K. *Clay Miner.* **1974,** *10,* 231.

91. Borisov, S. N. et al. Organosilicon Heteropolymers and Heterocompounds, pp297, New York, Plenum, 1970.

92. Ackerman, W. C.; Smith, D. M.; Huling, J. C.; Kim, Y. W.; Bailey, J. K.; Brinker, C. J. *Langmuir*, **1993**, *9(4)*, 1051.

93. Johnson, I.J.; Werpy, T. A.; Pinnavaia, T. J. *J. Am. Chem. Soc.* **1988,** *110,* 8545-8547.

94. Pinnavaia, T. J.; Kwon, T.; Yun, S. K. In "Zeolite Microporous Solids: Synthesis, Structure, and Reactivity", Derouane, E. G. et al Edsl 1992, Kulwer Academic Publishers, pp91-104.

95. U. S. Patent 4,621,070, 1986.

96. Werpy, T. A.: Michot, L. J.; Pinnavaia, T. J. ACS symposium series, *437,* Am. Chem. Soc.: 1990, pp119-128.

CHAPTER TWO

SYNTHESIS OF BEIDELLITE AT LOW TEMPERATURE BY A SOL-GEL PROCESS AND CHARACTERIZATION OF SYNTHETIC AND NATURAL BEIDELLITES

A. OBJECTIVE OF RESEARCH

In beidellite, a member of the smectite family of 2:1 layered silicate clays, the net negative charge on the oxygen framework arises mainly from the substitution of Al^{3+} for Si^{4+} in the tetrahedral sites. This structural analogy to zeolite suggests that Brönsted acid sites may arise from the conversion of Si-O-Al linkages to Si-OH··Al entities. Indeed, it has been suggested that the presence of Brönsted acid sites makes this clay and its aluminum pillared derivatives more attractive for acid catalytic application relative to montmorillonite and other smectites in which the layer charge arises from metal ion substitution on the octahedral sheet.[1, 2] Beidellite rarely is found in commercial quantity in nature. Also, the natural mineral even when available usually contains paramagnetic impurities such as Fe(III) that can promote undesirable coke formation in acid catalytic organic reactions.[3] Thus, there is considerable incentive for developing efficient routes to synthetic forms of this mineral.

The aim of this work is to synthesize well-crystallized beidellite at lower temperature than has been achieved in the past. In order to enhance the reactivity of the reactants, we have made use of a hydrated gel rather than a calcined oxide for hydrothermal synthesis. In addition, strongly hydrated Mg^{2+} is used as the exchangeable cation to help order the layer environment. We also incorporate natural beidellite as a seed to promote

nucleation. We find that the use of an active gel is the most critical step. Beidellite can be formed at 200 °C under hydrothermal conditions from active gels. Also the crystallinity of the product is substantially improved relative to beidellite prepared by conventional methods. The factors that influence the activity of the gel are discussed. Two kinds of natural beidellite obtained from the U. S. A. and from China, and synthetic beidellites are characterized. The properties of synthetic beidellite are compared with the properties of natural beidellites. Also, the method of identifying and measuring the kaolin impurity in natural beidellite is investigated.

B. EXPERIMENTAL

1. Clay Preparation

Volatile impurities in natural Chinese beidellite (CB) were removed by heating at 120 °C for 12 hours; the mineral was then exchanged with 1 M NaCl. Natural American beidellite (GS-3) was converted to the Na^+ exchanged form after eliminating carbonate and ferric oxide impurities by treatment with sodium acetate and sodium dithionite[1]. All clay samples were fractionated by conventional sedimentation techniques and the < 2 μm fractions were collected.

2. Synthesis of Beidellite at Low Temperature

Synthesis of beidellite at 200 °C was performed by hydrothermal reaction of a wet, co-precipitated magnesium aluminosilicate gel, instead of from calcined oxides. A typical gel preparation was as follows: Aluminum

tri-*sec* butoxide 16.2 mL, 0.064 mol and 15 wt% silica sol (Nalco silica sol #1115) 42.4 g, 0.106 mole SiO_2 were hydrolyzed in 150 mL 0.2 M NaOH solution, and then 0.935 g, 0.0046 mole $MgCl_2 \cdot 6H_2O$ was added into the gel to co-precipitate $Mg(OH)_2$. The resulting mixture was aged overnight at pH near 10 and then washed by centrifugation until the pH was reduced to 7 and the gel was free of Cl^-. The solid material thus obtained was re-dispersed in deionized water and natural beidellite (1wt%) was added as seed. The wet gel was allowed to undergo hydrothermal reaction at 200 ^oC for 3 to 7 days in Parr acid digestion bombs fitted with a teflon-lined cup. The product was suspended in water and air-dried to form continuous self-supporting films for x-ray diffraction analysis.

3. Characterization Methods

a) Chemical Analysis

Samples for elemental analysis by ICP emission spectroscopy were prepared by using the lithium metaborate ($LiBO_2$) technique.[4] A 50 mg quantity of sample was mixed with 300 mg of lithium metaborate and heated 10 minutes at 1000 ^oC. The fused product was then dissolved in 50 mL of 5% of HNO_3 for chemical analysis.

b) CEC Measurement

Cationic exchange capacities (CEC) were determined according to the procedure described by Busenberg and Clemency.[6] The clays were exchanged with ammonium acetate and air dried. The amount of ammonia

liberated from the NH_4^+- exchanged clays when suspended in 10M NaOH was measured with an ammonia electrode.

c) Physical Measurements

X-ray diffraction patterns were obtained for oriented powder samples using a Rigaku diffractometer equipped with a Cu target and curved crystal graphite monochromator.

The morphology of the clay and pillared clay was investigated with a JEOL 100 CX II transmission electron microscope operated at 100 KV.

Adsorption / desorption experiments using N_2 as the sorbate were carried out at -196 °C on a Coulter Ominosorb 360 CX sorptometer. The samples were outgassed overnight at 150 °C under dynamic vacuum (10^{-5} torr). Nitrogen isotherms were obtained by using the quasi-equilibrium volumetric method.[7-9] Surface areas were obtained from the BET equation.

FTIR spectra were recorded on powdered samples dispersed in KBr tablets (sample concentration is about 1 wt%) with an IBM IR44 spectrometer. To obtain the FTIR spectrum for chemisorbed pyridine, a self-supported sample wafer was outgassed at 300 °C under flowing helium prior to pyridine adsorption at 25 °C. Weakly adsorbed pyridine was removed by outgassing the sample at 150 °C.

A Varian 400 VXR solid state NMR spectrometer was used to obtain ^{29}Si and ^{27}Al MAS NMR spectra at 79.5 MHz and 104.3 MHz, respectively. The spinning frequencies were 4-5 KHz. ^{29}Si chemical shifts were reported relative to TMS. The relaxation recovery time used to accumulate spectra of synthetic and natural beidellite was 19 and 60 second, respectively. The ^{27}Al chemical shifts were relative to $AlCl_3 \cdot 6H_2O$.

Thermal gravimetric analysis (TGA) was run on a CAHN TG-121 apparatus. The sample was heated from 30 °C to 700 °C at the rate of 5 °C/min.

Temperature programmed desorption (TPD) of ammonia was carried out by outgassing the sample at 400 °C or 500 °C in flowing Ar for 4 hours, cooling to 100 °C, passing anhydrous ammonia gas over the sample for 30 minutes, flushing with pure Ar for another 30 minutes, then switching to an on-line GC system and ramping the temperature at 10 °C/min up to 500 °C. A thermal conductivity detector was used to detect the amount of ammonia as a function of temperature.

d) Catalysis

MBOH Reaction

A new model reaction,[10] which is sensitive simultaneously to the presence of acidic/basic sites, was applied to characterize the acid/base functionality on external clay surfaces. The probe molecule used in the catalytic reaction was 2-methyl-3-butyn-2-ol (MBOH). Upon an acid site, MBOH mainly undergoes dehydration to yield 3-methyl-3-buten-1-yne (Mbyne). Reaction at a basic site results in the formation of acetylene and acetone cleavage products. Also, certain amphoteric surfaces give by products 3-hydroxy-3-methyl-2-butanone (HMB) and its corresponding dehydrated product 3-methyl-2-butene-2-one (MIPK). The reaction schemes are shown in Figure 2.1. From the conversion and selectivity, information concerning reactivity and acid/base properties can be obtained under conditions close to those used for most common catalytic reactions.

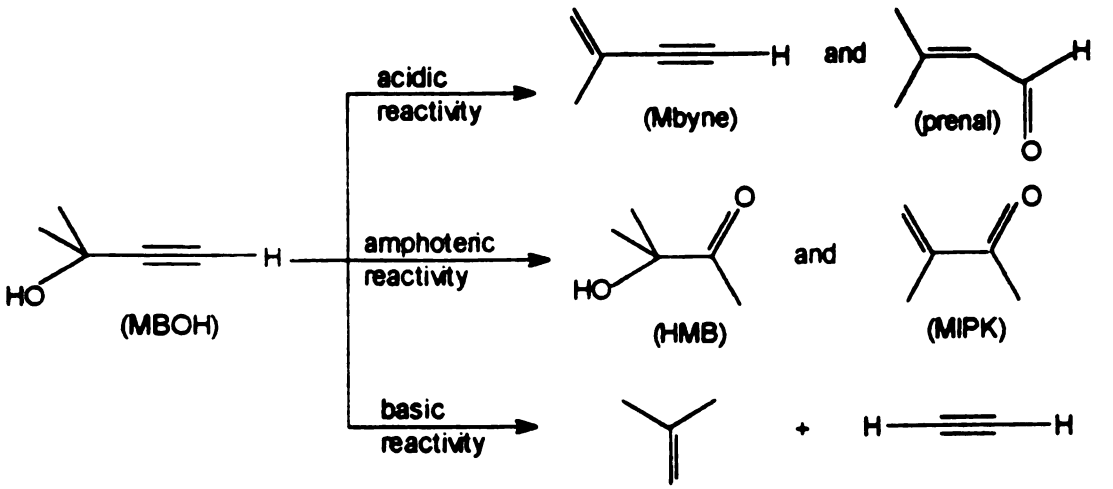

Figure 2.1. 2-methyl-3-butyn-2-ol (MBOH) reaction scheme.

In this work, the above probe reaction was used to characterize the external surface properties of smectites clays and their cation exchanged forms. The study was carried out in a fixed-bed flow reactor constructed in a 10 mm diameter quartz tube. A 0.2 g quantity of catalyst was activated at 300 °C for 2 hours. The dehydration temperature of MBOH over the catalyst was carried out at 180 °C. MBOH vapor was carried to the reaction by He flow through a saturator maintained at 25 °C. The reactant stream consisted of 2.5 % MBOH in He. The rate of reactant flow was 1.2 l/h. The products were analyzed after 2 hours when steady state conditions were reached.

C. RESULTS

1. SYNTHESIS OF BEIDELLITE AT LOW TEMPERATURE

As described in the experimental section, the gel used to synthesize beidellite was prepared by hydrolysis of aluminum tri-*sec* butoxide, Si sol and magnesium chloride in NaOH solution. After removal of extraneous ions by washing, the gel was divided into three potions. The first portion was redispersed by deionized water directly without drying. The second portion was air-dried on a glass plate at room temperature, and then dispersed with deionized water. The third portion was heated in an oven at 150 ^{o}C for 4 hours, and redispersed with deionized water. All the gels so obtained allowed to be performed hydrothermal reaction at 200 ^{o}C for 7 days. The XRD (film) diffraction patterns of the products is shown in Figure 2.2. The good crystallinity as seen in Figure 2.2 (A) was obtained from wet gel which was the gel without drying. Figure 2.2 (B) showed much lower intensity and broaden peak, indicating that the air - dried gel had poor crystallinity. A non - crystalline product was obtained if the gel was pre - dried at 150 ^{o}C. Figure 2.3 gives the XRD patterns of products from a wet gel with reaction periods of 1, 3 and 7 days. Good crystallinity was obtained after 3 days. The higher reactivity of the wet gel was indicated by the shorter reaction time needed to obtain good crystallinity of the product.

XRD enables one to check the quality of the product from both active and inactive gels, but it can not provide structural information due to the absence of long-range order. To compare structural differences between an air - dried gel and one dried at 150 ^{o}C, ^{29}Si MAS NMR spectra were obtained as shown in Figure 2.4(A, t=0) and Figure 2.4(B, t=0), respectively.

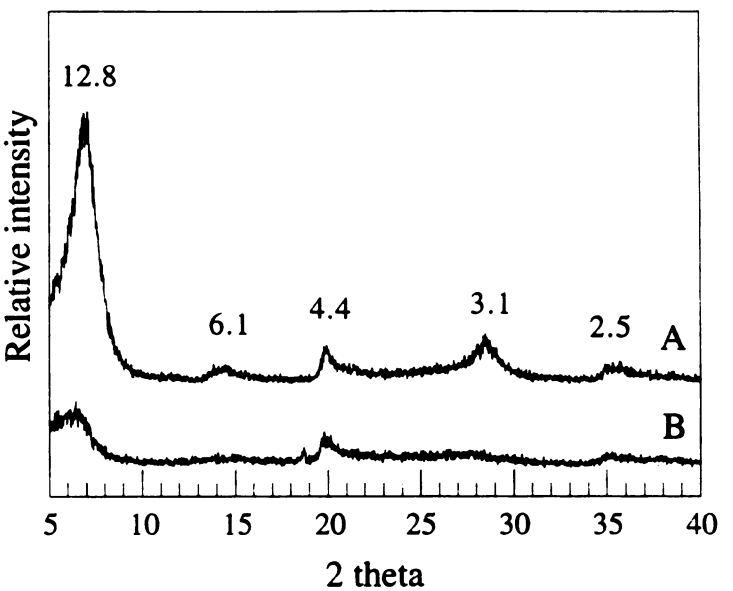

Figure 2.2 XRD pattern (film samples) of beidellites prepared by hydrothermal synthesis at 200 °C (7 days) and converted to Na^+- exchanged form from (A) wet gel; (B) air-dried gel.

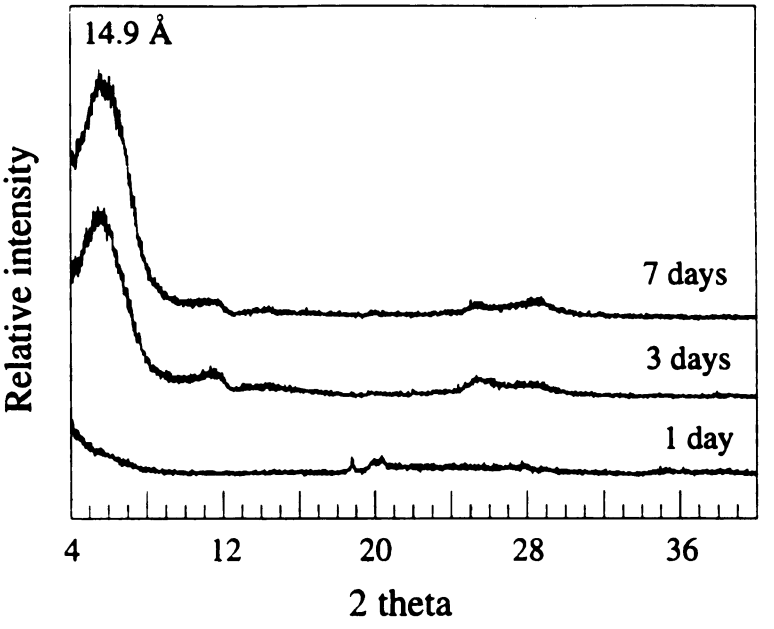

Figure 2.3 XRD patterns (film samples) of Mg^{2+}-beidellites prepared from a wet gel after reaction periods 1, 5, and 7 days.

Both gels gave a very broad band of overlapping from -80 ppm to -120 ppm, indicative of a broad range of silicon Q^1 to Q^4 sites. By using cross-polarization (CP), well resolved ^{29}Si NMR spectra were obtained. The short contact times were chosen to compare the content of OH group attached to different Si. For both gels CP led to an enhancement of the signal. Figure 2.4(A) for air - dried gel allowed a clear distinction among silicon sites: Q^1 peak at about -64 ppm, Q^2 peak at about -90 ppm, Q^3 site at about -100 ppm and Q^4 peak at about -110 ppm. In Figure 2.4(B) for the gel dried at 150 ^oC, there were no obvious distinctions between different silicon sites by applying CP, basically a broad peak centered around -97 ppm which belongs to Q^3 sites. Therefore, more OH groups attached to Si and Al existed in the air -dried gel than in the gel dried at 150 ^oC. The differences in gel structures are presumably related to the greater reactivity of the wet gel for beidellite synthesis.

Tetraethyl orthosilicate (TEOS) can be used in place of a silica sol for the preparation of beidellite. The composition, internal surface structure and kinetics of silica gel formation prepared by hydrolysis and condensation of TEOS are influenced by molar proportions of TEOS: EtOH: H_2O, temperature, pH, aging and drying of the reaction mixture.[11-12] In order to investigate the activities of gels prepared from TEOS, three different hydrolysis and aging procedures were applied to the gel synthesized at the same stoichoimetries used to prepare gels from a silica sol:

(A) TEOS was added to 150 mL, 0.2 M NaOH solution, then $[C_2H_5CH(CH_3)O]_3Al$ and $MgCl_2$ were added immediately into the this aqueous solution. The resulting gel was aged for 1 day before washing and performing the hydrothermal reaction at 200 ^oC for 7 days. The XRD pattern of the product is as given in Figure 2.5(A).

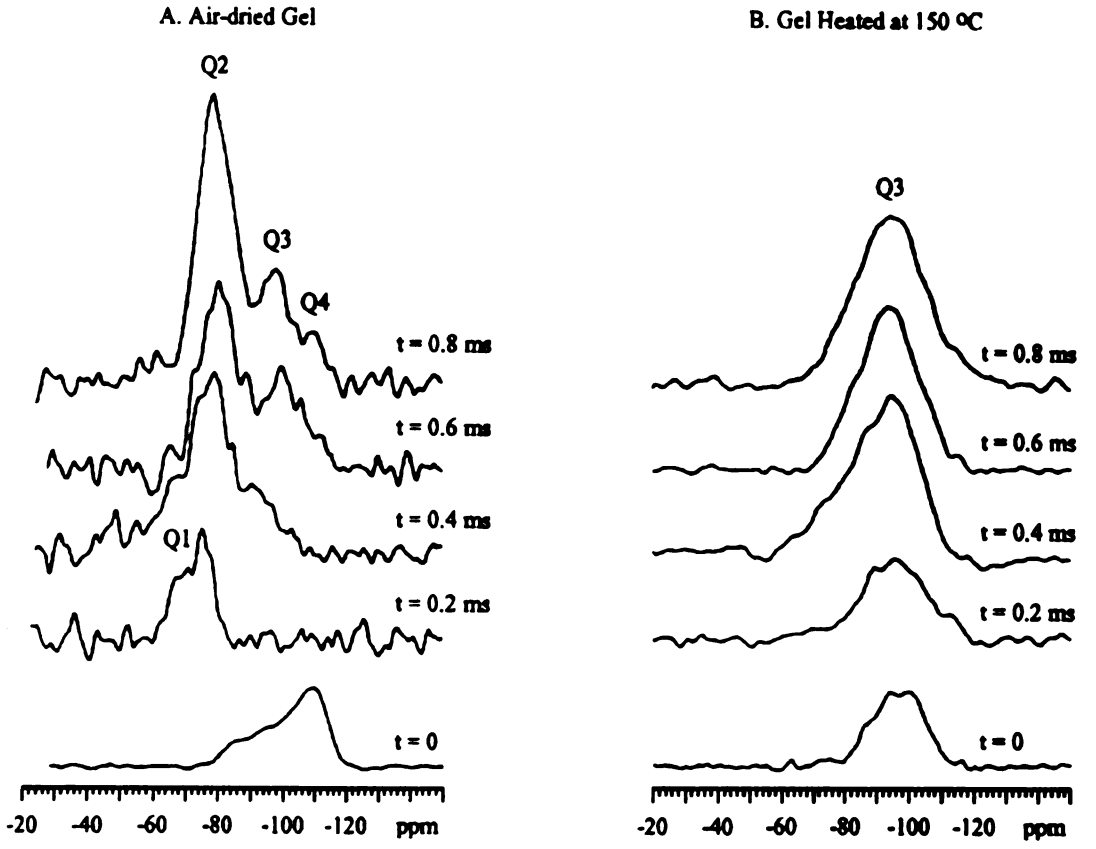

Figure 2.4 ^{29}Si CP MAS NMR spectra of magnesium aluminosilicate gels prepared from Si sol and aluminum tri-*sec* butoxide and used for the hydrothermal systhesis of beidellite. (A) air-dried gel; (B) gel dried at 150 °C. Cross-polarization spectra were obtained with the contact times specified.

(B) TEOS was hydrolyzed in 150 mL, 0.2 M NaOH solution for 3 days, then $[C_2H_5CH(CH_3)O]_3Al$ and $MgCl_2$ were added. The aging and washing procedures were same as those used in method (A). The XRD of the product is as shown in Figure 2.5(B).

(C) the mixture of TEOS and EtOH in a 1:1 volume ratio was added to 150 mL 0.2 M aqueous NaOH solution, aged for 1 day before $[C_2H_5CH(CH_3)O]_3Al$ and $MgCl_2$ were added, then aged overnight and washed. The XRD pattern is shown in Figure 2.5(C).

A more active gel was produced by pre - hydrolysis of TEOS in water - ethanol. The crystallinity of the products is influenced by the process used for TEOS hydrolysis. At the same base concentration, solvation effects are important for hydrolysis of TEOS.

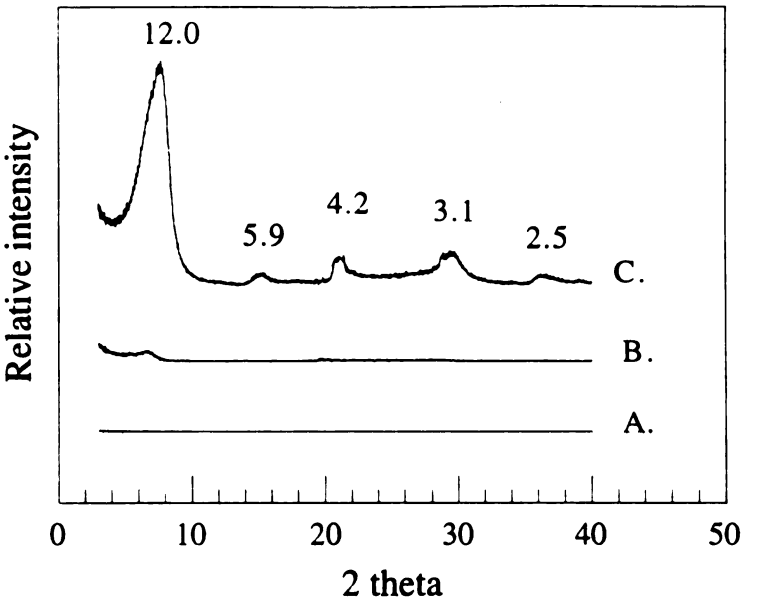

Figure 2.5 XRD patterns (film samples) of products obtained by hydrothermal reaction (at 200 °C, 7 days) of magnesium aluminosilicate gel prepared from TEOS under different conditions: gel prepared by (A) hydrolysis of TEOS in an aqueous NaOH in the presence of Al(*sec*-BuO)$_3$ and $MgCl_2$, (B) hydrolysis of TEOS in aqueous NaOH for 3 days prior to reaction with Al(*sec*-BuO)$_3$ and $MgCl_2$, (C) hydrolysis of TEOS in 1:1 ethanol:water for 1 day prior to reaction with Al(*sec*-BuO)$_3$ and $MgCl_2$.

2. CHARACTERIZATION OF BEIDELLITE SYNTHESIZED AT LOW TEMPERATURE

The beidellite characterized below was synthesized from the wet gel at 200 ^{o}C for 7 days. The gel was formed by the hydrolysis reaction of $MgCl_2$, $Al[O(CH_3)CHC_2H_5]_3$, and Si sol. Unlike the conventional synthesis of beidellite, where the metal oxide compositions were determined from the composition of starting materials, the gel used in the present work for the low temperature synthesis was washed free of extraneous ions. The washing process changes the compositions of starting materials slightly as the data in Table 2.1 show. The unit cell composition from the chemical analysis was written as: $Mg_{0.39}Al_{0.02}(Al_4)^{oct}(Si_{7.16}Al_{0.84})^{tet}O_{20}(OH)_4$. The CEC value was 101 meq/100g for air - dried clay as compared to a value of 114 meq/100g calculated from the anhydrous unit cell fomula.

Table 2.1. Compositions of Gel and Product[1]

	Mg/Al	Si/Al
Unwashed gel	0.071	1.64
Beidellite	0.080	1.47

[1]product composition from chemical analysis.

When Mg^{2+} was used as the exchangeable cations instead of Na^+, gel composition affected not only the crystallinity of the products, but also the charge distribution remarkably. To examine charge distribution, a Green-Kelly test was applied to confirm the tetrahedral origins of the layer charge.[13]

Figure 2.6(A) shows the SEM of Mg-beidellite which possesses a flakelike morphology. A regular layer stacking was observed in TEM images of ultrathin sections of synthetic beidellite as shown in Figure 2.6(B).

The X-ray powder diffraction pattern of the Na^+-exchanged form of synthetic beidellite is shown in Figure 2.7. The powder pattern yielded a sharp basal spacing at 12.8 Å. The high diffraction intensity indicated that the beidellite synthesized at 200 °C had very good crystallinity. The indexing of peaks for this work and that of other synthetic beidellites is listed in Table 2.2.

Table 2.2. X-ray Powder Diffraction Data for Na^+-Beidellites Prepared by Hydrothermal Synthesis

hkl Index[1]	d (obs)[2]	d (obs)[3]
001	12.87	12.44
002	6.22	6.19
020, 110	4.40	4.43
024	3.19	3.12
201	2.53	2.54
242	1.676	1.670
060, 330	1.496	1.490

[1]index assignments from ref.15 and from ref.16.

[2]this work, prepared at 200 °C from a wet magnesium aluminosilicate gel using silica sol as the source of silicon.

[3]from ref. 14, prepared at 340 °C from calcined metal oxides.

Figure 2.6 (A) SEM; (B) TEM images of Mg^{2+}-beidellite synthesized at 200 ^{o}C for 7 days from the wet gel.

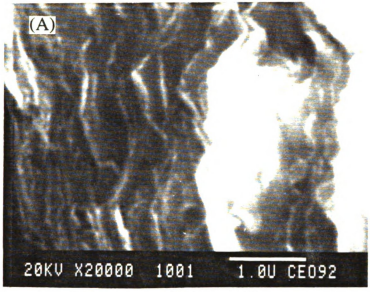
(A)
20KV X20000 1001 1.0U CE092

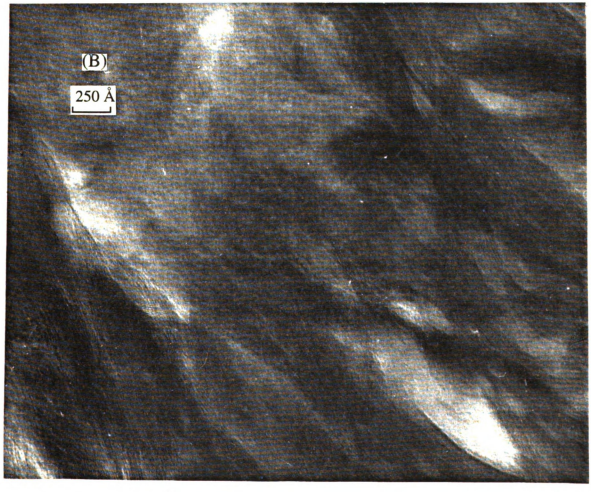
(B)
250 Å

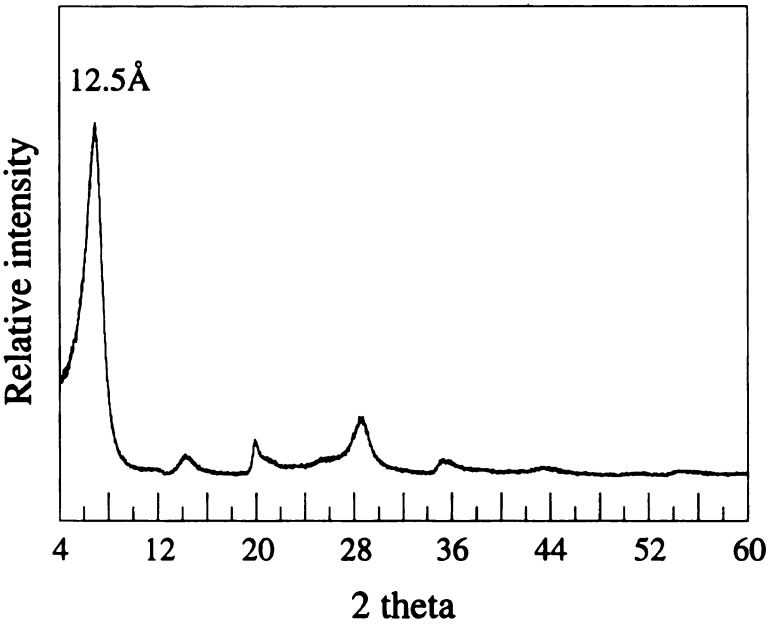

Figure 2.7 XRD powder pattern of Na^{+}-beidellite prepared by Na^{+} exchange of Mg^{2+}- beidellite synthesized at 200 °C for 7 days from the wet gel.

Additional piece of information concerning the local structure of synthetic beidellite was provided by ^{29}Si and ^{27}Al MAS NMR. In Figure 2.8, the Q^4 Si sites for the gel are replaced by Q^3 sites upon beidellite formation. The chemical shifts of the main components for beidellite occurred at -94 ppm and -89 ppm, corresponding to $Q^3(0Al)$ and $Q^3(1Al)$, respectively. Figure 2.9 presents the ^{27}Al NMR spectra of synthetic Mg^{2+}-beidellite. The two peaks at 4.4 ppm and 71 ppm belong to aluminum in octahedral and tetrahedral coordination, respectively.

In order to obtain the relative abundance of silica environments in the beidellite, the two ^{29}Si NMR components were deconvoluted by using a Lorentzian-line shape program. Based on Loewenstein's rule, the $(Si/Al)^{tet}$ ratio can be estimated from following equation:[17]

$$(Si/Al)^{tet} = \sum_{n=0}^{n=3} I_{Si(nAl)} \Big/ \sum_{n=0}^{n=3} \frac{n}{3} I_{Si(nAl)}$$

where I is the peak intensity of Q^3 sites of Si with nAl neighbors.
The results are summarized in Table 2.3.

Table 2.3. ^{29}Si Chemical Shifts (ppm), Line Width (ppm) and Relative Signal Intensities (%)[1] for Synthetic Beidellite

sample	line width (ppm)	$(Si/Al)^{tet}$	Si-(OAl) %	Si-(OAl) (ppm)	Si-(1Al) %	Si-(1Al) (ppm)
beidellite	6.0	10.6	72	-93.3	28	-89.4

[1]The relaxation recovery time used to accumulate spectra was 19 sec.

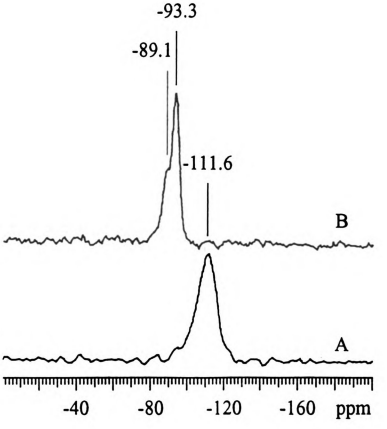

Figure 2.8 ^{29}Si MAS NMR spectra. (A) air-dried gel; (B) synthetic Mg^{2+}-beidellite crystallized at 200 ^{o}C for 7 days from a wet gel.

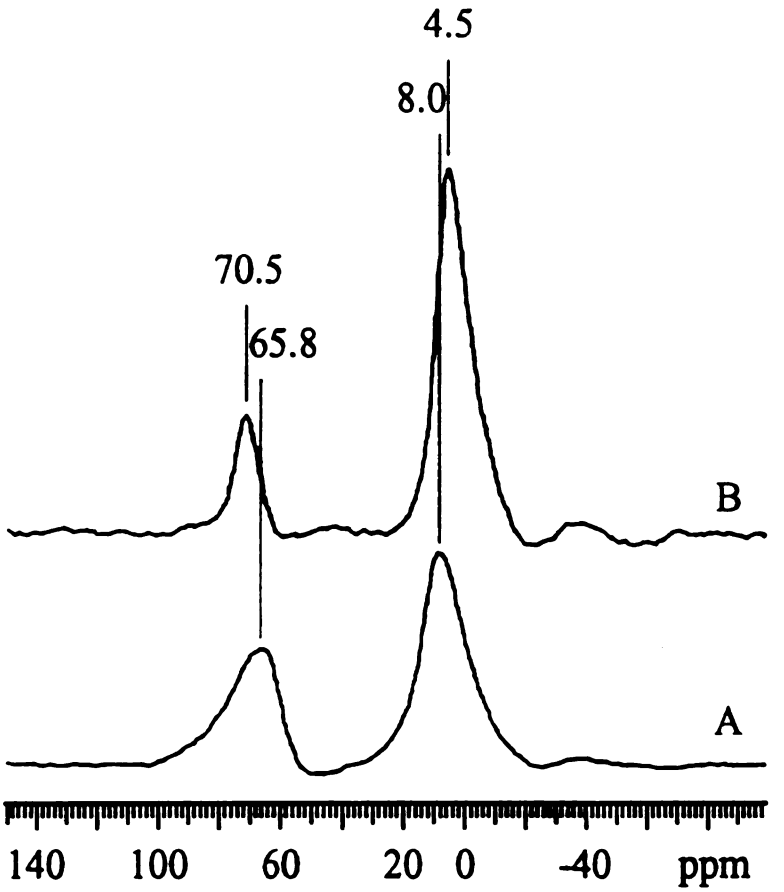

Figure 2.9 ^{27}Al MAS NMR spectra. (A) air-dried gel; (B) synthetic Mg^{2+}-beidellite crystallized at 200 °C for 7 days from a wet gel.

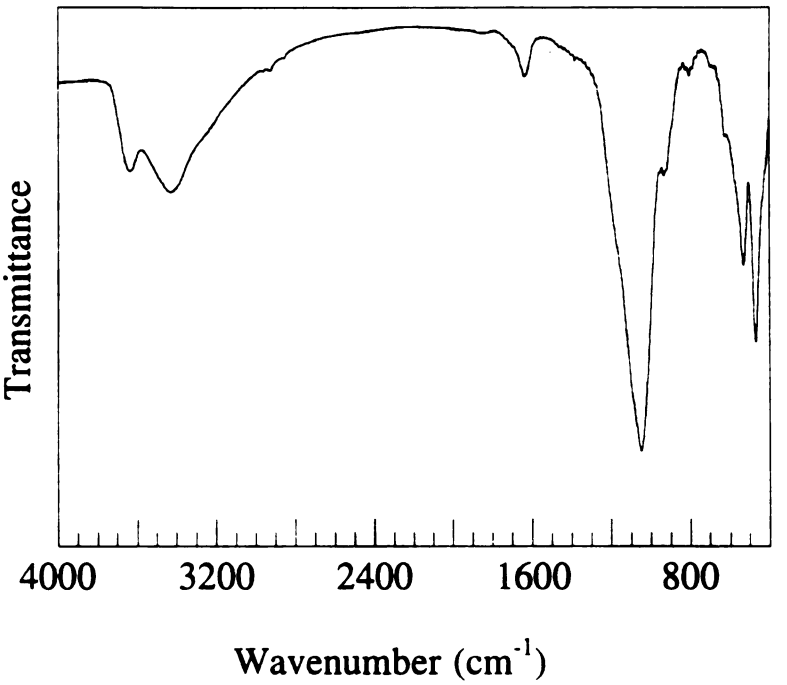

Figure 2.10 Infrared spectrum of synthetic Mg^{2+}-beidellite.

The IR spectrum of synthetic beidellite is shown in Figure 2.10. The bonding characters are summarized and compared in Table 2.4 with former work[14].

Table 2.4. Infrared Absorption Maxima (cm^{-1}) of Synthetic Mg^{2+}-Beidellite Prepared from the Wet Gel

Synthetic Mg^{2+}-Beidellite frequency (cm^{-1})	Na^{+}-Beidellite[1] frequency (cm^{-1})	Assignment[2]	
3636(s)	3655	Al-O-H	stretching
3447(s)	3450	H-O-H	stretching
1637 (m)	1638	H-O-H	bending
1042 (s)	1047	Si-O-Si	stretching
924 (m)	935	Al-O-H	bending
	883	Al-O-H	bending
810 (w)	800	Al-O-H	bending
694 (w)	700	Si-O-Al	bending
610 (w)	627	Al-O-H	bending
532 (s)	531	Si-O-Al	bending
468 (s)	470	Si-O	bending
442 (shoulder)	440	Si-O	bending

[1]from ref. 14, prepared at 340 °C from calcined metal oxides.

[2]Index assignments from ref. 18 and ref. 19.

TGA plots depicting the dehydration and dehydroxylation process of Mg^{2+}-beidellite is shown in Figure 2.11. After air-drying, the weight loss was measured. The first weight loss (up to 55 °C) was due to absorbed water. The second weight loss from 55 °C to 600 °C was attributed to the

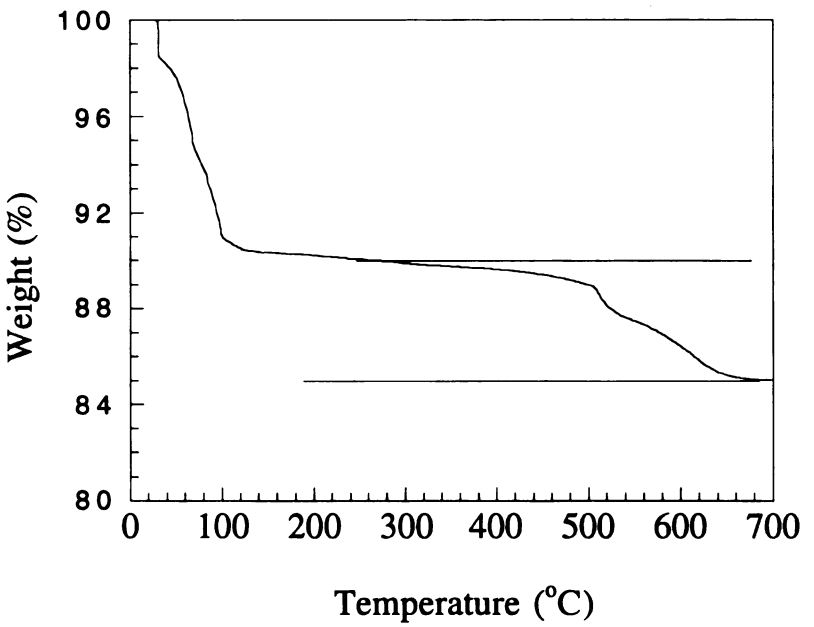

Figure 2.11 Thermogravimetric analysis of synthetic Mg^{2+}-beidellite (heating rate = 5 °C/min).

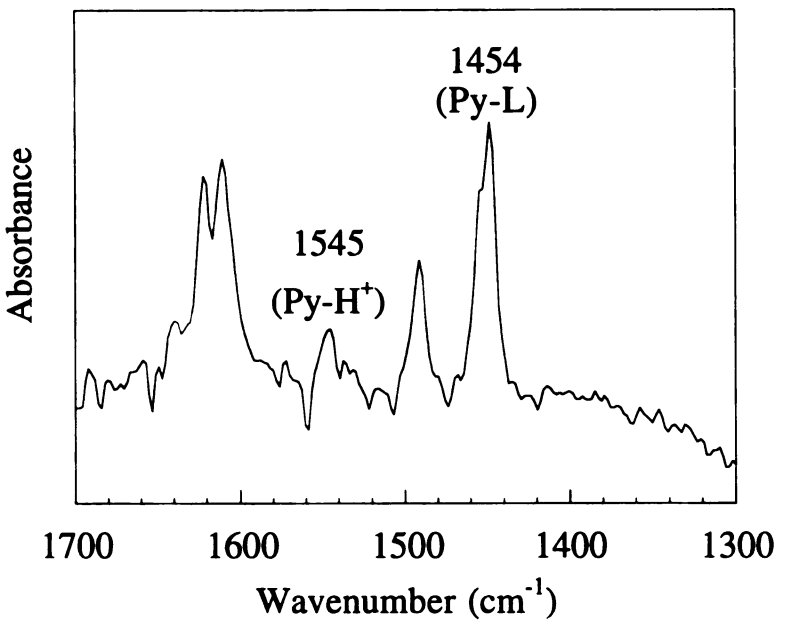

Figure 2.12 FTIR spectrum of pyridine chemisorbed at 150 °C on synthetic Mg^{2+}-beidellite.

removal of interlayer water and to the dehydroxylation of the 2:1 layers. The loss above 400 ^{o}C was considered due to dehydroxylation. Since there are four OH groups in one mole of beidellite, complete dehydroxylation should produce two moles of H_2O with a 4.9 % weight loss. The observed weight loss for the synthesized beidellite was 5.0 %.

Infrared spectroscopy (Figure 2.12) revealed chemisorption of pyridine at both the Lewis and Brösted acid sites of Mg^{2+}-beidellite. The ring stretching frequencies[20] at 1454 cm^{-1} and 1545 cm^{-1} are characteristic of Lewis pyridine and Brönsted pyridine, respectively. Both Lewis and Brönsted acid sites are observed in the synthetic beidellite.

In order to compare the effects of exchangeable cations on the surface acidity and on the activity for the reaction, temperature programmed desorption (TPD) of adsorbed ammonia was measured. The desorption of ammonia on various exchanged cations was recorded from 100 ^{o}C to 300 ^{o}C as shown in Figure 2.13.

The data for the MBOH catalytic test on various cation exchanged synthetic beidellites are listed in Table 2.5. From the product distributions, The major product was mbyne with a trace amount of MIPK due to the amphoteric reactivity. Prenal and HMB were absent. It seems that the acid-catalyzed dehydration process was the preferred route in the clay system. Although acid sites are predominant on the clay surface and the NH_4^+-exchanged form is more acidic than other cation exchanged forms, small amounts of base sites coexist with acid sites as evidenced by some base-catalyzed products.

When the interlayer cation was varied, the acid reactivity decreased in the order of $NH_4^+ > Li^+ > Mg^{2+} > Na^+$. The effect the of interlayer cation on reactivity was verified by using Wyoming montmorillonite, which

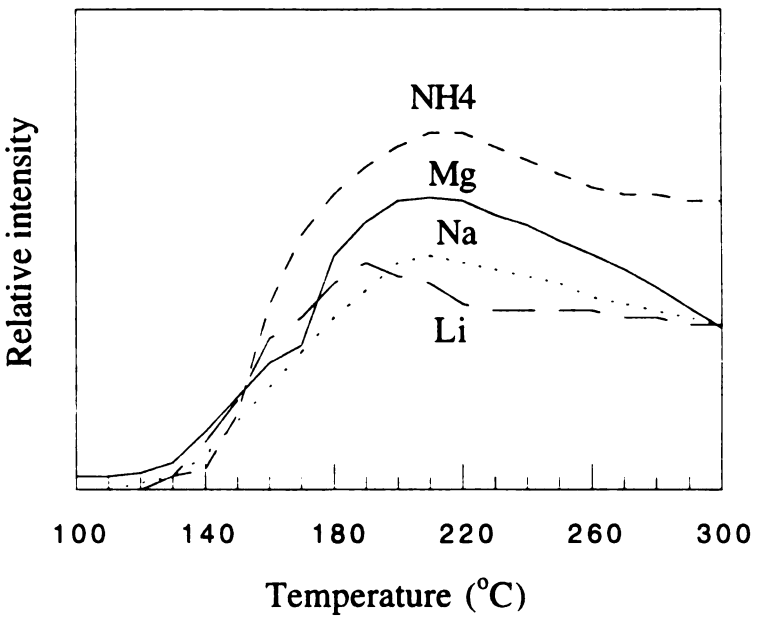

Figure 2.13 Temperature programmed desorption of ammonia as a function of temperature on various exchanged synthetic beidellites.

showed the same trend as the beidellite (see Table 2.5). In ammonia TPD, the acidity order became $NH_4^+ > Mg^{2+} > Li^+ \geq Na^+$. Moreover, we noticed that there were no major differences in the amount of desorbed ammonia when the exchangeable cations were varied. However, exchangeable catons seemed to influence the activity greatly. The strength of the electrostatic field and the electronic polarizability induced by cations may affect the surface acidity. In TPD all the acid sites which were able to adsorb a strong base such as ammonia were counted. For the catalytic process, the factors are more complicated. Active catalysts might need more accessible acid sites which can provide H^+ efficiently and have appropriate acid strength. Li^+-exchanged clay is more favorable over the Mg^{2+}- and Na^+- exchanged form for the acid catalyzed reaction.

Table 2.5. Reaction of 2-methyl-3-butyn-2-ol (MBOH)[1] on Various Ion Exchanged Forms of Synthetic Beidellite and Natural Montmorillonite

sample	conv.	selectivity (%)			
	(%)	C_2H_2	acetone	Mbyne	MIPK
NH_4-beidellite[2]	77.9	0.4	0.5	98.4	0.7
Li-beidellite	59.0	0.6	0.2	99.0	0.2
Mg-beidellite	30.9	0.5	0.7	98.6	0.2
Na-beidellite	20.4	1.1	1.1	97.7	0.1
NH_4-montmorillonite	23.8	3.3	2.7	94.0	0
Li-montmorillonite	13.9	4.3	3.7	91.2	0.9
Mg-montmorillonite	5.6	3.2	2.2	94.6	0
Na-montmorillonite	3.7	20.0	12.3	65.9	1.9

[1]Reaction conditions: 0.2 g of catalyst was activated at 300 °C *in situ* for 2 hours. Reation temperature was 180 °C.
[2]BET surface area = 129 m^2/g.

3. CHARACTERIZATION OF NATURAL BEIDELLITES

Two kinds of natural beidellites from different geological locations were characterized for comparison with synthetic beidellite. Also, as described in the introduction, most natural beidellites contain impurities. It was necessary to develop a convenient laboratory method in the lab to identify and estimate quantitatively the impurities in the clay minerals.

The most common impurity in the clay mineral is quartz, which mostly can be removed by sedimentation. However, sometimes in the < 2 μm fraction, small amount of quartz still exist, which usually gives rise to higher Si content by chemical analysis and lower CEC value. The existence of quartz is usually revealed by XRD and is identifiable by the strongest peak at 27~28° (2θ). In the Appendix B, the index of quartz is listed for the reference. ^{29}Si MAS NMR is another way to identify quartz. The peak at about -110 ppm belongs to the Q^4 sites of quartz.

The molar ratio of metal was for GS-3 and CB obtained by using the chemical analysis listed in Table 6. The unit cell composition for CB was written as $M^{n+}_{0.74/n}[Al_{3.31}Fe_{0.15}Mg_{0.74}]^{oct}(Si_{7.40}Al_{0.60})^{tet}O_{20}(OH)_4$

where $M^{+n} = Na^+$, K^+, and Ca^{2+}.

It does not seem reasonable to obtain a GS-3 unit cell composition from the molar ratio due to the quite high Al content obtained from chemical analysis data.

The measured CEC values for CB and GS-3 were 100 and 60 meq/100g, respectively.

The morphology of both samples was investigated by SEM and TEM. SEM of CB revealed a flakelike morphology (Figure 2.14(A)). The small aggregates on the surface of GS-3 (Figure 2.15(A)) might be the impurity.

Figure 2.14 (A) SEM; (B) TEM images of Na^+-CB (Chinese beidellite).

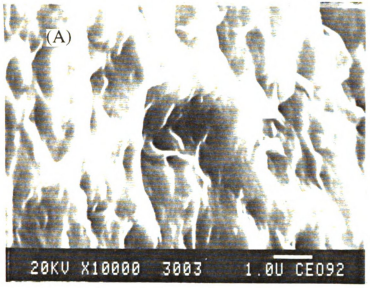
(A)
20KV X10000 3003 1.0U CE092

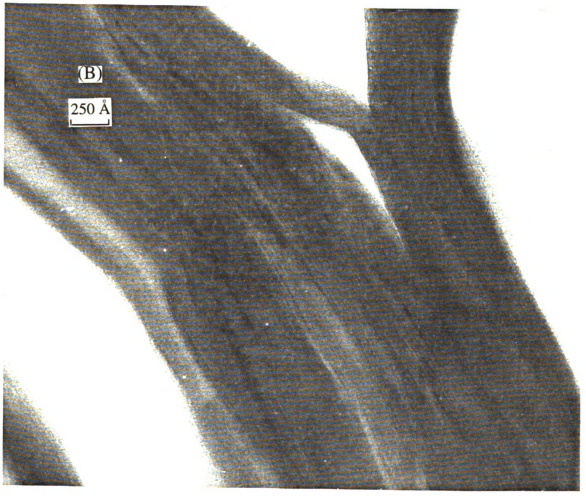
(B)
250 Å

Figure 2.15 (A) SEM; (B) TEM images of Na^{+}-GS-3 beidellite.

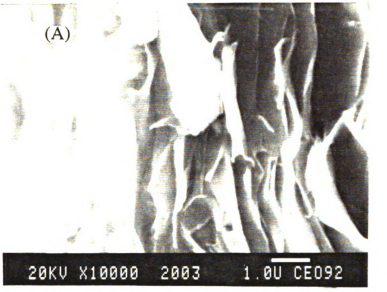
(A)
20KV X10000 2003 1.0U CE092


(B)
250 Å

Table 2.6. Metal Ion Content of Naturally Occurring Beidellites from Chemical Analysis

sample	molar compositions
GS-3	$Na_{0.44}\ Mg_{0.10}\ Fe_{0.16}\ Al_{5.10}\ Si_{6.90}$
CB	$Na_{0.74}\ Mg_{0.74}\ Fe_{0.15}\ Al_{3.91}\ Si_{7.40}$

The TEM images of thin sections in Figure 2.14(B) and Figure 2.15(B) clearly illustrate layer stacking. Most of the layers have their largest dimensions smaller than 0.2 μm.. A single layer along the c-axis could not be resolved. The tactoids are formed by stacking of approximately 10 layers.

GS-3 and CB were subjected to a Green-Kelly test. When Li^+-exchanged beidellites were heated at 200 °C, a d-spacing of 9.5 Å resulted. The expansion of the d-spacing to 17.8 Å after saturation by glycerol confirmed that charges originated from the tetrahedral sheets.

XRD patterns yielded basal spacing of 12.4 Å and 12.5 Å for GS-3 and CB, respectively at room temperature. When the temperature was increased above 55 °C, d(001) decreased gradually to 9.8 Å due to the loss of interlayer water. The d-spacings of the hkl indices of CB agreed well with the reported data.[14] However for GS-3, two broad peaks at d=7.2 Å and 3.5 Å could not be indexed as the diffraction peaks of the beidellite. These two peaks could be a possible indication of a kaolinite impurity. Figure 2.16 illustrates the XRD patterns of CB, GS-3 and pure kaolinite (Aldrich). The diffraction data are summarized in Table 2.7 and Table 2.8.

IR spectra provide a convenient way to distinguish kaolinite in smectite clays. The FTIR spectra of beidellite and kaolinite are shown in Figure 2.17. Pure kaolinite has a doublet Al-O-H stretch at 3697 cm^{-1} and

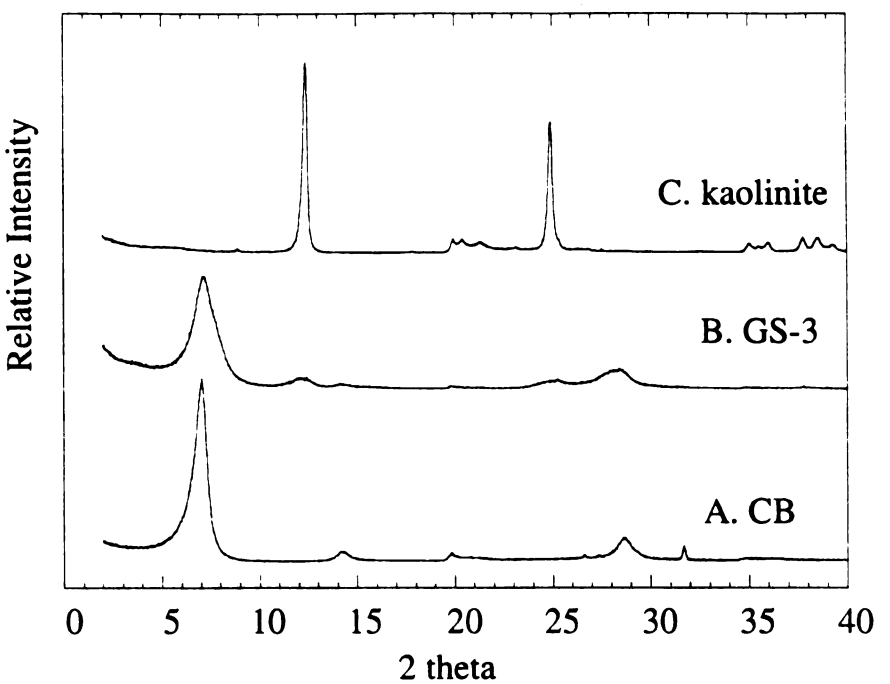

Figure 2.16 XRD patterns of (A) Na^+-CB (Chinese beidellite); (B) Na^+-GS-3 (beidellite); (C) kaolinite.

Table 2.7. X-ray Powder Diffraction Data for GS-3 and CB Na^+-Beidellites

d(obs)[1]	d(GS-3)	d(CB)	I/I_0[1]	hkl[1]
12.44	12.45	12.48	100	001
6.19	6.15	6.21	5	002
4.43	4.44	4.48	75	020, 110
3.12	3.16	3.12	55	004
2.59	2.59	2.57	15	200, 130
2.54				201
	7.2			
	3.5			

[1]index assignments from ref. 14.

Table 2.8. X-ray Powder Diffraction Data for Kaolinite[1]

d	I/I_0 (%)	hkl	d	I/I_0 (%)	hkl
7.17	100	001	3.155	20	112
4.487	35	020	3.107	20	112
4.366	60	110	2.754	20	022
4.186	45	111	2.556	35	130, 201
4.139	35	111	2.553	25	130
3.847	40	021	2.535	35	131
3.745	25	021	2.519	10	112
3.579	80	002	2.495	45	131, 200
3.420	5	111	2.385	25	003
3.376	35	111	2.347	40	202

[1]index assignments from ref. 13.

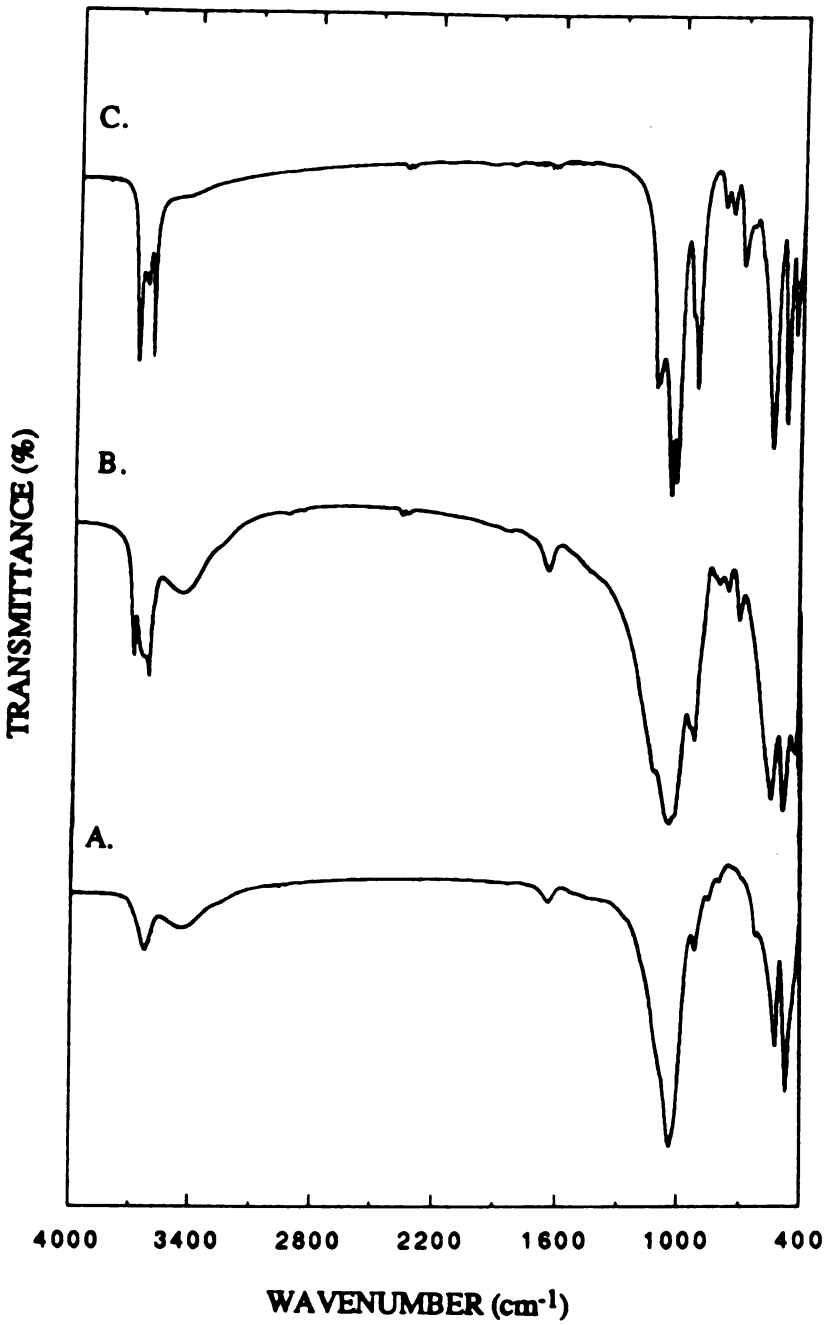

Figure 2.17 IR spectra of (A) Na^+-CB (Chinese beidellite); (B) Na^+-GS-3 (beidellite); (C) kaolinite.

3620 cm^{-1}. For beidellite, on the other hand, only one Al-O-H stretch at 3630 cm^{-1} is observed. Also, the absorption band of Al-O-H bending around 915 cm^{-1} is stronger for kaolinite than for beidellite. In comparison with pure kaolinite, GS-3 showed very similar absorption bands of Al-O-H stretching and bending. Thus, these observations confirm the kaolin impurity in GS-3.

TGA plots of GS-3 depicting dehydration and dehydroxylation processes are presented in Figure 2.18. The weight loss after air-drying was measured. The first weight loss below 100 ^{o}C of about 6% for CB was due to loss of absorbed water. The corresponding weight loss in GS-3 was about 4%. The weight loss for the kaolinite impurity is very small. The second weight loss from 350 ^{o}C to 600 ^{o}C is attributed to dehydroxylation. Since one mole of beidellite contains four OH^- groups, complete dehydroxylation will produce two moles of H_2O which corresponds to a weight loss of 4.9%. The weight loss by CB due to dehydroxylation was in good agreement with this expected value. Beidellite GS-3 lost 7.5% due to dehydroxylation from 350 ^{o}C to 700 ^{o}C. Dehydroxylation of one mole kaolinite ($Al_2Si_2O_5(OH)_4$) would correspond to a 12% weight loss. The higher weight loss in the GS-3 sample during dehydroxylation is an additional evidence for the presence of a kaolinite impurity. The kaolinite in GS-3 can be quantitatively estimated from the weight loss due to dehydroxylation. For pure kaolinite, the weight loss due to dehydroxylation is 14.0% (12.0% in Figure 2.18). For pure beidellite, the dedydroxylation loss is 5.0%. Therefore, the 7.5% weight loss for GS-3 during dehydroxylation corresponds to about a 28% kaolinite content.

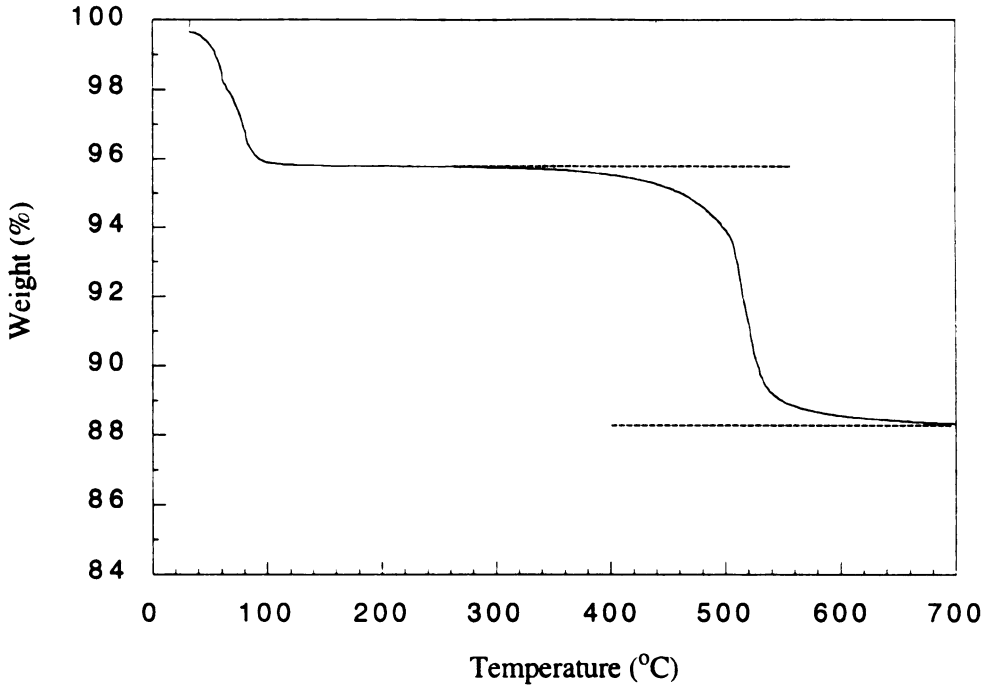

Figure 2.18 Thermogravimetric analysis of natural beidellite Na^+-GS-3 (heating rate = 5 °C/min).

Table 2.9. CEC Values of Natural Na^+-Beidellite as Determined by the Different Methods

	CEC (meq/100g)		
Methods	chemical analysis[1]	^{29}Si MAS NMR	NH_4^+-exchange
GS3	59	98	61
CB	95	95	101

[1]Only Na^+ was considered an exchangeable cation in the CEC calculation. The formula weight used for the unit cell was 737.

Table 2.10. Reaction of 2-methyl-3-butyn-2-ol (MBOH)[1]on NH_4^+-exchanged Smectite Clays

sample	BET surface area	conv.	selectivity (%)			
	(m^2/g)	(%)	C_2H_2	acetone	Mbyne	MIPK
GS-3	33	54.4	0.4	0.3	99.1	0.2
CB	28	35.1	1.1	1.0	97.4	0.5
mont.	41	23.8	3.3	2.7	94.0	0
saponite	37	23.0	1.0	1.0	97.8	0.2
hectorite	17	15.4	3.0	2.9	93.9	0.2
flurohect.	21	17.7	1.3	1.2	97.5	0

[1]Reaction conditions: 0.2 g of catalyst was activated at 300 °C *in situ* for 2 hours. Reaction temperature was 180 °C.

Table 2.9 lists the observed CEC values as determined by chemical analysis, ^{29}Si NMR, and NH_4^+ exchange. The high value estimated for GS-3 by ^{29}Si NMR is due to the contribution of kaolinite resonances at -92 ppm which overlap with the beidellite peaks.

The results for acid catalyzed dehydration of MBOH over NH_4^+-exchanged GS-3, CB and other natural smectite clays were given in Table 2.10 along with the BET surface areas. Among the smectite clays, beidellite was the most active as an acid catalyst, an activity usually believed due to the zeolite-like tetrahedral charge on the layers. However, the higher reactivity of GS-3 over CB can not be explained by the cation exchange capacity value and surface area. There might be more active defects on the edges of GS-3.

D. DISCUSSION

1. Synthesis

The high reactivity of wet gel precursors is a prerequisite for the synthesis of beidellite under mild reaction conditions. Although a high surface area (over 400 m^2/g) plays a role in enhancing the activity of oxides prepared by calcining a wet gel, calcined oxides do not possess sufficient activity to allow beidellite synthesis at low temperature. Even for air- dried gels, the reaction rate is much slower than that for freshly prepared wet gels. The reactivity of a beidellite precursor increases in the order of oxides < gel dried at 150 ^oC < air-dried gel < hydrated gel. From the CP MAS NMR studies, more Q^2 sites, e. g. siloxane chains, are present in the air-dried gel

than in the gel heated at 150 °C. Thus the reactivity of the precursor for beidellite synthesis Q^2 groups is related to the higher reactivity. It is likely that these less cross-linked Q^2 aluminosilicates readily form a 2:1 layered skeleton, whereas the Q^3 and Q^4 sites in a heated gel, which are a more cross-linked network, are more difficult to rearrange into the 2:1 layered skeleton. It might require the breaking of some Q^4 or Q^3 sites, a phenomenon which occurrs mostly at higher temperature before layer formation.

The silica gels have been investigated extensively because of their significant importance as ceramic and glass materials. The product distribution and kinetics for the TEOS hydrolysis reaction have been studied under acidic and basic conditions.[21-23] The process of silica gel formation is slower and more complicated than that for alumina gel formation. When silicon and aluminum alkoxides are hydrolyzed together, a rapid formation of small dense particles takes place by condensation between Al-OH groups. These particles are then agglomerated by a cluster aggregation process chemically limited by the hydrolysis of Si-OR groups.[24-25] It is easy to control the hydrolysis of aluminum alkoxides to form a gel which is suitable for hydrothermal reaction at low temperature. But for silicon the activity is affected greatly by the rate of hydrolysis polycondensation. Silica sol is the most active source of silicon for beidellite synthesis, since its hydrolysis is complete and as a result its condensation process is rapid. The active gel formed from a silica sol can form well-crystallized beidellite in three days. If TEOS is used as a precursor, it was necessary to pre-hydrolyze the TEOS in ethanol-water before mixing with aluminum tri-*sec* -butoxide. We found that the media (e.g. existence of EtOH) and base content for the hydrolysis are the two important factors that control the rate of hydrolysis. Since OH^- is a

good nucleophilic catalysts, deprotonation of silanol groups is facilitated and condensation rates are enhanced by its presence.

2. Comparison of Synthetic Beidellite with Natural Beidellite

The structural characteristic of beidellite synthesized at low temperature are consistent with the features of natural beidellite, including morphology, tetrahedral charge location, and acidity. Thus, the synthesis of beidellite at low temperature was successful. Nevertheless, differences were revealed in the surface areas and catalytic reactivities which are most likely related to the differences in crystallinity of the synthetic beidellites. For example, the BET surface area for the synthetic beidellite is 129 m^2/g, whereas for natural beidellite, it is around 30 m^2/g. The higher corresponding conversion of the MBOH reaction for synthetic beidellites could be explained by the fact that the reaction takes place mainly on the external surface.

In addition, an impurity usually accompanies with the natural beidellite; for example, GS-3 has about 28% kaolinite. CB contains quartz. The presence of such impurities complicated determination of chemical properties, such as the acid catalytic reactivity of GS-3 for the MBOH reaction, and led to the disagreement of CEC value measured by different methods. Synthetic beidellite on the other hand is free of these impurity problems.

REFERENCE

1. Schutz, A.; Plee, D.; Borg, F.; Jacobs, P.; Porcelet, G.; and Fripiat, J. J. Proc. Int. Conf., The clay society; Bloomington, Indiana, 1987; pp305-310.
2. Poncelet, G.; Schutz, A. In *"Chemical reactions in organic and inorganic constrained systems"*, Setton, R. Ed.; New York, 1986; pp165-178.
3. Occelli, M. L.; Stencel, J. M.; Suib, S. L. *J. Mol. Catal.* **1991,** *64,* 221-236.
4. Tzou, M. S. Ph.D. thesis, Michigan State University, 1983.
5. Wash, J. N. *Spectrochim,* **1980**, *35B*, 107.
6. Busenberg, E.; Clemency, C. V. *Clay and Clay Miner.* **1973**, *21*, 213.
7. Grillet, Y.; Rouquerol, F.; Gaualas, G. R. *Langmuir*, **1977**, *74*, 179.
8. Northrop, P. S.; Flagan, R. C.; Gavalas, G. R. *Langmuir*, **1987**, *3*, 300.
9. Michot, L. J.; Francois, M.; Case, J. M. *Langmuir*, **1990**, *6*, 677.
10. Lauron-Pernot, H.; Luck, F.; Popa, J. M. *Applied Catal.* **1991**, *78*, 213.
11. Bogush, G. H.; Zukoki, C. F. J. *Colloid. and Interface Sci.* **1991**, *142 (1)*, 1.
12. Wijner, P. W. *Collo. & Interface Sci.* **1991**, *145(1)*, 17.
13. MacEwan, D.M. D.; Wilson, M. J. In "*Crystal Structures of Clay Minerals and Their x-ray Diffraction*", Brindley, G. W.; Brown, B. Eds.; London, 1980, Chapter 3.
14. Lloprogge, J. T.; Jansen, J. B. H.; Geus, J. W. *Clays and Clay Miner.* **1990**, *38(4)*, 409.

15. Brown, G. Ed. The X-ray Indentification and Crystal Structures of Clay Minerals: Mineralogical Society, London, pp544.

16. Weir, A. H.; Greene-Kelly, R. *Amer. Mineral*, **1962**, *47*, 137.

17. Plee, D.; Gatineau, L.; Fripiat, J. J. *Clays and Clay Miner.* **1987**, *35(2)*, 81.

18. Stubican, V.; Roy, R. Z. *Kristallogr.* **1961**, *115*, 200.

19. Farmer, V. C. in "The Infrared Spectra of Minerals", London, pp 331.

20. Parry, E. P. *J. Catal.*, **1963**, *2*, 371.

21. Maniar, P.; Navrotsk, A.; Rabinovich, E. M.; Wood, D. L. In " Chemistry, Spectroscopy and Application of Sol-Gel Glasses", Reisfeld R. and Jorgerser, C. K. Ed.; Structure and Bonding 77, Verlag Heideberg, 1992, pp 323.

22. Bogush, G. H.; Dickstein, G. L.; Lee, P.; Zukaski, C. F. In " Chemistry, Spectroscopy and Application of Sol-Gel Glasses", Reisfeld R. and Jorgerser, C. K. Ed.; Structure and Bonding 77, Verlag Heideberg, 1992, pp 57.

23. Kilmperer, W. G.; Mainz, V. V.; Ramamurthi, S.D.; Rosenberg, F. S. In " Chemistry, Spectroscopy and Application of Sol-Gel Glasses", Reisfeld R. and Jorgerser, C. K. Ed.; Structure and Bonding 77, Verlag Heideberg, 1992, pp 15.

24. Pouxuiel, J. C.; Boilot, J. P.; Smaihi, M.; Dauger, A. *J. Non-Cryst. Solids*, **1988**, *106*, 147.

25. Loqet, T. *J. Non-Cryst. Solids*, **1989**, *108*, 45.

CHAPTER THREE

PREPARATION OF ALUMINA PILLARED MONTMORILLONITE WITH HIGH THERMAL STABILITY, REGULAR MICROPOROSITY AND LEWIS/BRÖNSTED ACIDITY

A. OBJECTIVE OF RESEARCH

As we noted in Chapter 1, the thermal stability of pillared clays depends on the method of synthesis as well as the nature of the host clay. The distribution of oligomeric cations in the initial pillaring agent solution, the pillaring reaction conditions, and the processing of the reaction products, all play a role in determining the thermal stability and corresponding properties, such as surface areas, acidities and catalytic activities. Simple variations in the synthesis procedure, such as the method of washing, can affect the hydrolytic chemistry of the pillaring agent and consequently the fundamental properties of the final products.

In order to improve the thermal stability of pillared smectites, in this work we report a synthesis procedure for the preparation of alumina pillared montmorillonites. Our procedure reliably affords products with exceptional performance properties, in particular, high BET surface areas, microporosity, and Brönsted/Lewis acidity, when calcined at elevated temperatures. These latter properties are especially important in determining the catalytic utility of alumina pillared clays. Our approach utilizes a common pillaring agent (base-hydrolyzed $AlCl_3$) and typical montmorillonite compositions. However, we have optimized certain synthesis and processing conditions that afford pillared products superior

in structural thermal stability to those reported previously. Also, our discussion focuses on the hydrolytic chemistry of the alumina pillar which is the crucial factor that determines the thermal stability in the synthesis process.

B. EXPERIMENTAL

1. Starting materials

A natural sodium-type montmorillonite was obtained from Zhejiang province, China, and a natural Wyoming montmorillonite, SWy-1, was obtained from the Source Clay Minerals Repository at the University of Missouri, Columbia, MO. The starting clays were designated ZM and WM, respectively. Both clay samples were fractionated by conventional sedimentation techniques, and the < 2 μm fractions (about 80%) were collected. The concentration of the ZM and WM clay slurries were 18.2 and 10.0 g/L and the pH values for the slurries were 9.1 and 8.4, respectively. The < 2 μm fraction of the ZM sample contained small amounts of quartz and kaolinite, whereas WM sample contained small amounts of quartz. The measured CEC values for ZM and WM were 78, and 80 meq/100g, respectively, as determined by the ammonium exchange method.[1]

H^+-Exchanged Montmorillonites: A 4.0 wt% slurry of Na^+-montmorillonite made 0.25 M in H_2SO_4 was aged for 2 h. The slurry was then centrifuged and washed with deionized water until the pH of the

suspension was in the range 3.8 - 4.5. This slurry was used to prepare alumina pillared derivatives by the procedure described above.

2. Pillaring Solution

The pillaring solution used in this study was prepared as follows. To 600 mL of 0.20 M $AlCl_3$ (120 mmol) in a three liter 3-neck flask was added dropwise with vigorous stirring 1440 mL of 0.20 M NaOH (288 mmol). The addition required approximately 6 h. During this time the temperature of the reaction mixture was increased from room temperature to 80 °C. The solution was allowed to age overnight (12-16 h) while being stirred and cooled to room temperature. Then the pH was adjusted to a value of 3.6 - 4.0 by dropwise addition of a small amount of 0.2 M NaOH. The solution was placed in a screw-cap glass bottle, where it could be stored at room temperature for a period of at least one year without noticeable effect on the properties of the final alumina pillared clay.

3. Pillaring Reaction

A 10-g quantity of Na^+- or H^+- exchanged montmorillonite in 0.5-3.0 wt% aqueous suspension at ambient temperature was added at an approximate rate of 150 mL/min to the vortex of a vigorously stirred pillaring solution at 70 °C. The Al^{3+}/clay ratio was maintained in the range of 1.8 - 2.5 mmol/g. The stirred mixture was allowed to age at 70 °C for an additional 2 h and then cooled under running tap water to room temperature. The suspension was immediately centrifuged at 10,000 rpm for 12 min, and the clay was washed four times by re-suspending it in an

equivalent volume of deionized water and centrifuging. The entire washing procedure was completed within 3 h. The chloride-free suspension was poured onto a plate glass sheet and allowed to dry overnight at room temperature. The air-dried products were then calcined in a programmable oven. Some of the pillared products were freeze-dried and dried in an oven at 150 °C before calcining. The heating rate and cooling rates were 10 °C/min. For samples calcined above 400 °C, the material was first heated to 400 °C at a rate of 10 °C/min, held at 400 °C for 1 h, ramped to a new temperature at a rate of 5 °C/min, held at the desired temperature for 4 h, and then cooled by using the reverse process.

4. Characterization Methods

a) Chemical Analysis

Samples for elemental analysis by ICP emission spectroscopy were prepared by using the lithium metaborate ($LiBO_2$) technique.[2] A 50 - mg quantity of sample was mixed with 300 mg of lithium metaborate and heated 10 minutes at 1000 °C. The fused product was then dissolved in 50 mL of 5% of HNO_3.

b) Physical Measurements

X-ray diffraction patterns were obtained for oriented powder samples using a Rigaku diffractometer equipped with rotating anode and Ni-filtered Cu-K_α radiation.

Adsorption / desorption experiments with N_2 as the sorbate were carried out at -196 °C on a Coulter Ominosorb 360 CX sorptometer. The samples were outgassed overnight at 150 °C under dynamic vacuum (10^{-5} torr). Nitrogen isotherms were obtained by the quasi-equilibrium volumetric method.[3-5] Surface areas were obtained from the BET equation. The t-plot method[6] was used to determine the total micropore volume, as well as the non-microporous surface area. The desorption branch was treated according to a parallel plate mesopore model developed for phyllosilicates.[7] The micropore size distribution was determined by using the model developed by Horvath and Kawazoe.[8]

The FTIR spectrum for chemisorbed pyridine was obtained on an IBM IR44 spectrometer. A self-supported sample wafer was outgassed at 300 °C under flowing helium prior to pyridine adsorption at 25 °C. Weakly adsorbed pyridine was removed by outgassing the sample at 150 °C.

^{27}Al NMR spectra of pillaring solutions were obtained on a Varian 300 spectrometer operated at 104 MHz. Spectra were obtained using tubes containing a coaxial external reference solution of sodium aluminate. A Varian 400 VXR solid state NMR spectrometer was used to obtain ^{29}Si and ^{27}Al MAS NMR spectra at 79.5 MHz and 104.3 MHz, respectively. The spinning frequencies were 4-5 KHz. ^{29}Si chemical shifts were reported relative to TMS. The ^{27}Al chemical shifts were relative to $AlCl_3 \cdot 6H_2O$.

C. RESULTS

1. Characterization

Two sodium montmorillonites from different locations, but with similar unit cell formulas, were selected for pillaring with aluminum polycations. One specimen was from Upton Wyoming (abbreviated, WM), and the other was from Zhejiang China (abbreviated, ZM). Chemical analysis of the pristine minerals indicated the anhydrous unit cell composition of WM to be:

$$M^{n+}_{0.72/n}[Al_{2.98}Fe_{0.30}Mg_{0.72}](Si_{8.00})O_{20}(OH)_4$$

where M^{+n} = Na^+, K^+, and Ca^{2+}. The corresponding formula for ZM was:

$$M^{n+}_{0.66}[Al_{2.97}Fe_{0.37}Mg_{0.66}](Si_{8.00})O_{20}(OH)_4$$

Pristine Na^+-exchanged forms of WM and ZM were allowed to react at 70 °C within an aluminum polycation solution formed by basic hydrolysis (OH^-/Al^{3+} = 2.4) and aging (70 °C, 12 - 16 h). The freshly formed reaction products were then efficiently washed free of Cl^-, dried in air at room temperature, and calcined at the desired temperature to afford the final alumina pillared derivatives. The alumina pillared form of WM (abbreviated AlWM) contained 1.58 pillaring Al ions per $O_{20}(OH)_4$ unit cell, whereas the ZM derivative (abbreviated AlZM) contained 1.84 pillaring Al ions per unit cell.

The exceptional thermal stabilities of our pillared reaction products are illustrated by the X-ray powder diffraction patterns in Figure 3.1A for AlZM products calcined at selected temperatures in the range 350 - 900 °C. As the calcination temperature is increased, the 001 reflection shifts from

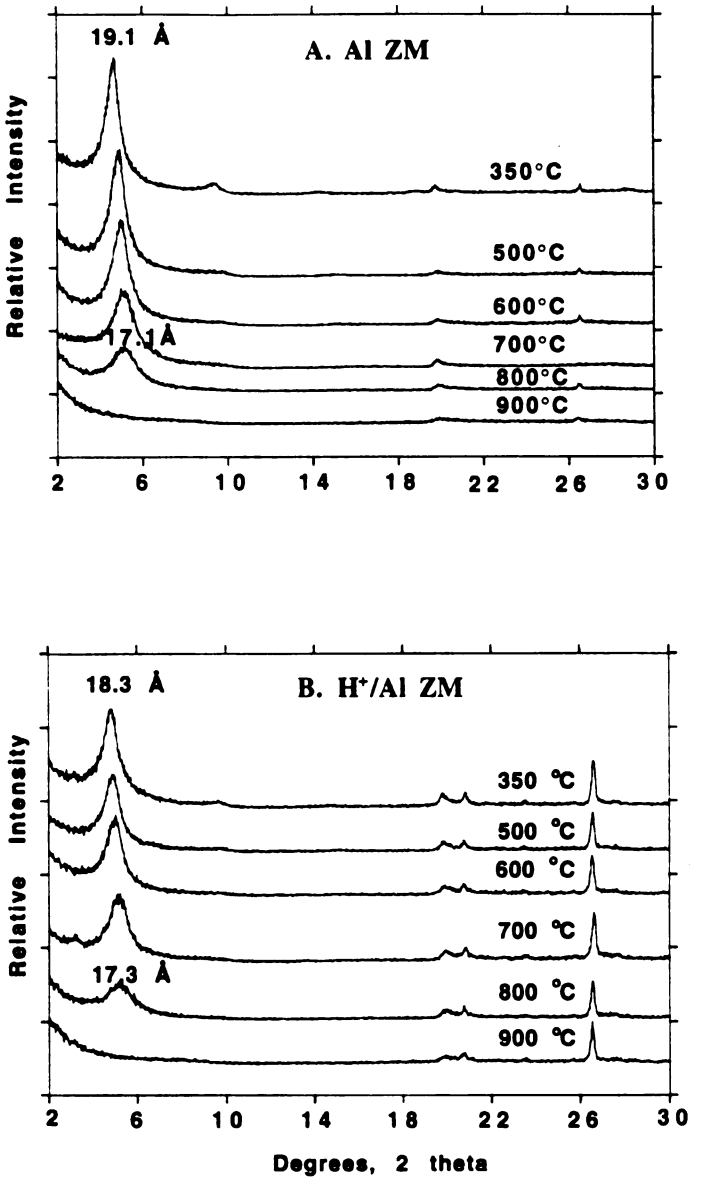

Figure 3.1. X-ray powder diffraction patterns (Cu-K_α) for calcined forms of alumina pillared Zhejiang montmorillonites: (A) AlZM, prepared from the pristine mineral (Na^+ form); (B) H^+/AlZM, prepared from the H^+-exchanged precursor.

19.1 Å at 350 °C to 17.1 Å at 800 °C. At the same time the width of the line increases, indicating that as the temperature increases, a reduction in the c-axis layer stacking order occurs in addition to a lowering of the average basal spacing. At a calcination temperature of 900 °C the clay decomposes and crystallinity is lost.

The diffraction patterns for the H^+/AlZM analogs prepared from the H^+-exchanged form of ZM (*cf.*, Figure 3.1B) also show a basal spacing of 18.3 - 17.1 Å over the 350 - 800 °C temperature range. However, as will be shown later based on surface area studies, the H^+/AlZM series of products are inferior to AlZM materials, especially when calcined above 500 °C. That is, basal spacings alone are not an adequate indication of overall thermal stability. X-ray powder diffraction patterns very similar to those represented in Figure 3.2 also are observed for AlWM and H^+/AlWM calcined at 800 °C.

Table 3.1 provides the basal spacings and N_2 BET surface areas for alumina pillared AlWM and AlZM samples prepared from the corresponding Na^+-exchanged montmorillonites and calcined at three different temperatures. Included in the table for comparison purposes are analogous data for alumina pillared products formed from the intrinsically more acidic H^+-exchanged forms of WM and ZM. These latter pillared derivatives are abbreviated H^+/AlWM and H^+/AlZM, respectively. The basal spacings of the pillared products air-dried at 25 °C, which correspond to gallery heights in the range 8.8 - 9.8 Å, are in agreement with most previously reported alumina pillared montmorillonites prepared by pre-intercalation of aluminum polycations. However, the basal spacings and N_2 BET surface area obtained for the products calcined at 500 °C and 800 °C, especially those prepared from the Na^+ forms of the pristine

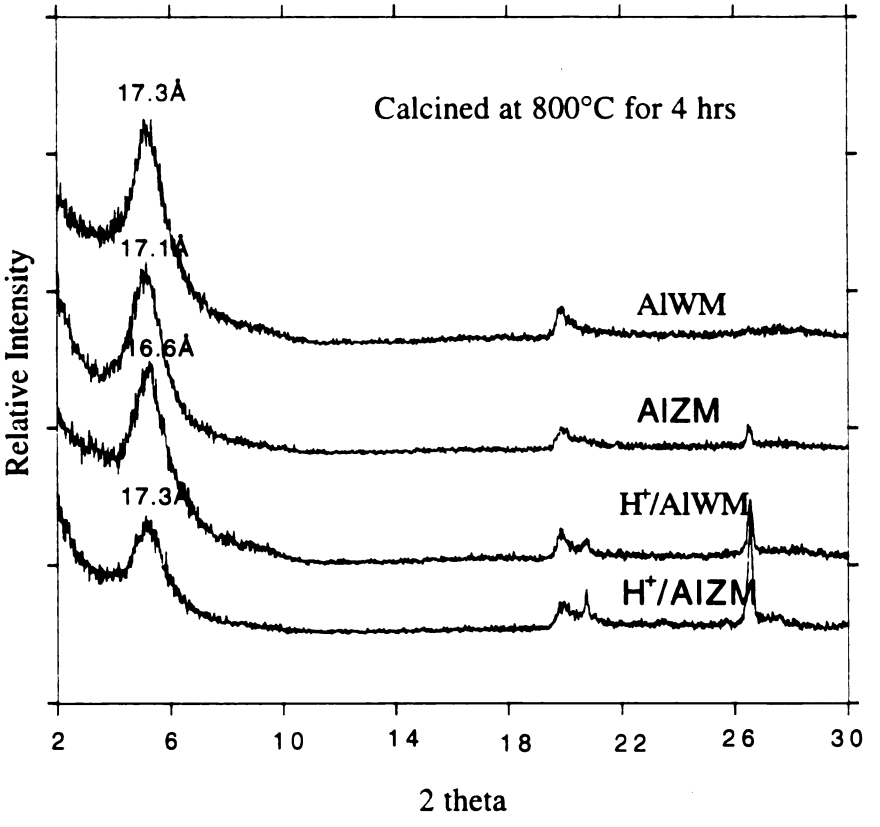

Figure 3.2. X-ray powder diffraction patterns for 800 °C calcined forms of alumina pillared Zhejiang montmorillonites (AlZM, H^+/AlZM) and alumina pillared Wyoming montmorillonites (AlWM, H^+/AlWM).

minerals, are exceptionally high relative to the values reported in previous work.

Table 3.1. Basal Spacings and N_2 BET Surface Areas for Alumina Pillared Montmorillonites Calcined at Different Temperatures

		Basal Spacing, Å			BET Surface Areas[1], m^2/g		
Sample	Exchange Ion	25 °C	500 °C	800 °C	150 °C	500 °C	800 °C
AlWM	Na^+	19.7	17.7	17.3	458	230	219
AlZM	Na^+	20.0	18.1	17.1	393	221	212
H^+/AlWM	H^+	19.2	17.5	16.6	—	203	153
H^+/AlZM	H^+	19.6	18.1	17.1	381	187	121

[1]Outgassing conditions: 150 °C, 12 h in vacuum.

In order to verify the presence of a microporous structure for the high temperature forms of pillared montmorillonite, we determined the microporous surface areas from t-plots of the N_2 adsorption data. Values of S_{micro}, along with the total surface areas S_T, are presented in Table 3.2. For both AlZM and H^+/AlZM, the total surface area after calcination at 150 °C was ~440 m^2/g, with ~310 m^2/g (~70%) falling in the microporous (< 20 Å) range. The high temperature forms of AlZM calcined at 500 °C and 800 °C exhibit total surface areas of 260 and 238 m^2/g, respectively,

with 78-62% of the total area occurring in the micropore size domain. H^+/AlZM materials are thermally less stable than the AlZM analogs, as judged from substantially lower values of S_T (130 m^2/g) and S_{micro} (61 m^2/g) for the sample calcined at 800 °C. Completely analogous microporous behavior was observed for the high temperature calcined forms of AlWM and H^+/AlWM.

Table 3.2. Total Surface Areas (S_T) and Microporous Surface Areas (S_{micro}) for Alumina Pillared Montmorillonites as Determined by the t-Plot Method[1]

Sample	Calcination Temperature, °C	S_T, m^2/g	S_{micro}, m^2/g
AlZM	150	444	319
	500	269	201
	800	238	148
AlWM	500	253	201
	800	247	175
H^+/AlZM	150	440	297
	500	215	166
	800	130	61
H^+/AlWM	500	247	188
	800	173	87

[1]Determined from t-plots of the N_2 adsorption data; outgassing conditions: 12 h in vacuum at 150 °C; calcination time at 500 °C and 800 °C was 4h.

Micropore size distributions for alumina pillared montmorillonites AlZM and AlWM were determined from the N_2 adsorption data using the parallel plate model of Horvath - Kawazoe.[8] Figure 3.3, parts A and B, provides the pore distributions obtained for these two derivatives after calcination at three different temperatures. Both samples after calcination at 150 °C exhibit bimodal pore distributions in the range 5-11 Å Calcination at 500 °C and 800 °C causes the pore distribution to become more uniform. A qualitatively similar narrowing of the pore distribution with increasing calcination temperature was observed for the H^+/AlZM and H^+/AlWM, series, as shown by the plots in Figure 3.3, parts C and D, respectively.

Infrared spectroscopy revealed the chemisorption of pyridine at both the Lewis and the Brönsted acid sites of each alumina pillared montmorillonite reaction product, regardless of calcination temperature over the range 400 - 800 °C. As shown in Figure 3.4 for the chemisorption of pyridine on calcined samples of AlZM, the ring stretching frequencies[9] characteristic of Lewis pyridine (1454 cm^{-1}) and Brönsted pyridine (1545 cm^{-1}) are observed even after calcination at 800 °C for 20 h. Lewis pyridine sites predominate over Brönsted sites at all calcination temperatures over the range 300 - 800 °C. The predominance of Lewis over Brönsted sites is a normal characteristic of alumina pillared clays, regardless of the synthesis method. Note, however, the general decrease in the total number of acid sites, especially Lewis sites, with increasing calcination temperature. Table 3.3 summarizes the relative intensities of the Lewis and Brönsted type pyridine sites as a function of calcination temperature.

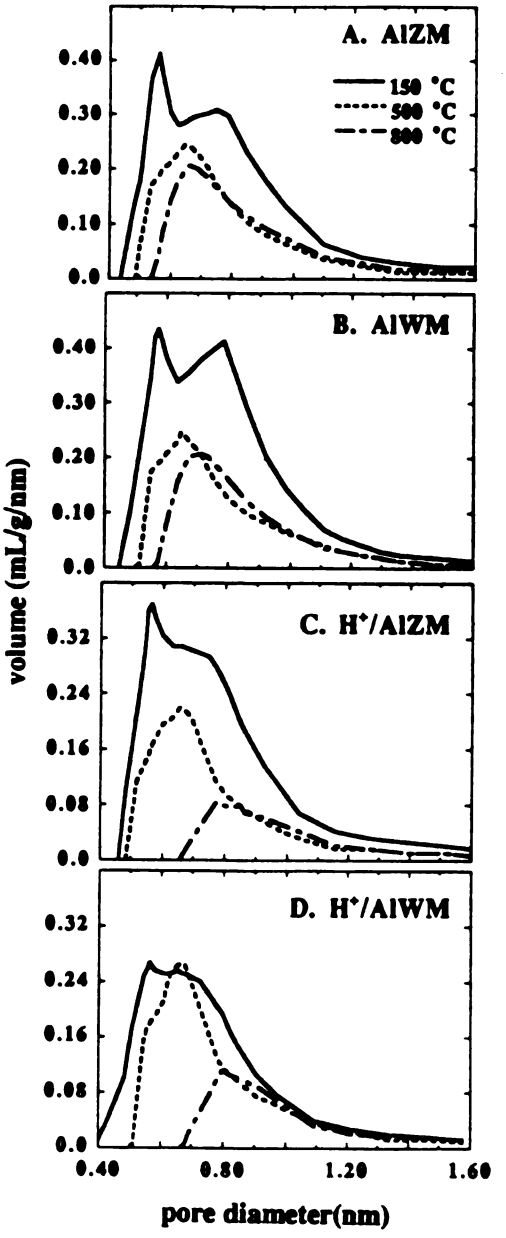

Figure 3.3 Horvath-Kawazoe pore distributions for calcined forms of alumina pillared Wyoming and Zhejiang montmorillonites.

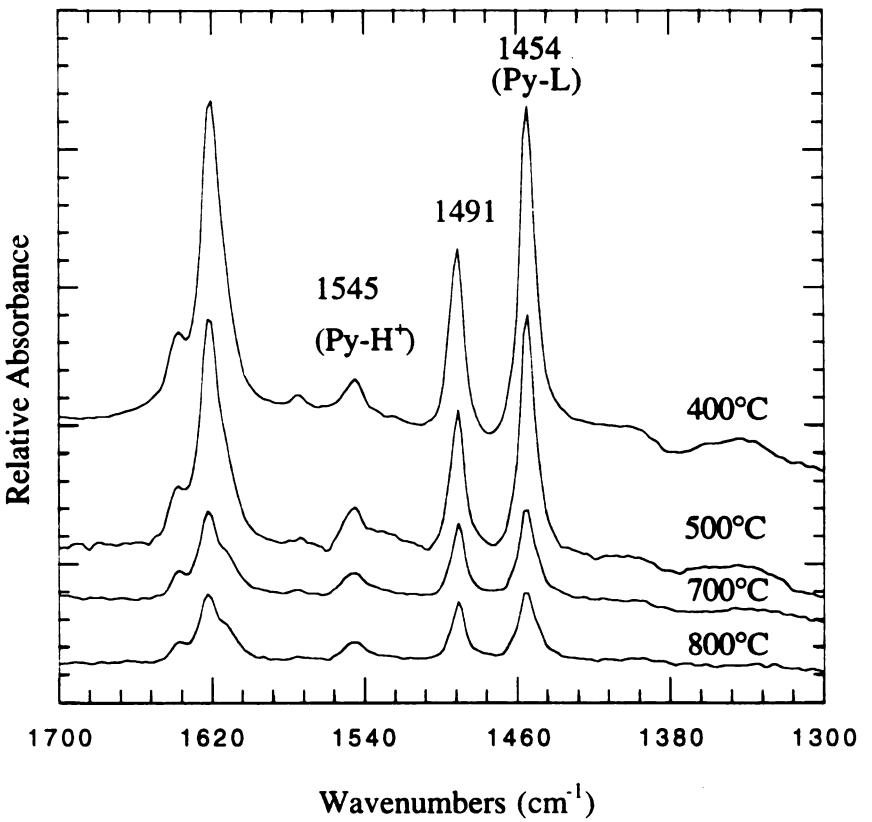

Figure 3.4. FTIR spectra of pyridine chemisorbed at 150 °C on calcined samples of AlZM.

Table 3.3. The Ratio of Lewis to Brönsted Pyridine Chemisorbed to Calcined Forms of Alumina Pillared Clays

Calcination Temperature[1], °C	AlZM	AlWM	H^+/AlZM	H^+/AlWM
300	4.42	4.21	3.83	3.42
400	4.61	4.87	4.47	3.58
500	5.42	6.16	4.79	3.78
700	3.73	5.35	3.38	2.55
800	3.21	4.15	3.08	2.38

[1]Sample were allowed to rehydrate in air following calcination and then outgassed at 300 °C for 1.5 h prior to pyridine adsorption. Weakly adsorbed pyridine was removed by outgassing under vacuum at 150 °C prior to recording the spectra at room temperature.

2. Hydrolysis Chemistry of Pillaring Species

The pillaring solution used in our synthesis contains primarily Al_{13} oligomers, as judged by ^{27}Al NMR spectroscopy. The spectra in Figure 3.5 show that the pillaring solution formed at $OH^-/Al = 2.4$ (pH = 3.6) exhibits only one line at 63 ppm characteristic of the tetrahedral site in $[Al_{13}O_4(OH)_{24+x}(H_2O)_{12-x}]^{7+x}$ cations.[10-14] Approximately 80% of the total aluminum under these conditions is in the form of Al_{13} oligomers. The remaining aluminum is NMR silent, presumably due to the formation of higher oligomers of lower symmetry. Increasing the pH of the pillaring solution over the range 3.6 - 6.0 causes the fraction of NMR silent

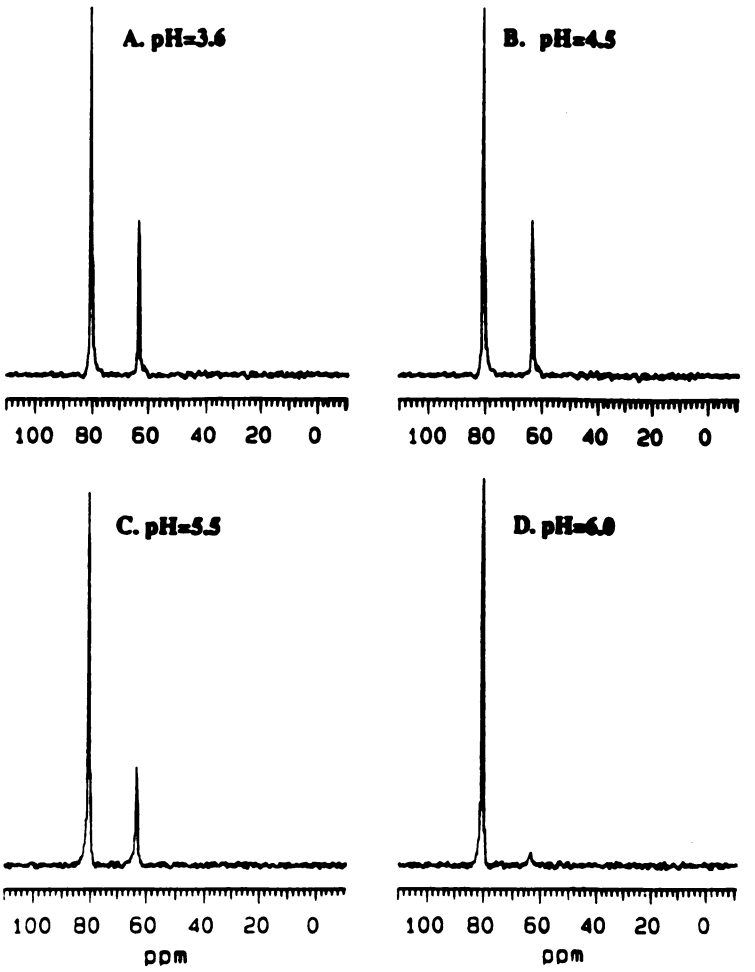

Figure 3.5. ^{27}Al NMR spectra of base - hydrolyzed $AlCl_3$ solutions. The solutions were prepared at 80 °C by the addition of 0.2M NaOH to 0.2M $AlCl_3$ until OH^-/Al^{3+} = 2.4, ageing at 80 °C for 16 h, and then titrating with NaOH to pH values of (A) 3.6, (B) 4.5, (C) 5.5, (D) 6.0. Each solution was then allowed to age an additional 20 hr at 25 °C before NMR measurement. The line at 80 ppm is the resonance of an external reference solution of sodium aluminate.

oligomers to increase at the expense of the Al_{13} cations. At pH = 6.0, where turbidity is observed due to the formation of $Al(OH)_3$, only 10% of the total aluminum is in the form of Al_{13} oligomer. Thus, it is preferable to retain the pH of the pillaring solution between values of 3.6 and 4.5.

The pH dependence of Al_{13} hydrolysis as shown in Figure 3.5 also implies that it is important to minimize the undesirable hydrolysis, e. g. when pH is higher than 5.0, the Al_{13} fraction decreases remarkably in the whole synthesis process. We have observed that if the washed, chloride-free clay is allowed to age in aqueous suspension for more than a few hours before initiating the air - drying procedure, the final product even after calcining tends to exhibit inferior thermal stability and generally lower surface areas. Also, a dramatic reduction in thermal stability occurs in the case of AlWM if the Al_{13}-Na^+ montmorillonite reaction product is allowed to age overnight before being washed free of Cl^-. As the data given in Table 3.4 indicate, the total surface area (S_T) and microporous surface area (S_{micro}) values after calcination at 800 °C dropped from S_T = 247 m^2/g and S_{micro} = 175 m^2/g for AlWM to S_T = 62 m^2/g and S_{micro} = 0 m^2/g for the equivalent analog prepared by the same procedures, except that the reaction mixture was allowed to age one day at room temperature before being washed to remove co-adsorbed Cl^- ions. Surface area values after calcination at 400 °C were S_T = 355 m^2/g and S_{micro} = 270 m^2/g for AlWM. The corresponding analog subjected to prolonged aging gave S_T = 309 m^2/g and S_{micro} = 240 m^2/g. Thus, the effect of prolonged aging of the initial reaction product in the presence of Cl^- is manifested most strongly at higher calcination temperatures.

Table 3.4. Total Surface Areas (S_T) and Microporous Surface Areas (S_{micro}) for AlWM and AlWM-1 Calcined at 400 °C and 800 °C

sample	S_T, m^2/g		S_{micro}, m^2/g	
	400 °C	800 °C	400 °C	800 °C
AlWM	355	247	270	175
AlWM-1[1]	309	62	240	0

[1]AlWM-1 was prepared by aging overnight, then washing over 5 h. Other pillaring procedures were the same as those for AlWM.

Compared with the hydrolysis of the pillaring species, other processing factors are less crucial for thermal stability, for example, methods of drying the product. Pillared ZM was divided into three portions for drying and then calcined at 800 °C for 4 h at the same time. Figure 3.6 shows XRD patterns of AlZM samples which have been air-dried, freeze-dried or oven dried at 150 °C. All three yield pillared products with spacing of about 16.6 Å after 800 °C calcination. Furthermore, the BET surface area data listed in Table 3.5 for different drying methods are very close. The AlZM using different drying methods which determine the textual structure of particles, but are not related to hydrolysis of pillars, exhibit similar thermal stability.

Table 3.5. N_2 BET Surface Area for AlZM Calcined at 800 °C Drying by Different Methods

Sample	Air-dried	Freeze-dried	Heated at 150 °C
BET Surface Area[1], m^2/g	171	178	189

[1]outgassing conditions: 150 °C, 12 h in vacuum.

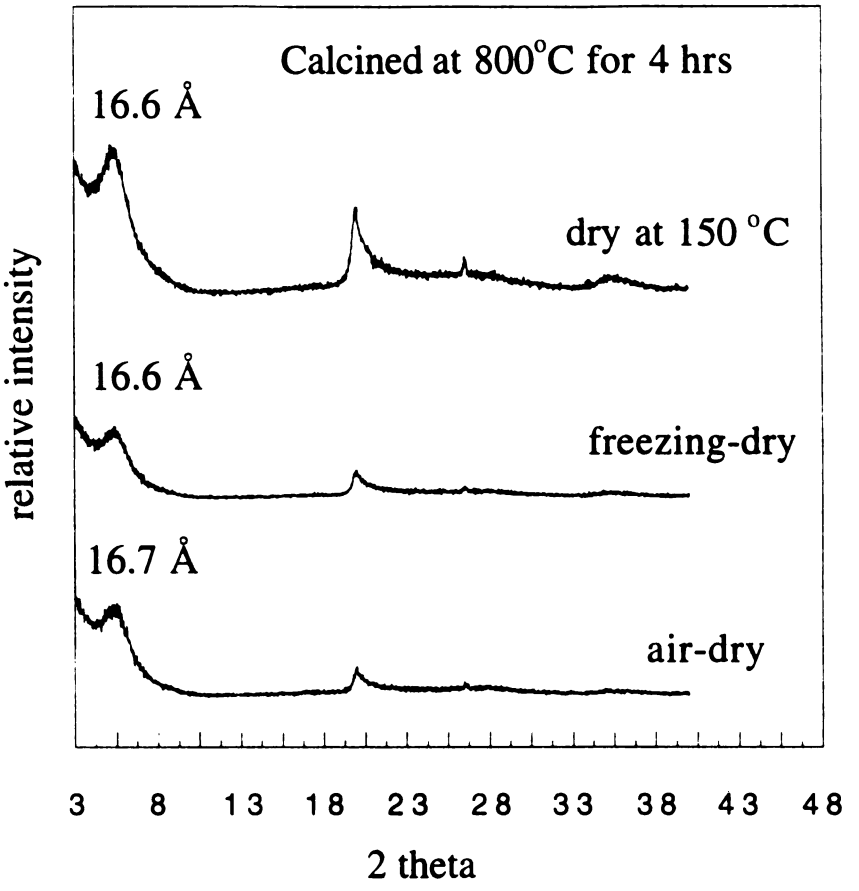

Figure 3.6. X-ray powder diffraction patterns for 800 °C calcined forms of Zhejiang montmorillonites (AlZM) using air-dry, freezing-dry, and oven dry at 150 °C.

D. DISCUSSION

Alumina pillared clay products AlZM and AlWM, as prepared by the reaction of Al_{13} oligocations with the Na^+-exchanged forms of Zhejiang and Wyoming montmorillonites, are among the most thermally stable metal oxide pillared smectite clays reported to date. Table 3.6 compares the surface areas and basal spacings of AlWM products at selected calcination temperatures with those for previously reported alumina pillared forms of Wyoming montmorillonites.[15-18] All of the previously reported derivatives are structurally decomposed at calcination temperatures near 800 °C, whereas AlWM retains an average basal spacing of 17.3 Å (gallery height ≈ 7.7 Å) at this temperature. In addition, the surface area of AlWM after 800 °C calcination (240 m^2/g) is almost twice as large as the best previously reported pillared montmorillonite under comparable processing conditions. Moreover, approximately 60% of the total surface area of AlWM at 800 °C arises from intracrystal micropores. Analogous basal spacings and surface areas were observed for high temperature (800 °C) calcined forms of AlZM. Complete loss of XRD crystallinity did not occur until 900 °C.

We note that both the Lewis acidity and the Brönsted acidity of our alumina pillared clay products are retained at all calcination temperatures. The ratio of pyridine chemisorbed at Lewis and Brönsted sites falls in the range 3.2 - 6.2 for all AlWM and AlZM derivatives formed by calcination at temperatures up to 800 °C (cf., Table 3.3). For H^+/AlWM and H^+/AlZM the analogous acidity ratio is maintained in the range 2.4 to 4.8.

Table 3.6. Range of the Surface Areas and Basal Spacings Reported for Calcined Samples of Alumina Pillared Wyoming Montmorillonites

Pillaring Agent[1] (OH^-/Al^{3+})	Calcination Conds. Temp., °C	Time h	S_T, m^2/g	d_{001}, Å	Reference
2.4	800	4	240	17.3	this work
2.0	800	5	~130	collapsed	26
--[2]	600	--	--	15.4	27
2.5	760	4	55	collapsed	28
2.5	800	3	91	collapsed	29

[1]Pillaring agent prepared by basic hydrolysis of aluminum trichloride at the OH^-/Al^{3+} mole ratios indicated.

[2]Aluminum chlorohydrate was the pillaring reagent.

The retention of Lewis acidity with increasing temperatures is not surprising since the Lewis sites arise from coordinatively unsaturated aluminum centers on the pillars. However, there is a tendency toward reduced Lewis acidity with increasing calcination temperature, which undoubtedly reflects the restructuring of the pillars. Although the origin of the Brönsted acidity in pillared clays is less certain, the protons most likely are associated with the structural hydroxyl groups of the layers.[19] It is important to note that the samples in these acidity studies were allowed to rehydrate by exposure to the atmosphere prior to pyridine chemisorption. Thus, the hydroxyl structural group and associated Brönsted acidity of the layers was largely restored even after calcination at 800 °C. Consequently, the pillared clay products, particularly the AlWM and AlZM series of materials, are remarkably resilient, chemically as well as structurally.

These two general characteristics are well suited to catalytic and sorptive applications at elevated temperatures.

Several synthesis variables are potentially important in determining the physicochemical properties of alumina pillared clay products. These include:

(i) the distribution of aluminum oligomers in the hydrolyzing aluminum pillaring solution, as determined by the OH^-/Al^{3+} ratio, hydrolysis temperature, and aging time.

(ii) the nature of the initial gallery exchange cation

(iii) the magnitude and origin of the clay layer charge

(iv) the reaction conditions and product work-up procedures, such as the rates of reagent addition, reaction temperature, washing and drying methods, and calcination temperature.

All of the above factors can influence the composition and structure of the pillaring species. However, it is difficult to accurately assess from available literature reports the relative importance of each synthesis variable, particularly with regard to the formation of thermally stable derivatives. For instance, one might expect the distribution of aluminum oligocations in the pillaring solution to be important in determining the thermal stability of pillared montmorillonites with basal spacing near 19 Å. In the present work, AlWM and AlZM were prepared from base-hydrolyzed $AlCl_3$ pillaring solutions in which ≈ 80% of the total aluminum ions are present as Al_{13} oligocations (*cf.* Figure 3.1). However, we also were able to prepare pillared montmorillonites of comparable thermal stability using commercially available aluminum chlorohydrate solutions containing a much smaller fractions of Al_{13} oligomers. These latter solutions, which are formed by the reaction of aluminum metal with

aqueous $AlCl_3$, contain oligomers larger than Al_{13}.[14] It is possible that the clay selectively adsorbs Al_{13} oligomers over higher oligomers. Recent work by several groups[20-22] has confirmed the original observation of Plee et al.[23] that intercalation of aluminum polycations does not occur until the reaction products are washed with water. This suggests to us that the initial adsorption of polycations may occur by an ion pairing mechanism, in which case the counter anion could also play an important role in determining cation binding selectivity. Additional studies are needed, however, before factor (i) above can be fully elucidated.

The effect of factor (ii), namely, the nature of the initial gallery cation, on the thermal stability of alumina pillared clays is clearly indicated by the results of the present study. Na^+-montmorillonites afforded pillared derivatives that were substantially more thermally stable than those derived from H^+- exchanged forms, as judged by surface area measurements (*cf.*, Table 3.1 and Table 3.2). Owing to the exceptional acidity of H^+- exchanged clays and the effect of acidic pH on lowering the nuclearity of aluminum polycations, these results may represent an extreme example of an exchange cation effect. However, the differences in thermal stability for the pillared Wyoming montmorillonites shown in Table 3.5 cannot be due to exchange cation effects, since the same Na^+-exchanged clay precursor was used for each synthesis.

Variations in the magnitude and origin of layer charge (*i.e..*, factor iii) also cannot be responsible for the differences in thermal stabilities for the pillared Wyoming montmorillonites shown in Table 3.5. The cation exchange capacities of naturally occurring montmorillonites may vary over a large range (e.g., 70 - 120 meq/100 g), but such large variations in layer charge density are unlikely for a mineral from a single locality.[24] Indeed,

the magnitude and origin of layer charge probably are of major importance in determining the exceptional hydrothermal stability of alumina pillared rectorite[25-27] and the high acidity of pillared beidellite.[28,29] But the smectite clays under consideration in the present work are relatively uniform in composition, and the variations that do occur are outside the range needed to explain the relatively large differences in their thermal stabilities.

Several groups have pointed out the importance of synthesis methods and processing variables (*i.e..*, factor iv) on pillared clay properties. For instance, the hydrolysis conditions used to form the pillaring solution,[30] the nature (particle size) of the clay suspension,[31] and the sequence of steps used to dry and calcine the final product[32] all have been identified as important operational variables. Keeping factor (iv) considerations in mind, we have utilized in the present work procedures that have consistently provided alumina pillared montmorillonites with exceptional thermal stability and regular microporosity.

Among the various steps incorporated in our synthesis procedure, perhaps the most important is the removal of chloride from the reaction product by efficient washing of the Al_{13} intercalate. The observed data in Table 3.4 suggest that aging of Al_{13}-exchanged clay in aqueous suspension facilitates the undesirable hydrolysis of the aluminum oligomers in a manner analogous to that which has been observed for the air - dried (uncalcined) pillared clay under ambient aging conditions.[33] Our results also indicate that the pillaring chemistry of smectite clays, particularly the hydrolysis reaction of the surface bound oligocations both in the presence and absence of Cl^- counter ions, is much more complex than generally realized. Thus, operational factors can be very important in regulating the

hydrolysis reactions of polycations intercalated in clay galleries, and such reactions can have a profound effect on the chemical and physical performance properties of the final products. There are several promising approaches to regulating in a more controlled way the pillaring chemistry of smectite clays which include improvements in processing conditions, as demonstrated in the present work, as well as more chemically based strategies, such as the use of surfactants to control polycation hydrolysis.[33,34]

The BET surface areas and pore sizes of the alumina pillared clays prepared in this work merit further comment. The maximum surface areas for AlWM (458 m^2/g) and AlZM (393 m^2/g) are observed at the lowest calcination temperatures (150 ^oC). However, these low temperature products exhibit a relatively broad micropore distribution which extends from 4 Å to beyond 11 Å (*cf.*, Figure 3.3). In addition, the pore distribution is bimodal with the maxima occurring near 5.5 Å and 7.5 Å. Increasing the calcination temperature to 500 ^oC or 800 ^oC causes the surface areas to decrease dramatically to values between 230 and 212 m^2/g (*cf.*, Table 3.1). Most of the surface area loss occurred in the micropore region (*cf.*, Table 3.2). Equally significant, the uniformity of the micropore distribution improves substantially with increasing calcination temperature, with single maxima being observed in the region 6-8 Å. Qualitatively similar relationships between surface area, pore size, and calcination temperature are found for the H^+/AlWM and H^+/AlZM series of products prepared in this study.

The improvement in micropore fidelity with increasing calcination temperature is caused by a reduction in the fraction of pores occurring at both the lower (< 6 Å) and the higher regions (> 8Å) of the micropore size

range. This enhanced uniformity in the pore distribution suggests that the pillars tend to aggregate or cluster non-uniformly at low temperature, but then laterally migrate and become more regularly spaced within the galleries with increasing temperature. The accompanying decrease in surface area, which is estimated from the extent of nitrogen monolayer coverage of the upper and lower surfaces of the galleries, most likely is caused primarily by the restructuring of the pillars and the concomitant reduction in gallery height from ~9.5 Å at 150 °C to ~7.6 Å at 800 °C. Migration of the pillars to the edges of the clay tactoids, where they may block access to some of the gallery surface, is another plausible mechanism for the reduction of surface area with increasing temperature. The importance of gallery blockage in reducing the surface area, however, cannot be assessed based on the present results.

REFERENCES

1. Busenberg E.; Clemency, C. V. *Clays and Clay Miner.*, **1973**, *21*, 213.
2. Wash, J. N. *Spectrochim*, **1980**, *35B*, 107.
3. Grillet, Y.; Rouquerol F.; J. Rouquerol, J. *J.Chim. Phys.*, **1977**, *74*, 179.
4. Northrop, P. S.; Flagan, R. C.; Gavalas, G. R. *Langmuir*, **1987**, *3*, 300.
5. Michot, L. J.; Francois, M.; Case, J. M. *Langmuir*, **1990**, *6*, 677.
6. De Boer, J. M.; Lippens, B. C.; Linsen, B. G.; Broekhoff, J. C. P.; Van den A. H.; Osinga, Th. *J. Coll. Interface Sci.*, **1966**, *21*, 405.
7. Delon, J. F.; Dellyes, R. *C. R. Ac. Sci. Paris, Série D*, **1967**, *265*, 1161.
8. Horvath, G.; Kawazoe, K. G. *J. Chem. Eng. Japan*, **1983**, *16*, 470.
9. Parry, E. R. *J. Catal.*, , **1963**, *2*, 371.
10. Bottero, J.-Y.; Cases, J. M.; Fiessinger, F.; Poirier, J. E. *J. Phys. Chem.*, **1980**, *84*, 2933.
11. Akitt, J. W.; Farthing, A. *J. Chem. Soc. Dalton Trans.*, **1981**, 1606.
12. Bottero, J-Y.; Axelos, M.; Tchoubar, D.; Cases, J. M.; Fripiat, J. J.; Fiessinger, F. *J. Coll. Inter. Sci.*, **1987**, *117*, 47.
13. Fu, G.; Nazar, L. F.; Bain, A. D. *Chem. Mater.*, **1991**, *3*, 602.
14. Fitzgerald, J. J. in *Antiperspirants and Deorderants*, Lader, J. J.; Felga, C. Eds.; Dekker, New York, 1988; p. 119.
15. Tichit, D.; Fazula, F.; Figueras, F. *Stud. Surf. Sci. Catal.*, **1985**, *20*, 351.
16. Bukka, K.; Miller, J. *Clays and Clay Miner.*, **1992**, *40*, 92.

17. Occelli, M.; Tindwa, R. M. *Clays and Clay Miner.*, **1983**, *31*, 22.

18. Sterte, J. *Clays and Clay Miner.*, **1990**, *38*, 609.

19. Tennakoon, D. T. B.; Jones, W.; Thomas, J. M. *J. Chem. Soc., Faraday Trans. 1*, **1986**, *82*, 3081.

20. Schoonheydt, R. A.; Leeman, H. *Clay Miner.*, **1992**, *27*, 253.

21. Doblin, C.; Corrigan, P.; Turney, T. W. Abstract of Paper, *10th Int. Clay Conf.*, Australia, 1993.

22. Molina, R.; A. Vieira-Coelho, A.; and G. Poncelet, G. *Clays and Clay Miner.*, **1992**, *40*, 480.

23. Plee, D.; Borg, F.; Gatineau, L.; Fripiat, J. J. *J. Am. Chem. Soc.*, **1985**, *107*, 2362.

24. Christidis, G.; and P.W. Scott, P. W.*Ind. Miner.* **1993**, *August*, 51.

25. Guan, J.; Min E.; Yu, Z. in *Proc.- Int. Congr. Catal. 9th.*, Philips, M. J.; Ternam, M. Eds.; Ottawa, Canada, 1988, p. 104.

26. Brody, J. F.; and J.W. Johnson, J. W. *Proc. Mat. Res. Soc.*, Materials Research Society; Pittsburgh, USA, p. 65.

27. Occelli, M. *Stud. Surf. Sci. Catal.*, **1991**, *63*, 287.

28. Poncelet, G.; Schutz, A. in *Chemical Reactions in Organic and Inorganic Constrained Systems*, R. Setton, R. Ed.; New York, 1986, p. 165.

29. Schutz, A.; Plee, D.; Borg, F.; Jacobs, P.; Poncelet, G.; Fripiat, J. J. *Proc. Int. Clay Conf.*, 1987, p. 305.

30. Sterte, J. *Catal. Today*, **1988**, *2*, 219.

31. Figueras, F.; Koapyta, Z.; Massiani, P.; Mountassir, Z.; Tichit, D.; Fajula, F. *Clays and Clay Miner.*, **1990**, *38*, 257.

32. Espinosa, J.; Gomez, S. A.; Fuentes, G. A. Abstracts of Papers, 13th North Am. Meeting, Catal. Soc.; Pittsburgh, 1993.

33. Michot, L.; Pinnavaia, T. J. *Chem. Mater.*, **1992**, *4*, 1433.

34. Michot, L.; Pinnavaia, T. J. *Langmuir*, **1993**, *9*, 1794.

CHAPTER FOUR
PILLARED BEIDELLITES WITH HIGH THERMAL STABILITY, REGULAR MICROPOROSITY AND HIGH REACTIVITY

A. OBJECTIVE OF RESEARCH

Chapter 1 summarized the structures and properties of beidellite and its pillared derivatives. Chapter 3 reported the preparation of alumina pillared montmorillonites that are thermally stable up to 800 ^{o}C. This Chapter focuses on the characterization of pillared beidellites, especially on the properties which distinguished alumina pillared beidellites from the corresponding alumina pillared montmorillonites.

Thermally stable pillared beidellites were prepared by using the procedure reported in Chapter 3 for the pillaring of montmorillonite. The pillared beidellites obtained from both the Na^{+}-exchanged form and the H^{+}-exchanged form are characterized in the terms of d-spacings, surface areas, regular microporosity, Brönsted/Lewis acidity and reactivity in the alkylation of biphenyl by propene. Furthermore, synthetic beidellites obtained by 200 ^{o}C hydrothermal reaction were pillared and the properties of the pillared synthetic derivatives were compared with those of the corresponding pillared natural beidellites. The formation of a pillared beidellite with superior thermal stability and catalytic activity is further investigated by designing a synthesis procedure starting from the H^{+}-exchanged form.

B. EXPERIMENTAL

1. Starting materials

Natural beidellite from China was obtained from Dr. J. Guan, Research Institute of Petroleum Processing, Beijing. The starting clay was designated CB. The volatile organic impurities in CB were removed by heating in air at 120 ^{o}C for 12 hours. After being exchanged into the Na^{+} form by using NaCl, the clay sample was fractionated by conventional sedimentation techniques and the < 2 μm fraction was collected. The concentration of the CB clay slurries used for pillaring reactions was between 1 and 2.5 wt%. The < 2 μm fraction of the CB sample contained small amounts of quartz as indicated by the presence of a diffraction peak at 3.34 Å ($2\theta = 26.6^{o}$). The measured CEC values for CB was 101 meq/100g, as determined by the ammonium exchange method.[1]

<u>$H^{\pm}$-Exchanged Beidellites</u>: A 4.0 wt% slurry of Na^{+}-natural beidellite was acidified to 0.25 M in H_2SO_4 by the dropwise addition of 98 wt% sulfuric acid and the mixture was aged for 2 h. The slurry was then centrifuged and washed with deionized water until the pH of the suspension was in the range 3.8 - 4.5. This slurry was used to prepare alumina pillared derivatives by the same procedure as described for the Na^{+}-exchanged form.

<u>Synthetic beidellites</u>: Synthesis of beidellite at below 200 ^{o}C was performed by hydrothermal reaction directly from a wet, co-precipitated aluminosilicate gel, instead of calcining the gel into oxides and hydroxides first. An example of gel preparation is as follow: Aluminum tri-*sec* butoxide 16.2 mL, 0.064 mol and 15 wt% silica sol (Nalco silica sol #1115) 42.4 g,

0.106 mole SiO_2 were hydrolyzed in 150 mL 0.2 M NaOH solution, and then 0.935 g, 0.0046 mole $MgCl_2 \cdot 6H_2O$ was added into the gel to co-precipitate $Mg(OH)_2$. The resulting mixture was aged overnight at pH near 10 and then washed by centrifugation until the pH was reduced to 7 and the gel was free of Cl^-. The solid material thus obtained was re-dispersed in deionized water and natural beidellite (1 wt%) was added as seed. The wet gel was allowed to undergo hydrothermal reaction at 200 °C for 3 to 7 days in Parr acid digestion bombs fitted with a teflon-lined cup. The solid material thus obtained was re-dispersed in deionized water. 1 wt% of natural beidellite was added as seed. The wet gel was allowed to undergo hydrothermal reaction at 200 °C for 3 to 7 days. The crystalline product was suspended in deionized water for use in the pillaring reaction.

2. Pillaring Solution

The pillaring solution used in this study was prepared as follows. To 600 mL of 0.20 M $AlCl_3$ (120 mmol) in a three liter 3-neck flask was added dropwise with vigorous stirring 1440 mL of 0.20 M NaOH (288 mmol). The addition required approximately 6 h to complete. During this time the temperature of the reaction mixture was increased from room temperature to 80 °C. The solution was then allowed to age overnight (12-16 h) at 80 °C while being stirred and then allowed to cool to room temperature. Then the pH was adjusted to a value of 3.6 - 4.0 by addition of a small amount of 0.2 M NaOH. The solution was placed in a screw-cap glass bottle, where it could be stored at room temperature for a period of at least one year without noticeable changes as a reagent for the pillaring of the clay.

3. Pillaring Reaction

A 1.0-2.5 wt% suspension of Na^+- or H^+- exchanged beidellites (see below) at ambient temperature was added at an approximate rate of 150 mL/min to the vortex of a vigorously stirred pillaring solution at 70 °C. The Al^{3+}/clay ratio was maintained in the range of 1.8 - 2.5 mmol/g. The stirred mixture was allowed to age at 70 °C for an additional 2 h and then it was cooled under running tap water to room temperature. The suspension was immediately centrifuged at 10,000 rpm for 12 min, and the clay was washed four times by re-suspending it in an equivalent volume of deionized water and centrifuging. The entire washing procedure was completed within 3 h. The chloride-free suspension was poured onto a glass plate sheet and allowed to dry overnight at room temperature. The air-dried products were then calcined in a programmable oven. The heating rate and cooling rates used in the calcination were 10 °C/min. For samples calcined above 400 °C, the material was first heated to 400 °C at a rate of 10 °C/min, held at 400 °C for 1 h, and ramped to the new temperature at a rate of 5 °C/min, held at the desired temperature for 4 h, and then cooled by using the reverse process.

4. Characterization Methods

Samples for elemental analysis by ICP emission spectroscopy were prepared by using the lithium metaborate ($LiBO_2$) technique.[2] A 50 - mg quantity of sample was mixed with 300 mg of lithium metaborate and heated 10 minutes at 1000 °C. The fused product was then dissolved in 50 mL of 5% of HNO_3.

X-ray diffraction patterns were obtained for oriented powder samples with a Rigaku diffractometer equipped with Cu target and curved crystal graphite monochromator.

Adsorption / desorption experiments with N_2 as the sorbate were carried out at -196 °C on a Coulter Ominosorb 360 CX sorptometer. The samples were outgassed overnight at 150 °C under dynamic vacuum (10^{-5} torr). Nitrogen isotherms were obtained by the quasi-equilibrium volumetric method.[3-5] Surface areas were obtained by using the BET equation. The t-plot method[6] was used to determine the total micropore volume, as well as the non-microporous surface area.

FTIR spectra for chemisorbed pyridine were obtained on an IBM IR44 spectrometer. A self-supported sample wafer was outgassed at 300 °C under flowing helium prior to pyridine adsorption at 25 °C. Weakly adsorbed pyridine was removed by outgassing the sample at 150 °C for 16 h. Chemisorbed pyridine was then further desorbed by evacuation at 250 °C. All spectra were recorded at 150 °C. The quantitative results were obtained by the method of Datka[7] by using the following formula.

$$c=\frac{A\cdot S}{\varepsilon\cdot w}$$

where c is the pyridine concentration in $umol.mg^{-1}$, A is the measured absorbance, ε is the extinction coefficient ($\varepsilon=0.059\pm0.004$ cm^2 μmol^{-1} for the 1545 cm^{-1} band of PyH^+ and $\varepsilon=0.084\pm0.003$ cm^2 $umol^{-1}$ for the 1457 cm^{-1} band of Lewis bonded pyridine), S is the area of the pellet (S= 1.3 cm^2) and w is the weight of the pellet ($w \approx 20mg$).

A Varian 400 VXR solid state NMR spectrometer was used to obtain ^{29}Si and ^{27}Al MAS NMR spectra at 79.5 MHz and 104.3 MHz, respectively.

The spinning frequencies were 4-5 KHz. ^{29}Si chemical shifts were reported relative to TMS. The ^{27}Al chemical shifts were relative to $AlCl_3 \cdot 6H_2O$.

5. Catalysis

Alkylation of Biphenyl by Propene: The alkylation of biphenyl by propene was carried out in a 300-mL batch reactor (n° 4561 Parr Instruments). Propene was CP grade (Matheson Company), and biphenyl was practical grade.

A 30-g quantity of biphenyl (0.194 mole) and 0.2 g or 0.1 g of pillared beidellite were heated at a ramp rate of 3 °C/min under a purge stream of propene with stirring until a temperature of 250 °C was reached. The reaction was carried out for 20 hours at 250 °C, and then the reactor was allowed to cool and the pressure was slowly released. The reaction mixture was dissolved in 300 mL hexane, the catalyst was filtered, and the products were analyzed by GC.

Gas chromatographic analyses were performed on a HP5890 GC equipped with a 60 m SPB1 column (Supelco) and a FID detector. Injection temperature was 230 °C, and the detection temperature was 250 °C. The column was heated from 100 °C to 225 °C at 4°/min to elute the analyte. A typical chromatogram for a typical reaction mixture is shown in Figure 4.1.

The conversion of biphenyl was calculated from the following equation:

$$\text{conversion (\%)} = \frac{(\text{Biphenyl})_{\text{converted}}}{(\text{Biphenyl})_{\text{unreacted}} + (\text{Biphenyl})_{\text{converted}}} \cdot 100$$

Where $(\text{Biphenyl})_{\text{unreacted}}$ refers to the area of the biphenyl peak in the GC and $(\text{Biphenyl})_{\text{converted}}$ was calculated as follows:

$$(\text{Biphenyl})_{\text{converted}} = \sum \left[(\text{area alkylbiphenyl}) \cdot \frac{12}{x} \right]$$

where x is the carbon atom number of the alkylbiphenyl considered.

The degree of biphenyl alkylation was determined by VG TROI-1000 GC MAS. Assignments are given in Table 4.1.

Table 4.1 Assignments Proposed for Alkylation of Biphenyl by Propene

Alkylated Biphenyl	Peaks (isomers)
monoalkyl[1]	3 (o), 4 (m), 5 (p)
dialkyl[1,2]	6 (0-p + o-m), 7 (o-m'), 8 (o-p'), 10 (m-m), 12(m-m'), 14 (m-p'), 16 (p-p')
trialkyl	9, 11,13, 15, 21, 27
tetraalkyl	17, 18, 19, 20, 22, 28, 33
pentaalkyl	23, 24, 25, 29, 30, 31

[1]The assignments of monoalkyl and dialkyl isomers were identified according to ref. 13.

[2]The assignment of no. 14 and no. 16 were confirmed by analysis of pure p-p' and m-p' samples supplied by the Dow Chemical Company.

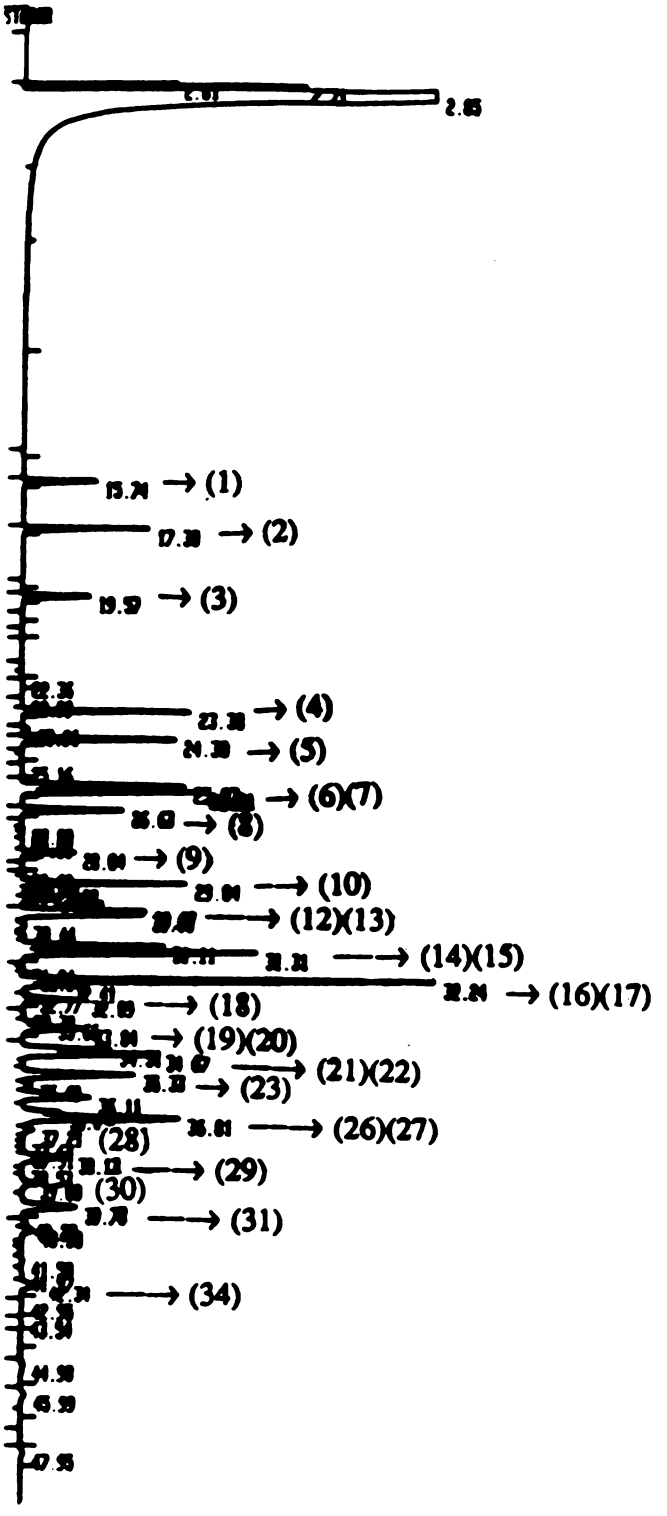

Figure 4.1 Typical gas chromatograms of products obtained by propene alkylation of biphenyl catalyzed by alumina pillared beidellites.

C. RESULTS

1. Alumina Pillared Natural Beidellite

1) XRD and Pore Structure

The pillared natural Chinese beidellites formed by reaction of the Na^+- and H^+-exchanged forms with Al_{13} oligomers are abbreviated AlCB and H^+/AlCB, respectively. Pillared synthetic beidellites to be discussed later, are abbreviated AlSB.

Table 4.2 and Table 4.3 provide the basal spacings, N_2 BET surface areas and N_2 adsorption t-plot data for AlCB and H^+/AlCB at different calcination temperatures, respectively. From the t-plot, values of microporous surface areas (S_{micro}) along with the total surface areas (S_{total}) are determined. The basal spacing from 19.1 Å for air-dried AlCB to 17.7 Å after 500 ^oC calcination are in agreement with previously reported alumina pillared beidellites. AlCB, after 150 ^oC calcination, exhibited a 452 m^2/g BET surface area. The t-plot results gave a 373 m^2/g microporous surface area and a total surface area of 464 m^2/g. As the calcination temperature is increased, the BET and the total surface areas decrease gradually, with 70-80 % of the total area occurring in the micropore size domain. The very high thermal stability of AlCB after calcination at 800 ^oC is shown by the basal spacing of 16.7 Å, as well as by the surface area data, which give 218 m^2/g of BET and 205 m^2/g microporous surface area out of 248 m^2/g total surface area.

Table 4.2 Basal Spacing, N_2 BET Surface Areas, Total Surface Areas (S_{total}) and Microporous Surface Areas (S_{micro}) for AlCB[1] Calcined at Different Temperatures

cal. temp. (°C)	150	300	400	500	800
basal spacing (Å)	19.1	18.6	18.1	17.7	16.7
BET (m^2/g)	452	370	287	279	218
S_{total} (m^2/g)	464	418	321	309	248
S_{micro} (m^2/g)	373 (80 %)	306 (73 %)	232 (72 %)	218 (71%)	205 (83 %)

[1] Outgassing conditions: 150 °C, 12 h in vacuum.

Included in Table 4.3 for comparison purpose are analogous data for alumina pillared products formed from the intrinsically more acidic H^+-exchanged form of CB (H^+/AlCB). Unlike alumina pillared montmorillonites prepared from the H^+-exchanged clay, which is less stable compared to the pillared products prepared from the Na^+-exchanged clay,[8] H^+/AlCB displays thermal stability compatible to that of AlCB. After 700 °C calcination, the BET area is 278 m^2/g and total area is 309 m^2/g with 201 m^2/g microporous surface area. After 800 °C calcination, analogous behavior which give 220 m^2/g of BET and 250 m^2/g total surface area with 208 m^2/g of microporous surface area observed for high temperature calcined H^+/AlCB.

Table 4.3 Basal Spacing, N_2 BET Surface Areas, Total Surface Areas (S_{total}) and Microporous Surface Areas (S_{micro}) for H^+/AlCB[1] Calcined at Different Temperatures

cal. temp. (°C)	150	300	400	500	700	800
basal spacing (Å)	19.3	18.6	18.1	17.9	17.5	16.9
BET (m^2/g)	434	435	330	327	278	222
S_{total} (m^2/g)	495	495	377	317	309	252
S_{micro} (m^2/g)	415 (84 %)	367 (74 %)	328 (87 %)	236 (75 %)	201 (65 %)	178 (71 %)

[1] Outgassing conditions: 150 °C, 12 h in vacuum.

The exceptional thermal stabilities of our pillared products formed from the H^+-exchanged form of beidellite also are further illustrated by the x-ray powder diffraction patterns in Figure 4.2 for H^+/AlCB products calcined at selected temperatures in the range 150 - 800 °C. As the calcination temperature is increased, the 001 reflection shifts from 19.3 Å at 300 °C to 17.5 Å at 800 °C. At the same time the width of the line increases, indicating that as the temperature increases, a reduction in the c-axis layer stacking order occurs, in addition to a lowering of the average basal spacing. At a calcination temperature of 900 °C the clay decomposes and crystallinity is lost. Similar XRD patterns are observed for AlCB.

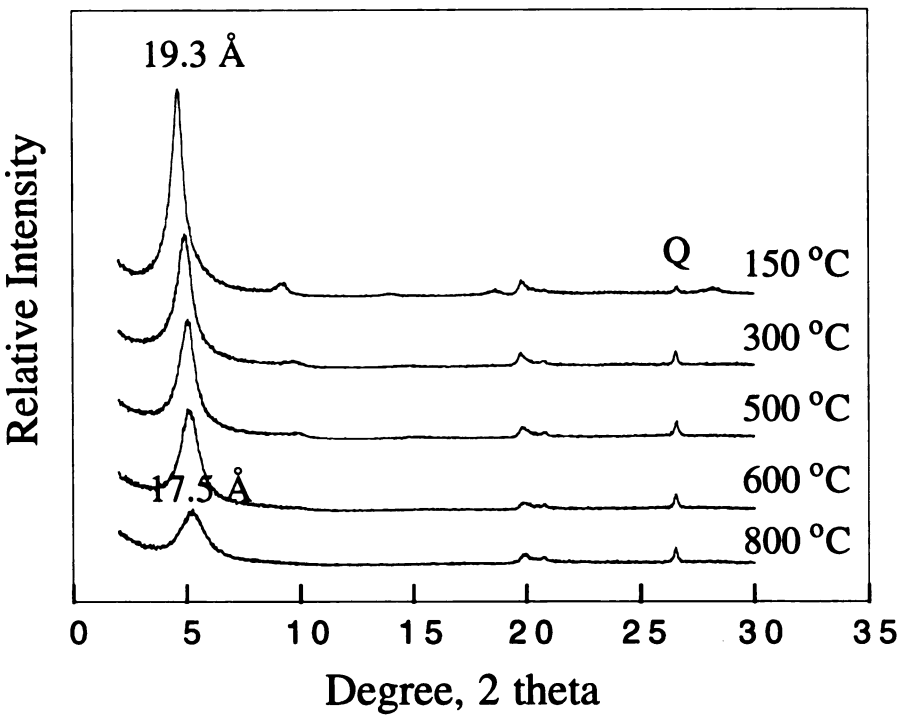

Figure 4.2. X-ray powder diffraction patterns (Cu-K_α) for calcined forms of H^+/AlCB (alumina pillared Chinese beidellites prepared from the H^+-exchanged precursor). The peak labeled Q is due to the presence of quartz.

In order to monitor the structural stability of pillared beidellite upon aging, the same samples that gave the data in Table 4.2 and Table 4.3 were remeasured after storage at room temperature for 18 months. The isotherms for freshly prepared samples and for 18 months samples are shown in Figure 4.3. The Figure 4.3 (a) and (c) correspond to AlCB, (b) and (d) are for H^+/AlCB, respectively. It is obvious that the characteristics of the isotherms remain unchanged after 18 months storage for both AlCB and H^+/AlCB, The well-expressed plateaus at the low pressure indicate that the micropore structure does not decrease with time of aging. The corresponding BET surface area and t - plot data listed in Table 4.4 for AlCB and Table 4.5 for H^+/AlCB are consistent with the isotherms. The

Table 4.4 N_2 BET Surface Areas, Total Surface Areas (S_{total}) and Microporous Surface Areas (S_{micro}) as Determined by the t-Plot Method for AlCB[1] Calcined at Different Temperatures after 18 Months Storage at Room Temperature

cal. temp. (°C)	300	400	500	800
BET (m^2/g)	397	286	239	202
S_{total} (m^2/g)	452	328	290	249
S_{micro} (m^2/g)	358	258	232	192

[1]Outgassing conditions: 150 °C, 12 h in vacuum.

microporous surface areas are retained and about 75% of total surface area is due to a micropore. These observations verify the stability of pillared beidellites.

Table 4.5 N_2 BET Surface Areas, Total Surface Areas (S_{total}) and Microporous Surface Areas (S_{micro}) as Determined by the t-Plot Method for H^+/AlCB[1] Calcined at Different Temperatures after 18 Months Storage at Room Temperature

cal. temp. (°C)	300	400	500	800
BET (m^2/g)	423	344	280	206
S_{total} (m^2/g)	483	398	348	251
S_{micro} (m^2/g)	393	310	275	201

[1] Outgassing conditions: 150 °C, 12 h in vacuum.

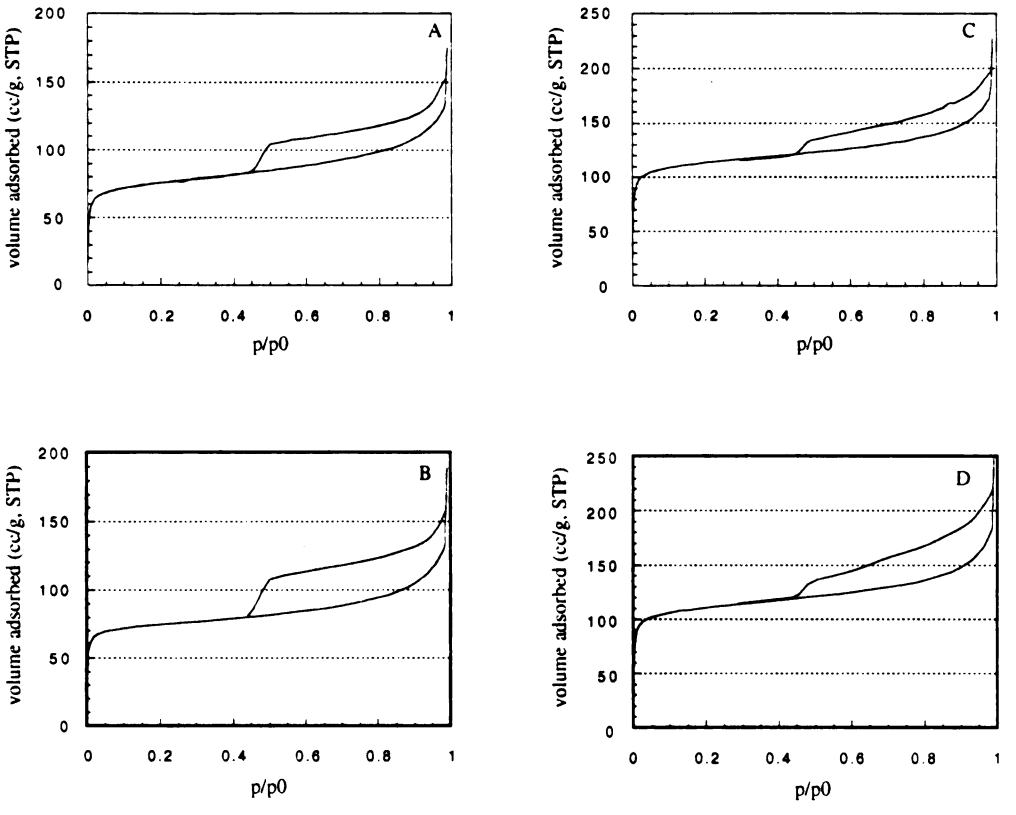

Figure 4.3 Nitrogen adsorption-desorption isotherms for (A) freshly prepared AlCB calcined at 500 °C; (B) sample A after 18 months; (C) freshly prepared H^+/AlCB calcined at 400 °C; (D) sample C after 18 months.

2) MAS NMR

The ^{29}Si MAS NMR spectra of Na^+ and Al_{13} ion-exchanged beidellites and calcined alumina pillared beidellites are shown in Figure 4.4. The parent clay shows two peaks. As shown in Figure 4.4-1, the first peak at -93.7 ppm can be deconvolved into two signals, at -93.8 ppm corresponding to a Q^3 tetrahedral silicon linked through oxygen to three other silicon and at -89.5 ppm corresponding to a Q^3 tetrahedral silicon linked through oxygen to two other silicon and one adjacent aluminum in the tetrahedral layer. The second peak appearing at -108 ppm was assigned to a silicon impurity (quartz) associated with the parent clay. The spectrum of the air-dried pillared clay is similar to that of the parent clay, but after calcination the ^{29}Si signal shifts negatively with a concomitant broadening of the peak. As shown in Figure 4.4 (C) and (D), the peak shifts to -95.2 ppm after 500 ^oC calcination and to -98.0 ppm after calcination at 800 ^oC.

Similar ^{29}Si MAS NMR spectra were observed for alumina pillared saponites when the pillared analogues were calcined at elevated temperatures.[9-10] The slight differences in pillared montmorillonites and hectorite[11] is that a more negative shift was observed at lower temperature compared with the shift of pillared beidellite and saponit. For example, after heating at 500 ^oC pillared hectorite shifted negatively from -95.0 ppm to -98.5 ppm and pillared montmorillonite from -93.5 ppm to -95.5 ppm, e. g. a 2-3 ppm shift, whereas tetrahedral charged pillared analogue yielded a 1-1.5 ppm negative shift.

For alumina pillared Beidellite and montmorillonite, the explanation of ^{27}Al MAS NMR is difficult because of the near coincidence of the signals from the constituent aluminum of the parent clay and from the aluminum

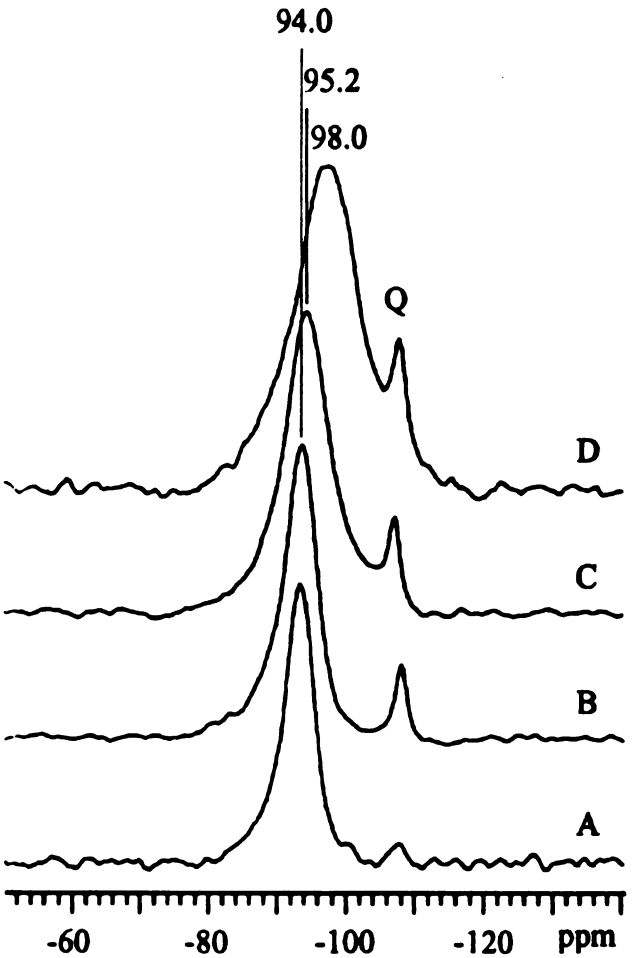

Figure 4.4 ^{29}Si MAS NMR spectra of (A) Na^+-exchanged beidellite; and of AlCB after (B) air-dry; (C) 500 °C calcination; (D) 800 °C calcination. The peak labeled "Q" at -108 ppm is due to the presence of quartz.

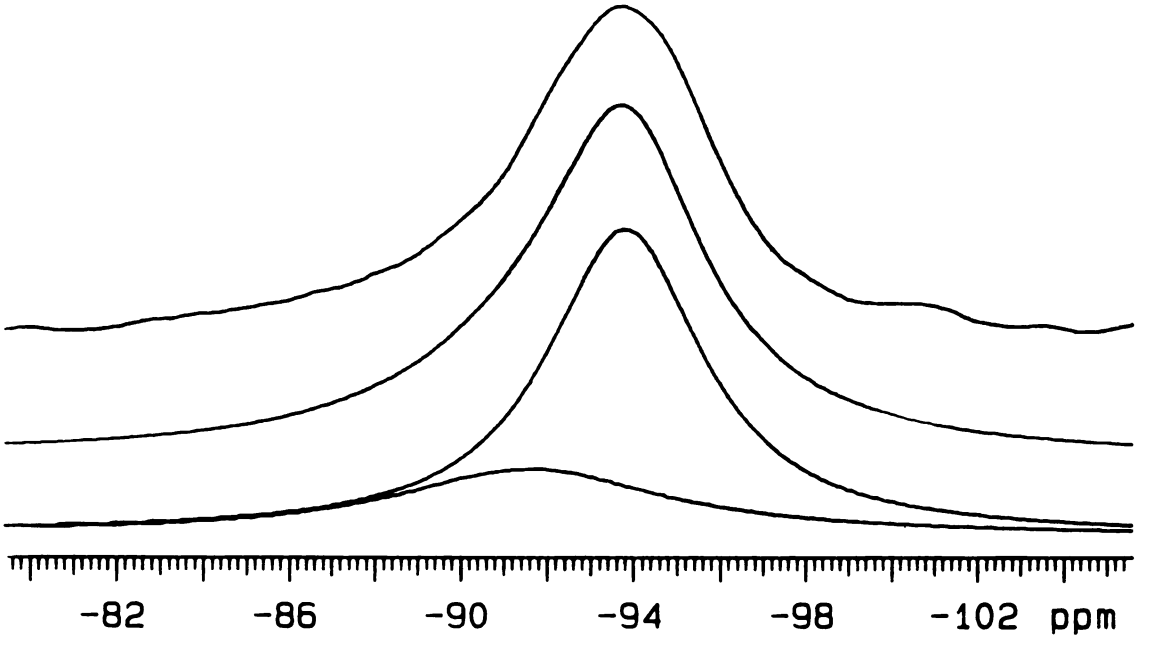

Figure 4.4-1 Deconvolution of the ^{29}Si MAS NMR spectrum of Figure 4.4 A (upper curve) into two components given by the bottom two lines. The second curve from the top is the simulated spectrum. The relative intensities for Q^3 (Si-OAl) and Q^3 (Si-1Al) components are 2.5.

within the pillar. It is necessary to consider the alumina pillar structure separately under our experimental condition in order to obtain information on the influence of pillar and calcination. Figure 4.5 shows the ^{27}Al MAS NMR spectra of alumina pillars prepared by hydrolysis of $AlCl_3$ with NaOH (OH^-/Al^{3+}= 2.4) dried at room temperature and after heating to 700 ^oC at two different heating rates. The calcination results in a decrease and broadening of the sharp tetrahedral peak and an increase in the corresponding octahedral peak, which is the result of pillar dehydration and dehydroxylation. The amount of tetrahedral and octahedral aluminum cannot be quantitatively determined under our experimental conditions. However, the spectral changes reflect the change in the Al environment symmetry. The spectra in Figure 4.5 (B) and (C) indicate that more tetrahedral aluminum ia pewawnr at the low heating rate than the high heating rate, which means that heating rate also affects the symmetry of the pillar alumina.

Figure 4.6 illustrates ^{27}Al MAS NMR spectra for pillared beidellite. The clay layers and the pillar give a tetrahedral aluminum resonance at 68 ppm and an octahedral aluminum resonance at 3 ppm. On calcination a slight upfield shift for both tetrahedral Al and octahedral Al, as well as a broadening and decrease of tetrahedral Al are observed. A change of pillar structure itself may be partly responsible for the structural modification upon calcination.

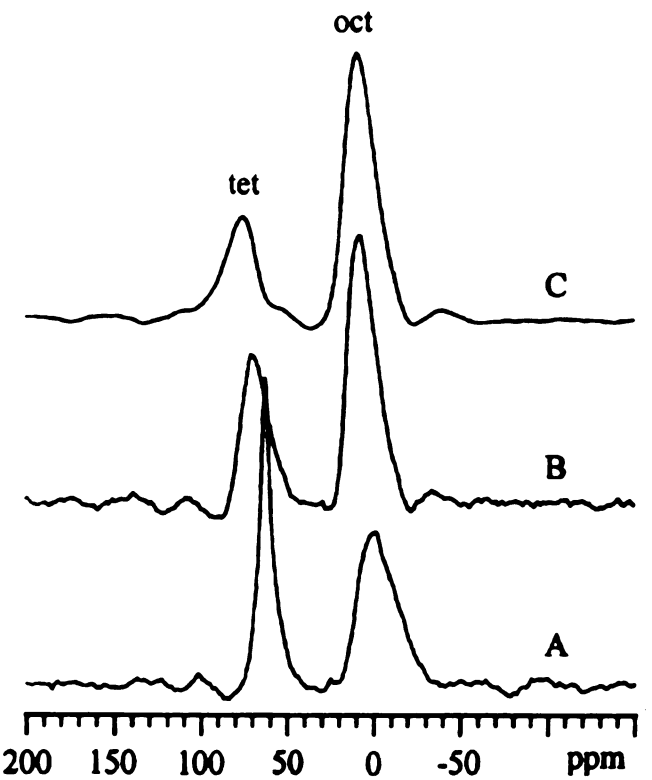

Figure 4.5 ^{27}Al MAS NMR spectra of aluminum polycations prepared by hydrolysis of $AlCl_3$ with NaOH (OH^-/Al^{3+}= 2.4) (A) residue obtained by evaporation at room temperature; (B) after heating to 700 °C at the rate of 3 °C/min; (C) after heating to 700 °C at the rate of 10 °C/min.

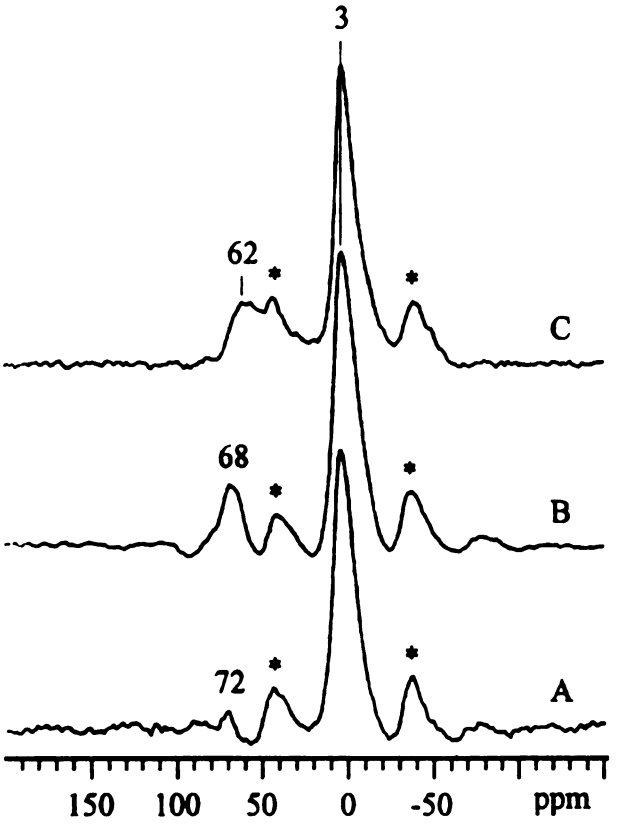

Figure 4.6 ^{27}Al MAS NMR spectra of (A) Na^+-exchanged beidellite; and of AlCB after (B) air-dry; (C) 800 °C calcination.

3) FTIR

Infrared spectroscopy revealed the chemisorption of pyridine at both the Lewis and the Brönsted acid sites of each alumina pillared beidellite reaction product, as long as the calcination temperature range was 300 - 800 ^{o}C. Table 4.6 summarizes the amount of the Lewis and Brönsted type pyridine sites as a function of calcination temperature. The amounts of adsorbed pyridine are similar for AlCB and H^+/AlCB at the same calcination temperature, e.g. pillared beidellites formed by H^+-exchange do not adsorb significantly more pyridine than pillared beidellites prepared by Na^+-exchange. The predominance of Lewis over Brönsted sites is a normal characteristic of alumina pillared clays, regardless of synthesis method. Lewis pyridine sites predominate over Brönsted sites at all calcination temperatures over the range 300 - 800 ^{o}C. Note, however, the general decrease in the total number of acid sites, especially Lewis sites, with increasing calcination temperature. As shown in Figure 4.7 for the chemisorption of pyridine on calcined samples of H^+/AlCB, the ring stretching frequencies[12] characteristic of Lewis pyridine (1454 cm^{-1}) and Brönsted pyridine (1545 cm^{-1}) are observed even after calcination at 800 ^{o}C.

Table 4.6 Pyridine Adsorbed on Alumina Pillared Beidellites Calcined at Different Temperatures

Catalyst	cal. temp. °C	degassing temp. °C	Lewis[3]	Brönsted[4]	Total[5]	Lewis/ Brönsted
AlCB[1]	300	150	14.9	5.0	19.8	3.0
		250	10.5	2.7	13.2	3.9
	500	150	10.9	3.4	14.3	3.2
		250	9.6	1.7	11.3	5.6
	800	150	4.3	1.3	5.6	3.3
		250	3.9	0.3	4.2	13.0
H^+/ AlCB[2]	300	150	12.8	7.6	20.4	1.7
		250	11.8	4.4	16.2	2.7
	500	150	10.8	3.3	14.1	3.3
		250	9.6	1.6	11.2	6.0
	800	150	4.1	3.8	7.9	3.4
		250	2.2	0.2	2.4	11.0

[1] pillared beidellite prepared from Na^+ exchange form.

[2] pillared beidellite prepared from H^+ exchange form.

[3] Lewis-bonded pyridine determined from 1450 cm^{-1} absorption band (mmol/100g of clay).

[4] Brönsted -bonded pyridine from 1545 cm^{-1} absorption band (mmol/100g of clay).

[5] Total of acid-bonded pyridine (mmol/100 g of clay).

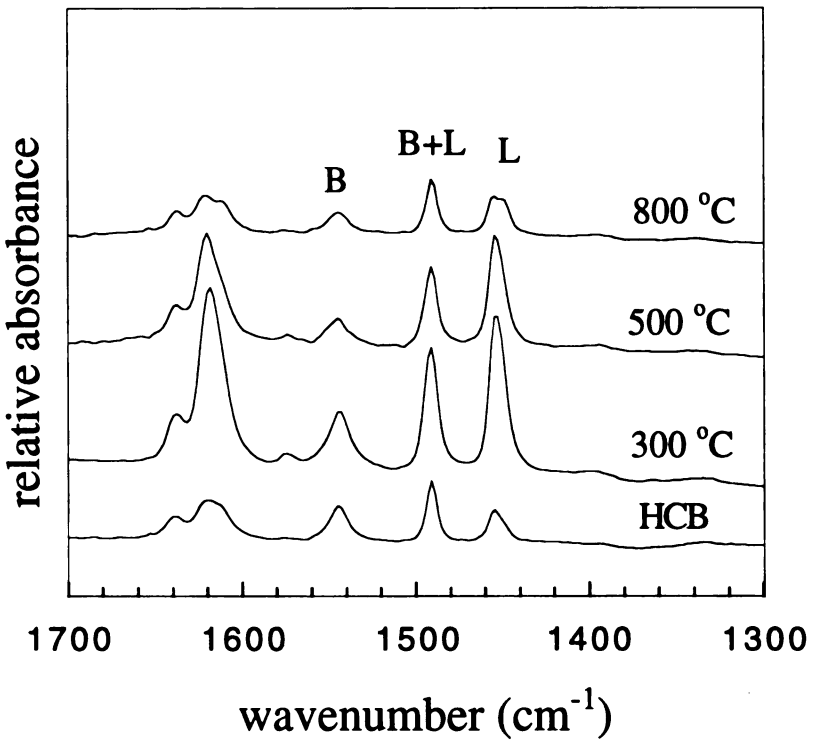

Figure 4.7 FTIR spectra of pyridine chemisorbed at 150 °C on calcined samples of H^+/AlCB.

4) Alkylation of Biphenyl by Propene

The catalytic activities of pillared beidellite calcined at the different temperatures are listed in the Table 4.7, 4.8, 4.9 for alkylation of liquid phase biphenyl by propene at 250 °C by using either 0.2 g or 0.1 g catalyst (100 -200 mesh, 75 - 150 μm fraction). Included in Table 4.10 for comparison purpose are analogous data of other solid catalysts.[13]

The previous studies have verified that catalytic activity of alumina pillared clays for propene alkylation of biphenyl is a function of the porosity and acidity.[14] A comparison with other solid catalysts in Table 4.10 indicates that alumina pillared beidellites (Table 4.7) belong to the most active group that includes K10 and alumina pillared flurohectorite (APFH), with most of the biphenyl converted to di, tri, tetra and even pentaalkylated products. Although pillared beidellites possess similar porosity and adsorb analogous amount of pyridine as those of pillared montmorillonites,[13] their activities are much higher. The activities of APFH decrease dramatically after 500 °C calcination due to the dehydroxylation of OH which replace F,[15] whereas as shown in Table 4.7 and 4.9 the alumina pillared beidellites are not very sensitive to calcination temperature. Even after 700 °C calcination the activities remain quite high. The higher activities of H^+/AlCB in Table 4.9 over these of AlCB in Table 4.8 are pronounced when 0.1 g catalyst is used. Therefore, alumina pillared beidellite, especially specimens prepared from an H^+-exchanged form, are exceptionally active catalysts for the alkylation of biphenyl by propene.

Table 4.7 Biphenyl Conversion and Product Isomer Distribution Obtained for AlCB[1]

cal. temp. (°C)	300	400	500	600	700
conversion %	99	99	99	99	74
% monoalkyl	5	4	4	11	49
% dialkyl	34	28	29	24	39
% trialkyl	28	24	18	25	10
% tetraalkyl	17	20	24	21	1
% pentaalkyl	16	24	25	19	1

[1]The reaction conditions were as follows: 30 g biphenyl, 0.2 g catalyst (alumina pillared CB prepared from Na^+-Chinese beidellites), 140 psi propene, 250 °C, 20 hours reaction time. All results were obtained with 100-200 mesh particle size catalysts.

Table 4.8 Biphenyl Conversion and Product Isomer Distribution Obtained for AlCB[1]

cal. temp. (°C)	300	400	500	600
conversion %	39	92	67	26
% monoalkyl	72	24	54	85
% dialkyl	18	41	33	12
% trialkyl	6	21	10	3
% tetraalkyl	4	8	2	0
% pentaalkyl	0	6	1	0

[1] The reaction conditions were as follows: 30 g biphenyl, 0.1 g catalyst (alumina pillared CB prepared from Na^+-Chinese beidellites), 140 psi propene, 250 °C, 20 hours reaction time. All results were obtained with 100-200 mesh particle size catalysts.

Table 4.9 Biphenyl Conversion and Product Isomer Distribution Obtained for H^+/AlCB[1]

cal. temp. (°C)	300	400	500	600
conversion %	98	99	98	94
% monoalkyl	8	3	7	19
% dialkyl	37	26	35	45
% trialkyl	26	27	27	22
% tetraalkyl	15	19	17	9
% pentaalkyl	14	24	14	5

[1] The reaction conditions were as follows: 30 g biphenyl, 0.1 g catalyst (alumina pillared CB prepared from H^+-Chinese beidellites), 140 psi propene, 250 °C, 20 hours reaction time. All results were obtained with 100-200 mesh particle size catalysts.

Table 4.10 Biphenyl Conversion and Product Isomer Distribution Obtained for Different Solid Catalysts[1]

catalysts	APFH[2]	K10	ADL[3]	USY	APWM[4]
conversion %	98	96	89	78	64
% monoalkyl	11	16	29	45	63
% dialkyl	33	36	39	40	30
% trialkyl	38	37	25	14	7
% tetraalkyl	17	11	7	2	0
% pentaalkyl	0	0	0	0	0

[1] The reaction conditions were as follows: 30 g biphenyl, 0.2 g catalyst after 350 °C calcination, 140 psi propene, 250 °C, 20 hours reaction time. All results were obtained with 100-200 mesh particle size catalysts. All the data are taken from ref. 13.

[2]Alumina pillared fluorohectorite.

[3]Alumina pillared laponites.

[4]Alumina pillared Wyoming montmorillonite.

5) Chemical and Structural Data for NaCB and HCB

Although AlCB and H^+/AlCB exhibit very similar thermal stabilities, pore structures, and amounts of acid sites detected by pyridine adsorption, certain properties, such as catalytic activity, are strikingly different. These differences arise from the clay hosts used to prepare the pillared clay. In Table 4.11, the chemical analysis, BET surface area and cell parameters for NaCB (Na^+-exchanged CB) and HCB (acid treated CB) are compared. The high BET surface area (103 m^2/g) for HCB probably is due to more external

surface than that of NaCB (30 m^2/g). Acid treatment creates exposed defect sites. Chemical analysis data given in Table 4.11 provide the following information: firstly, the interlayer cation of Na^+ is replaced by H_3O^+ ions; secondly, a notable decrease of Al content occurs in the acid-treated sample, indicating dissolution of the Al from the layer. Most of the leached Al might be from the octahedral sheet. On the other hand, the cell parameters[16] measured by XRD yield identical values of dimension for both NaCB and HCB. This means that mild acid treatment leaves the lattice structure of the parent clay intact, which is consistent with the fact that AlCB and H^+/AlCB have similar XRD patterns and pore structures.

Table 4.11 BET Surface Area, Element Contents (wt%) and Cell Parameters[a)] of NaCB and HCB

sample	BET surface area	Element content (wt%)				Parameters (Å)		
	m^2/g	Si	Al	Mg	Na	a[1]	b	c
NaCB	30	26.1	13.9	2.0	3.9	5.186	8.892	12.5
HCB	103	29.6	10.6	2.3	0.2	5.186	8.892	14.4

[1] $a = b / \sqrt{3}$

2. Alumina Pillared Synthetic Beidellites

Our studies of the preparation and structural characterization of pillared beidellites were carried out on natural beidellite derivatives in order to avoid the possible effects of impurities contained in synthetic beidellite. So the differences in the pillared analogues arise from the parent clays.

Some previous work[22] claimed that the low surface area of 156 m^2/g for alumina pillared synthetic beidellite may be due to a low CEC. However, pillared Wyoming montmorillonites with low CEC (CEC=60 meaq/100 g) have over 300 m^2/g of BET surface area. In this case, the influence of starting material and pillaring reaction can not be distinguished.

Table 4.12 Basal Spacing, N_2 BET Surface Areas, Total Surface Areas (S_{total}) and Microporous Surface Areas (S_{micro}) as Determined by the t- Plot Method[1] for AlSB[2] Calcined at Different Temperatures

cal. temp. (°C)	150	300	400	500	700
basal spacing (Å)	19.6	19.3	19.0	18.3	17.6
BET (m^2/g)	338	266	235	223	186
S_{total} (m^2/g)	380	266	235	223	201
S_{micro} (m^2/g)	253	159	141	122	118

[1] Outgassing conditions: 150 °C, 12 h in vacuum.

[2] Alumina pillared synthetic beidellite prepared from Na^+-synthetic beidellites.

The synthetic beidellites prepared at 200 °C as described in Chapter Two are pillared successfully by using the same procedure as that used for preparing natural beidellites. The XRD pattern of the product calcined at selected temperatures is shown in Figure 4.8. The d-spacing shifts from 19.6

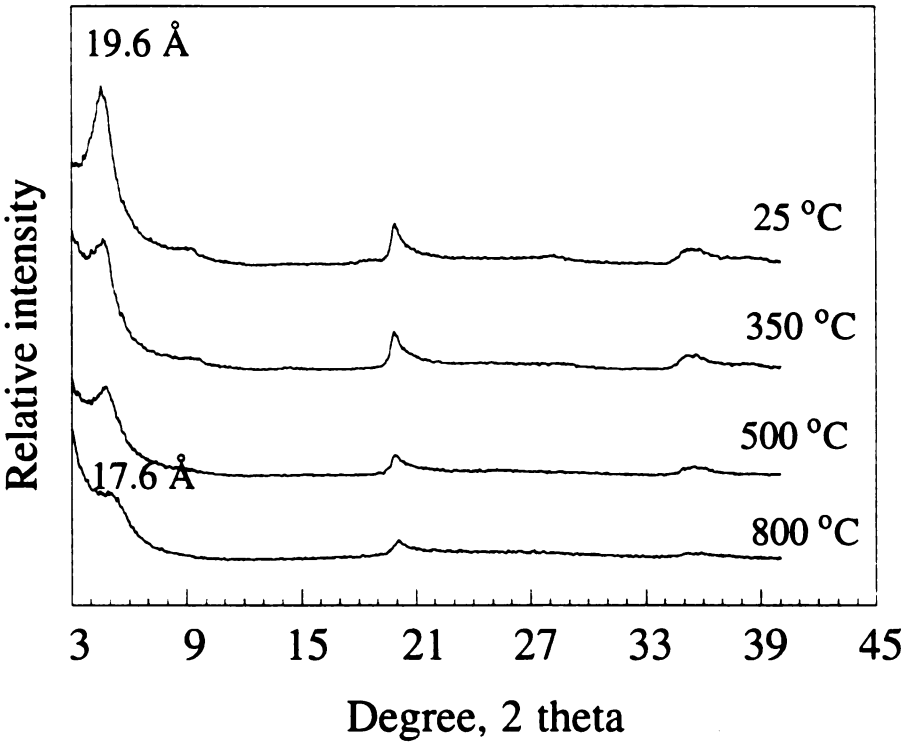

Figure 4.8. X-ray powder diffraction patterns (Cu-K_α) for calcined forms of AlSB (alumina pillared synthetic beidellites prepared from the Na^+-exchanged precursor).

Å for air-dried sample to 17.6 Å after 700 °C calcination. The N_2 BET surface areas and microporous surface areas are summarized in Table 4.12. The BET surface area as well as about 60 % of total surface area in the micropore range are in agreement with the XRD pattern. However, the synthetic pillared analogue exhibits lower surface area in comparison to the corresponding natural pillared beidellite (Table 4.2). According to the CEC results, both clays exhibit CEC values around 100 meq/100g clay. Therefore, the difference can not be due to CEC difference. The poor crystallinity of synthetic beidellite in term of high surface area might be the main reason. Also, the small amount of amorphous co-product which does not contribute to forming the pillared structure is another source of non-microporous surface area.

Table 4.13 Biphenyl Conversion and Product Isomer Distribution Obtained for Synthetic Beidellites [1]

cal. tem. (°C)	300	400	500	700
conversion %	99	94	77	63
% monoalkyl	28	18	45	59
% dialkyl	24	49	43	33
% trialkyl	20	18	9	7
% tetraalkyl	14	7	2	1
% pentaalkyl	14	7	1	0

[1]The reaction conditions were as follows: 30 g biphenyl, 0.2 g catalyst, 140 psi propene, 250 °C, 20 hours reaction time. All results were obtained with 100-200 mesh particle size catalysts.

The catalytic activities of pillared synthetic beidellites for the alkylation of biphenyl by propene are given in Table 4.13. Although pillared montmorillonites have higher surface area than pillared synthetic beidellites, the conversion of biphenyl and the product distribution show that pillared synthetic beidellites are more active than pillared natural montmorillonites. This is an good evidence for the effect of tetrahedral substitution on the acidity of clay host and pillared clay derivatives.

D. DISCUSSION

Alumina pillared clay beidellites AlCB and H^+/AlCB, prepared by the reaction of Al_{13} oligocations with the Na^+-exchanged and H^+-exchanged forms of China beidellites, respectively, not only are among the most thermally stable metal oxide pillared smectite clays known, but also they exhibit exceptionally high acid catalytic activities after calcination, as determined by the alkylation of biphenyl by propene. The crucial factor determining the thermally stability and reactivity seem to be the homogeneity of the pillar distribution affected by the preparation conditions.

The formation of pillared clay is achieved by intercalating polycations to prop open the clay sheet, resulting in a regular micropore gallery environment. It is not hard to conceive that the pillars should be as uniform as possible to achieve a stable structure. The microporous structures are likely to collapse at elevated temperature if pillars of various sizes are distributed between the clay sheets. The tetrahedral layer charge sites of beidellite minimizes the distance between the pillaring cations and the layers, thus optimizing the electrostatic interaction to the cations between the

layers. The influence of homogeneous distribution of pillar on the thermal stability is more important.

Improving the homogenous distribution of noble metals loaded on an inorganic support has been thoroughly investigated.[17] A more homogeneous distribution of metal can be obtained by increasing the dilution of the noble metal. Similarly, a high dilution of the clay slurry increases the surface area of PILC.[18-19] However, the use of a dilute clay slurry (<1 wt%) is not practical for large scale preparations of pillared clay. Our work emphasizes the important steps affecting the homogeneity of alumina oxide pillars between the layers. As we have reported recently for the synthesis procedure of thermally stable pillared montmorillonites, a high fraction of uniform aluminum oligomers in the pillaring solution is the prerequisite to stable derivatives. Heating the pillaring reagent speeds up the hydrolysis process. When hydrolysis is complete, pH or alumina species would not vary upon the aging. It has been noted that as alkali is added to a dilute aluminum salt solution there is only a slow change in pH until equilibrium is attained and aging must be allowed to take place before meaningful pH measurement can be obtained.[20] The pillaring solution used in our synthesis contains primarily Al_{13} oligomers, as judged by ^{27}Al NMR spectroscopy.[8] Secondly, shorter pillaring reaction and processing (washing) time minimize undesirable changes in the pillaring species. Exchange of aluminum polycations is complete within a half hour if stirring is efficient and the Al/clay ratio is high enough.[21] Increasing the number of washings increases the pH of the final products. For example, before washing the pH of an Al_{13}^{7+}-Na^+ beidellite reaction mixture is 4.3, after 4 washings, the pH increases to 5.6. ^{27}Al NMR showed that the fraction of Al_{13} in solution decreases with increasing pH over 5,[21] which implies a reduction in the

homogeneity of the pillars, and a reduced stability of pillared clay at elevated temperatures. Keeping all other synthesis conditions constant, we find that the washing procedure is very important. A mixture of pillaring solution and clay slurry was aged over night at room temperature with stirring and then washed over an additional 10 hour period. The resulting product was then dried and calcined at 350 °C and 500 °C, respectively. Although the BET surface area of 290 m^2/g after calcination at 500 °C was comparable to 287 m^2/g surface area of a product prepared using a much shorter time, the conversion of biphenyl for the aged catalysts declined dramatically from 99% at 350 °C to 16% at 500 °C. In contrast, the catalysts aged and washed in shorter time maintain most of the surface area, microporous structure and alkylation activity above 500 °C. Thus, the preparation conditions which optimize the homogeneous distribution of pillars are suggested to be most responsible for the high thermally stable and reactively pillared beidellites.

Several factors can contribute to the temperature sensitivity of an alumina pillared clay catalysts. For instance, a decrease in the reactivity of an alumina pillared montmorillonite catalyst has been observed for the gas phase conversion of 1,2,4 - trimethylbenzene when the catalyst is calcined at 500 °C. In this case the loss in reactivity most likely was due to loss of Brönsted acidity.[22] In contrast, the reactivity of pillared beidellite has been observed to be less sensitive to temperature in this work and in the hydrocracking of hydrocarbons.[23,24] If the hydroxyl groups of the clay sheet are associated with Brönsted acidity, the higher reactivity reveals more Brönsted sites in the pillared beidellite because both pillared montmorillonite and pillared beidellite have similar pore structures. It is noted that the hydroxyl groups were allowed to rehydrate by exposure to the

atmosphere prior to performing catalytic reaction or pyridine chemisorption after calcination at high temperature (> 500 ^{o}C). Although the amount of chemisorbed pyridine is similar for pillared montmorillonite and pillared beidellite, the number of Brönsted sites might be different. Since the measurement of pyridine chemisorption was made under vacuum, part of weak hydroxyl groups could have been condensed to form water. It seems that pillared beidellite is more capable of regenerating hydroxyl group from the dehydroxylated state.

The reason for the different acidic behavior could be looked at in terms of the different pillaring mechanism and relating that to the clay structures. When octahedrally charged montmorillonite is intercalated by hydroxy aluminum and calcined at moderate temperatures, for example 400 - 500 ^{o}C, the protons released from the pillars would defuse into the clay sheet. Meanwhile, the hydroxyl groups on the polymeric ion condense with lattice hydroxyls, resulting in a reduction of lattice hydroxyl groups. A substantial number of hydroxy groups would remain in the clay sheet, as evidenced by a negative shift to -95 ppm in the ^{29}Si MAS NMR spectra.[25] On heating up to 700 ^{o}C the rest of the hydroxyl groups would be lost, shifting the ^{29}Si signal to -100 ppm. In the case of tetrahedral charged clay, instead of proton diffusion, Si-O-Al linkage in the tetrahedral layer tend to open upon proton attack at elevated temperatures. This can be seen clearly by the ^{29}Si NMR spectra of alumina pillared saponite,[26] in which the $Q^3(0Al)$ and $Q^3(1Al)$ peaks are well resolved. The Si-OH groups then link to the pillar, or condense with hydroxyl groups on the polymeric ions. This means the hydroxyl groups of the clay remained unaffected by the stabilizing pillars. The loss of clay layer hydroxyl groups is caused by dehydroxylation upon heating. A slight negative shift in the Q^3 ^{29}Si

resonance was observed after calcination at 400 °C - 500 °C. A similar situation would occur for pillared beidellite, although the resolution of $Q^3(0Al)$ and $Q^3(1Al)$ lines is not as well defined as in pillared saponite. There is about 0.7 negative charge units and 1.8 intercalated aluminum ions per unit cell of pillared beidellite from chemical analysis. So there are enough Al-O-Si units in the clay to interact with the polycation pillars. When the temperature is increased further, dehydroxylation also occurs. The reconstructed clay yields a broader $Q^3(0Al)$ peak at -98 ppm. If a calcined sample is exposed to moisture, part of the hydroxyl groups rehydrate, corresponding to an increase in the intensity of the peak at -95 ppm as observed in the ^{29}Si NMR after calcination at 700 °C, which might overlap the shifted $Q^3(1Al)$ with unchanged or partly restored $Q^3(0Al)$. More dehydroxylated sites in pillared beidellite might become rehydrated than in pillared montmorillonite and pillared flurohectorite.

In a comparison of the thermal stability, pore structure, acidity and catalytic reactivity, H^+/AlCB should give rise to greater acidity. However, the acid sites measured by pyridine adsorption do not disclose the difference between AlCB and H^+/AlCB. This difference might be because pyridine is a relatively strong base and is unable to distinguish between the weak and strong acid sites upon adsorption. The acid sites counted would then be the sum of both weak and strong acid sites. It is well-known that the main Lewis acid sites are introduced by alumina pillars. The origin of stronger acid sites should be the parent clay. For HCB, acid sites created by acid treatment might be mainly those of the incompletely coordinated tetrahedral Al (Lewis sites, c.f. decrease of Al content) and those of silanol groups (Brönsted sites) which are accessible for substrate catalysis.

Generally, acid attack of a clay structure consists of 3 phenomena, observed for increasingly severe acidification conditions, (1) replacing the interlayer Mg^{2+} by H_3O^+ ions; (2) dissolution of the octahedral sheet cations; (3) expelling the tetrahedral cations, for example, when vermiculite is treated by 1 M HCl at 80 ^oC for 2 h.[27] The leached octahedral sheet has smaller dimensions than the parent material, so the tetrahedra should increase their rotation angle to ensure a fit between the sheets. Consequently, the acidified layers have smaller values of a and b parameters than the starting vermiculite.

Our milder conditions (0.2 M H_2SO_4 at 70 ^oC for 2 h) result in the replacing the interlayer ions by H_3O^+ and the expelling of the octahedral cations. But the constant cell parameter indicates that the twist of octahedral sheets due to disslution of the cations from them is negligible for HCB. The non-twisted lattice is desirable and important because the pillared beidellites prepared from this not only exhibit enhanced acid strength and catalytic reactivity, but also compatible thermal stability and pore structure compared with alumina pillared beidellite without acid treatment.

REFERENCE

1. Busenberg, E.; Clemency, C. V. *Clays and Clay Miner.*, **1973**, *21*, 213.
2. Wash, J. N. *Spectrochim* , **1980**, *35B*, 107.
3. Grillet, Y.; Rouquerol, F.; Rouquerol, J. *J. Chim. Phys.*, **1977**, *74*, 179.
4. Northrop, P. S.; Flagan, R. C.; Gaualas, G. R. *Langmuir*, **1987**, *3*, 300.
5. Michot, L. J.; Francois, M.; Case, J. M. *Langmuir*, **1990**, *6*, 677.
6. De Boer, J. M.; Lippens, B. C.; Linsen, B. G.; Broekhoff, J. C. P.; Heuvel, A. Van den; Osinga, Th. *J. Coll. Interface Sci.*, **1966**, *21*, 405.
7. Datka, J. *J. Chem. Soc., Faraday Trans I*, **1981**, *77*, 2877.
8. Ge, Z.; Li, D.; Pinnavaia, T. J. *Microporous Mater.*, to be published.
9 Malla, P. B.; Komarneni, S. *Clays and Clay Miner.*, **1993**, *41(4)*, 472-483.
10. Li, L.; Liu, X.; Ge, Y.; Xu, R. *J. Phys. Chem.*, **1993**, *97*, 10389-10393.
11. Tennakoon, D. T. B.; Jones, W.; Thomas, J. M. *J. Chem. Soc., Faraday Trans. 1*, **1986**, *82*, 3081.
12. Parry, E. P. *J. Catal.*, **1963**, *2*, 371.
13. Butruille, J. Ph. D thesis, Michigan State Univ. 1992.
14. Butruille, J.; Pinnavaia, T. J. *Pillared Clay, Catalysis Today 14*, 1992, 14-54.
15. Butruille, J.; Laurent, J. M.; Barrés, O.; Pinnavaia, T. J. *J. Catal.*, **1993**, *139*, 664-678.
16. MacEwan, D.M. D.; Wilson, M. J. In "*Crystal Structures of Clay Minerals and Their x-ray Diffraction*", Brindley, G. W.; Brown, B. Eds.; London, 1980, Chapter 2.

17. Brunelle, J. P. *J. Pure Applied Chem.*, **1978**, *50*, 229-237.

18. Lahav, N.; Shani, U.; Shabtai, J. *Clays and Clay Miner.*, **1978**, *26*, 107- 115.

19. Vaughan, D. E. W.; Lussier, R. J.; Mcgee, J. S. US Patent 4 248 739, 1988.

20. Schutz, A.; Stone, W. E. E.; Poncelet, G.; Fripiat, J. J. *Clays and Clay Miner*, **1987**, *35(4)*, 251-261.

21. Doblin, C.; Corrigan, P.; Turney, T. W. *10th Int. Clay Conf.*, Australia, 1993.

22. Kojima, M.; Hartford, R.; O'Connor, C. T. *J. Catal.*, **1991**, *128*, 487-498.

23. Schutz, A.; Plee, D., Borg, F.; Jacobs, P., Poncelet, G.; Fripiat, J. J., in *Proc. Int. Clay Conf.*, Denver, 1987. Schultz, L. G., Olphen, H. van, Mumpton, F. A., Eds.; The Clay Minerals Society: Bloomington, Indiana, 1987; pp 305-310.

24. Plee, D.; Schutz, A.; Poncelet, G.; Borg, F.; Jacobs, P.; Gatineau, L.; Fripiat, J. J. Fr. Patent 2 563 446, 1984.

25. Tennakoon, D. T. B.; Jones, W.; Thomas, J. M. *J. Chem. Soc., Faraday Trans. 1*, **1986**, *82*, 3081.

26. Li, L.; Liu, X.; Ge, Y.; Xu, R. *J. Phys. Chem.*, **1993**, *97*, 10389-10393.

27. Suquet, H.; Frank, R.; Lambert, J-F.; Elsass, F.; Marcilly, C.; Chevalier, S. *Applied Clay Sci.*, **1994**, *8*, 349-364.

CHAPTER FIVE
IMOGOLITE PILLARED BEIDELLITES

A. OBJECTIVE OF RESEARCH

The structure and properties of imogolite with an anhydrous formula of $(OH)_3Al_2O_3SiOH$ have been reviewed in the introduction. The properties of imogolite pillared montmorillonite were investigated in terms of structure, acidity and thermal stability.[1-2]

The objective of present work is to pillar imogolite into natural beidellite, a member of smectite clays in which negative charges arise from the tetrahedral sheets. In order to elucidate the properties of the TSLS (tubular silicate-layered silicate) complex, pure imogolite, especially its pore structure, is studied. The work focuses on the unique features of the TSLS complex which are different from conventional pillared clays, such as, alumina pillared smectites. The structures pillared by various amounts of imogolite are examined. XRD is used to monitor the structural variations caused by washing and dehydration processes. Nitrogen adsorption and desorption isotherms are analyzed in terms of microporous surface areas and micropore distributions. The acid-catalytic reactivity is tested in the alkylation of biphenyl by propene.

B. EXPERIMENTAL

1. Synthesis of Imogolite

A synthetic route to imogolite was described by Farmer.[3] Since imogolite suspensions corresponding to aluminum concentrations greater than 30 mM, will begin to flocculate, even in acidic solution, the aqueous imogolite suspension synthesized in this work contain 30 mM Al or less depending on the need. A concentration of 30 mM Al was used to pillar beidellite clay. The control of pH was a crucial step in forming tubes. A weak acidic environment is the most favorable. When imogolite tubes form, a decrease in pH is observed due to the release of H^+. If the proper pH conditions are not been met, nucleation and growth are inhibited and the pH of the solution either remains the same or increases slightly.

The synthesis of an aqueous imogolite suspension (30 mM Al) was achieved by the acid hydrolysis of aluminum tri-*sec*-butoxide in an amount of perchloric acid equal to half the number of moles of aluminum. About 4-8 hours were required for complete hydrolysis to be completed. Deionized water was added to bring the aluminum concentration to 30 mM, and then tetraetylorthosilicate was added in an amount equal to half the number of moles of aluminum, e. g. the Si/Al molar ratio was 0.5. The pH of the mixture was then raised to 5.0 with 1 M NaOH and then immediately re-acidified to pH 4.0 with 1 M acetic acid. The reaction suspension was heated at 90 - 100 ^{o}C for 2 days. The final solution was water-clear, indicating imogolite formation. The presence of imogolite is further verified by gel formation upon the addition of ammonia hydroxide. The resulting product

was dialyzed 5 days in a cellulose dialysis tube to remove soluble by-products.

2. Pillaring Beidellite by Imogolite

A natural Na^+-exchanged beidellite from China was used to pillar imogolite. The mineral was purified by removing organic impurities, and exchanging by Na^+. The < 2 μm fraction was collected. Chemical analysis of the pristine minerals indicated the unit cell to be:

$Na_{0.74}$ $(Mg_{0.74}$ $Fe_{0.15}$ $Al_{3.31})($ $Si_{7.40}Al_{0.60})$ O_{20} $(OH)_4$

The CEC value was 101 meq/100g, as determined by the ammonium exchange method.

An imogolite pillared beidellite (abbreviated IPB) was obtained by the dropwise addition of 1.0 wt % suspension of Na^+-beidellite to imogolite (30 mM Al) at a ratio of 2:1 (v / v) at 80 °C. The mixture was kept at 80 °C for 2 h with stirring, then it was cooled to room temperature by immersion of the reaction vessel in running water. After centrifuging, half the product was washed by centrifugation. The rest was redispersed in water, and the above pillaring process repeated. The amount of intercalated imogolite also can be controlled by varying the ratios of imogolite to beidellite, but because the concentration of imogolite was low, controlling the amount of intercalated imogolite by this method was found to be less efficient. The excess imogolite was removed by washing and centrifuging. The films used for XRD studies were prepared by dropping a suspension of the product on a glass slide and air-drying. The pillared-products obtained without washing and after washing 5 times are abbreviated as IPB0 and IPB5, respectively. Those pillared products obtained after two pillaring cycles without washing

and after 5 times washing are abbreviated as IPB2-0 and IPB2-5, respectively.

3. Characterization

X-ray diffraction patterns (Cu-Kα) of oriented film and powder samples were obtained with a Rigaku x-ray diffractometer equipped with a rotating anode.

Nitrogen adsorption/desorption isotherms were determined at -196 °C on an Ominisorb 360 CX (Coulter) Sorptometer. The samples were degassed at 150 °C for 12 hours under 10^{-5} torr. N_2 adsorption and desorption were measured by the quasi-equilibrium volumetric method. Surface areas were obtained using the BET equation. The t-plot method[4] was used to determine the total micropore volume, as well as non-microporous surface area. Micropore size distributions were determined using the model developed by Horvatha and Kawazoe.[5]

The FTIR spectrum was obtained on an IBM IR44 Spectrometer. The IR specimens were KBr pellets containing 1 wt% of air-dried samples.

A Varian 400 VXR solid state NMR spectrometer was used to obtain ^{29}Si MAS NMR spectra at 79.5 MHz. The spinning frequency was 4 KHz. The Si chemical shifts are reported relative to TMS.

TGA was run on a CAHN TG-121 electrobalance. The sample was heated from 30 °C to 700 °C at a rate of 5 °C/min.

The alkylation of biphenyl by propene was carried out in a 300-mL batch reactor. A 30-g (0.194 mole) quantity of biphenyl and 0.2 g of air-dry pillared beidellite (particle size between 100-200 mesh) were heated to 250

^{o}C at a temperature ramp rate of 3°/min while purging with propene. The reaction was carried out at 250 ^{o}C, 140 psi for 20 hours. The reaction mixture was dissolved in hexane, and analyzed by a HP5890 chromatograph equipped with a 60 m SPBI column and a FID detector.

C. RESULTS

1. Characterization of Imogolite

The simplest way to test for the presence of imogolite is to form gel upon addition of NH_4OH. After dialysis of the imogolite, the product was further identified by FTIR and ^{29}Si MAS NMR.[6]

FTIR is the easiest method of imogolite identification. Figure 5.1 provides a representative IR spectrum of a dialyzed imogolite. The prominent peaks near 3500 cm^{-1} is OH stretch of water and the 1630 cm^{-1} band is HOH bending vibration of water. The dialyzed sample contained two peaks characteristic of the Si-O-Al vibration in imogolite. One is at 995 cm^{-1} and the other at 940 cm^{-1}. In the region from 900-1000 cm^{-1}, the presence of two separate peaks is unique to imogolite. If absorbance greater than 1000 cm^{-1} due to Si-O-Si vibration, the peak is to be identified as impurities because there are no Si-O-Si bonds in the imogolite structure. For allophane, another aluminosilicates found with imogolite in the nature, there is only one broad peak observable in the 900-1000 cm^{-1} region.

^{29}Si MAS NMR is another useful means of characterizing imogolite. The single peak at -79 ppm in Figure 5.2 is due to the Q^0 site of the isolated

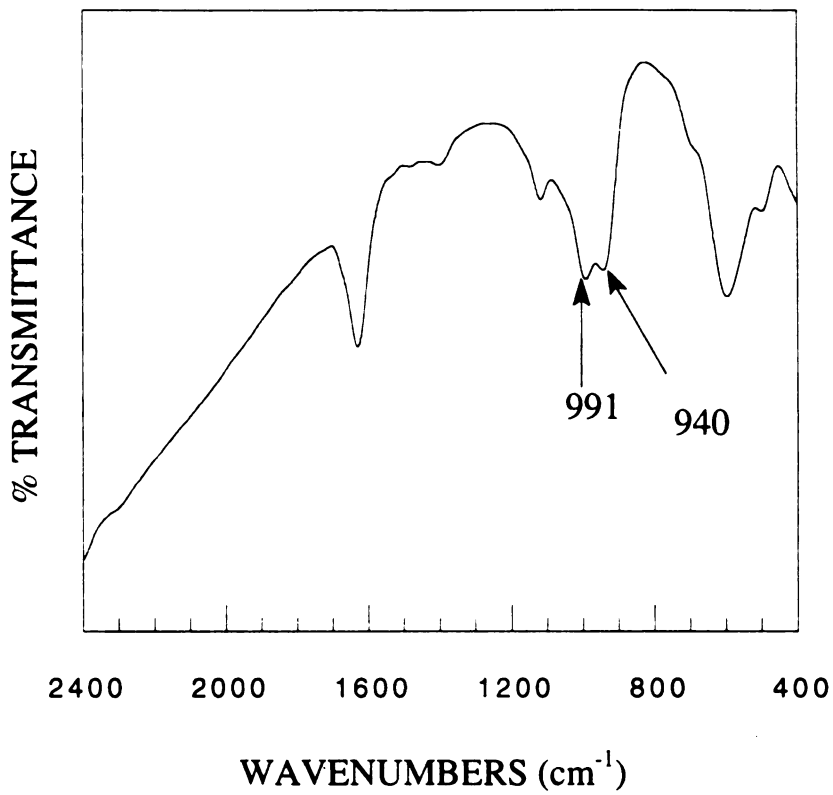

Figure 5.1 IR spectrum of air-dried imogolite as a KBr pellet sample.

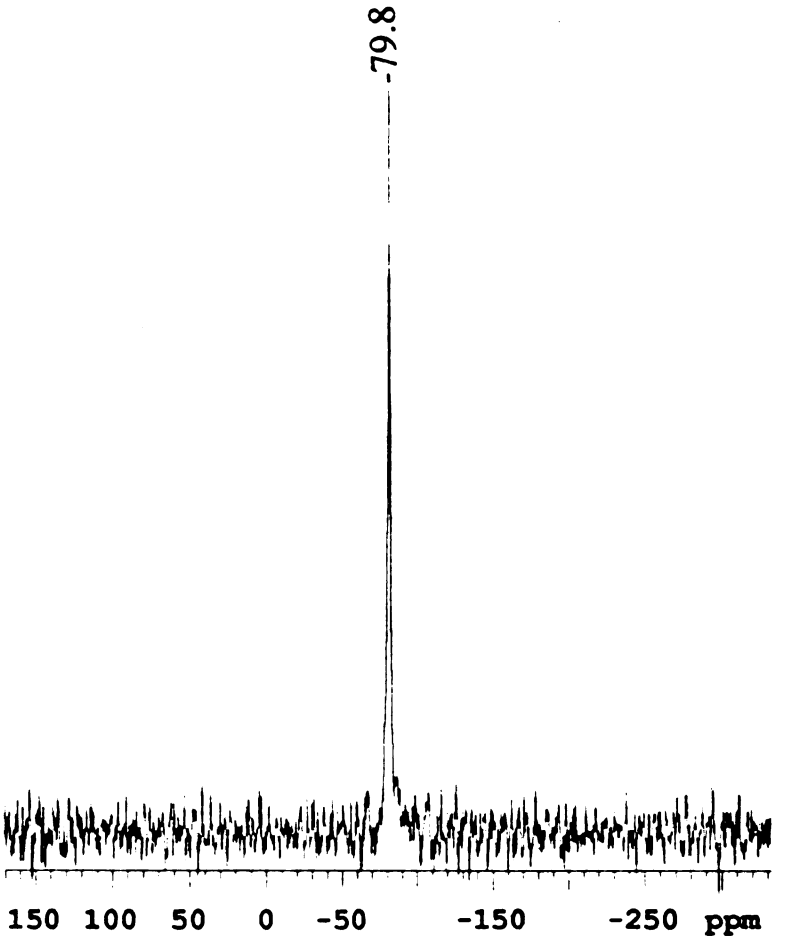

Figure 5.2 ^{29}Si MAS NMR spectrum of air-dried imogolite.

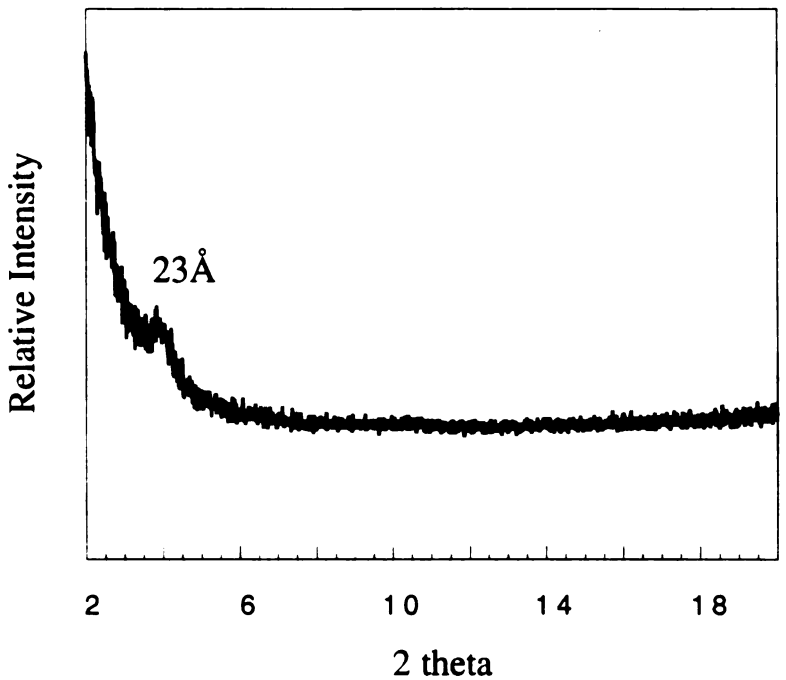

Figure 5.3 X-ray diffraction pattern of air-dried imogolite.

orthosilicate units wherein a silicon is bonded through oxygen to three aluminum atoms and to a single silanol group.[7]

In contrast to the sharp peak in the NMR, the XRD film pattern gives a weak and quite broad peak at a d-spacing around 23 Å as shown in Figure 5.3. The repeat packing order of 23 Å is the external diameter of the tubes.

Under ambient atmospheric and temperature conditions, imogolite tubes are filled with water. The water clearly will affect gas/vapor adsorption. It is important to know both the minimum temperature at which water is removed and the maximum temperature for structure stability. However, these two temperatures are difficult to distinguish because imogolite exhibits two different types of pores as shown in Figure 1.2. The effect of temperature on imogolite chemical structure has been previously studied by XRD and solid state NMR.[8] It was found that up to 275 ^{o}C, dehydroxylation of silanol groups did not occur. The TGA curve in Figure 5.4 shows the relation between weight loss and temperature. The weight loss from 30 ^{o}C to 150 ^{o}C counts for about 20 % of the total weight. In the range from 150 ^{o}C to 430 ^{o}C, another 13 % weight loss is continuous and nearly linear with increasing temperature. If the weight loss below 275 ^{o}C was due to the removal of pore water, then the amount loss between from 30 ^{o}C to 150 ^{o}C might mostly be associated with the mesopores formed by packing of tubes into bundles, e. g. type (C) pores and type (A) micropore of formed within the tubes as shown in Figure 1.7. The less accessible water in the space between three aligned tubes in a regular packing (B) should be lost at higher temperature. The dehydration and dehydroxylation process corresponding to 150 ^{o}C to 430 ^{o}C can not be distinguished from the TGA. Another factor which determines the temperature of water removal is the outgassing conditions. The TGA curve was run at atmospheric pressure,

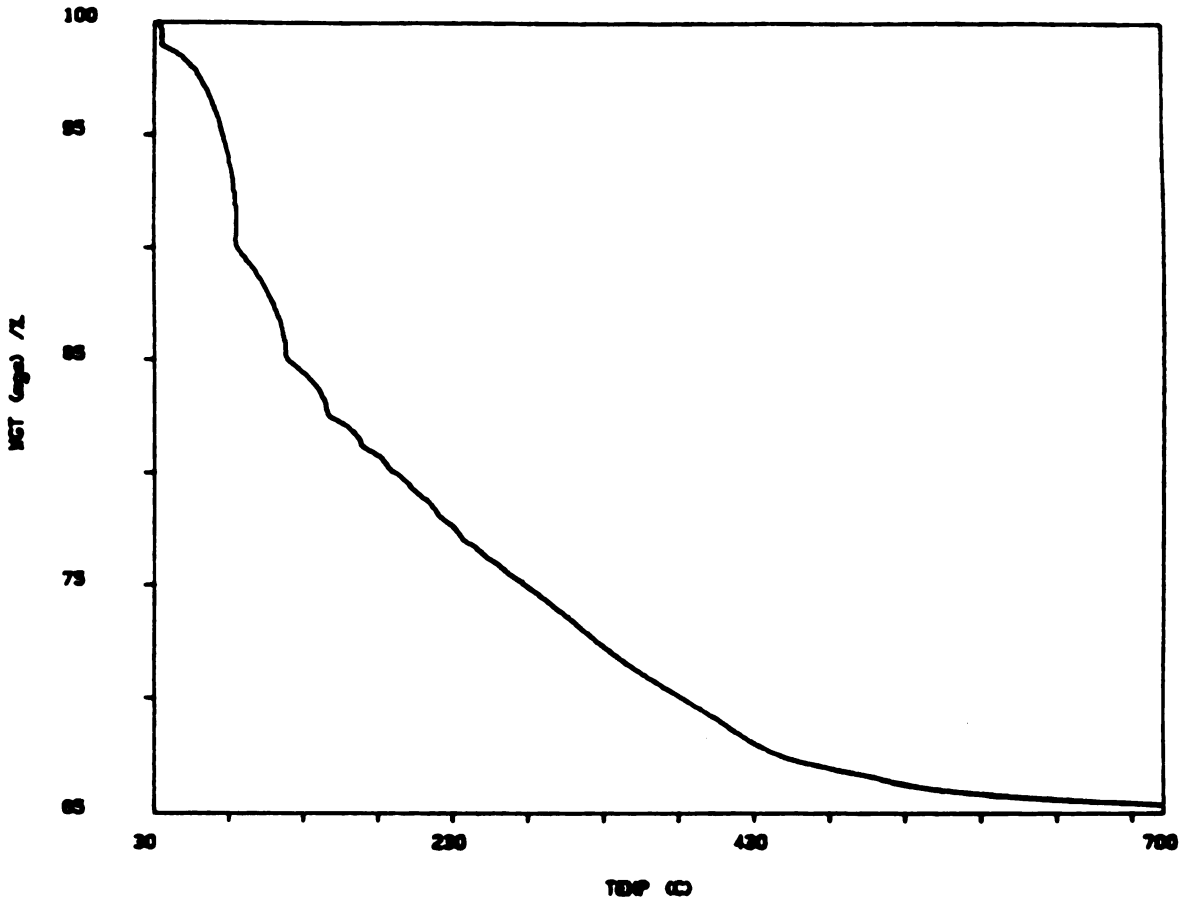

Figure 5.4 Thermogravimetric analysis of imogolite (heating rate= 5 $^{o}C/min$).

whereas the pore structure studies were carried out after degassing in a vacuum. The temperature to remove water at atmospheric pressure is higher than that needed under the vacuum.

In order to determine the pore structure of imogolite more precisely, the adsorption/desorption isotherms were studied after degassing temperatures of 150 ^{o}C and 275 ^{o}C. The nitrogen adsorption and desorption (kinetic diameter, 3.6 Å) isotherms for pure imogolite for the nitrogen are shown in Figure 5.5. The shape of the adsorption isotherm is a typical type I for a microporous powder.[9] Micropores with enhanced the quantity of gas adsorbed at relatively low pressure. At higher pressure, the pores are filled by adsorbate leading to the plateau, and indicating little or no additional adsorption after the micropores are filled. The small hysteresis loop of the desorption isotherm is a result of different degrees of pore blocking. The overlapping of the desorption branch with the adsorption curve can be ascribed to the close degree of spontaneity of both the adsorption and desorption process.

The BET surface area of pure imogolite degassed at 150 ^{o}C is 350 m^2/g. For the material degassed at 275 ^{o}C the surface area is 344 m^2/g. The t-plots for N_2 adsorption shown in Figure 5.6 yield a total surface area of 375 m^2/g, comparable to the values obtained from the BET equation. The intercept of 80 cm^3 STP g^{-1} obtained by extrapolation of the linear portion of the t-plot corresponds to a 350 m^2/g microporous area. Fairly low mesopore surface area of 25 m^2/g might be due to the efficient packaging of the tubes during the heating process under the vacuum. At both degassing temperatures, imogolites maintains the tubular structure. However, the sample color turns dark after degassing at 275 ^{o}C. A further increase in degassing temperature results in the collapse of the tube structure.

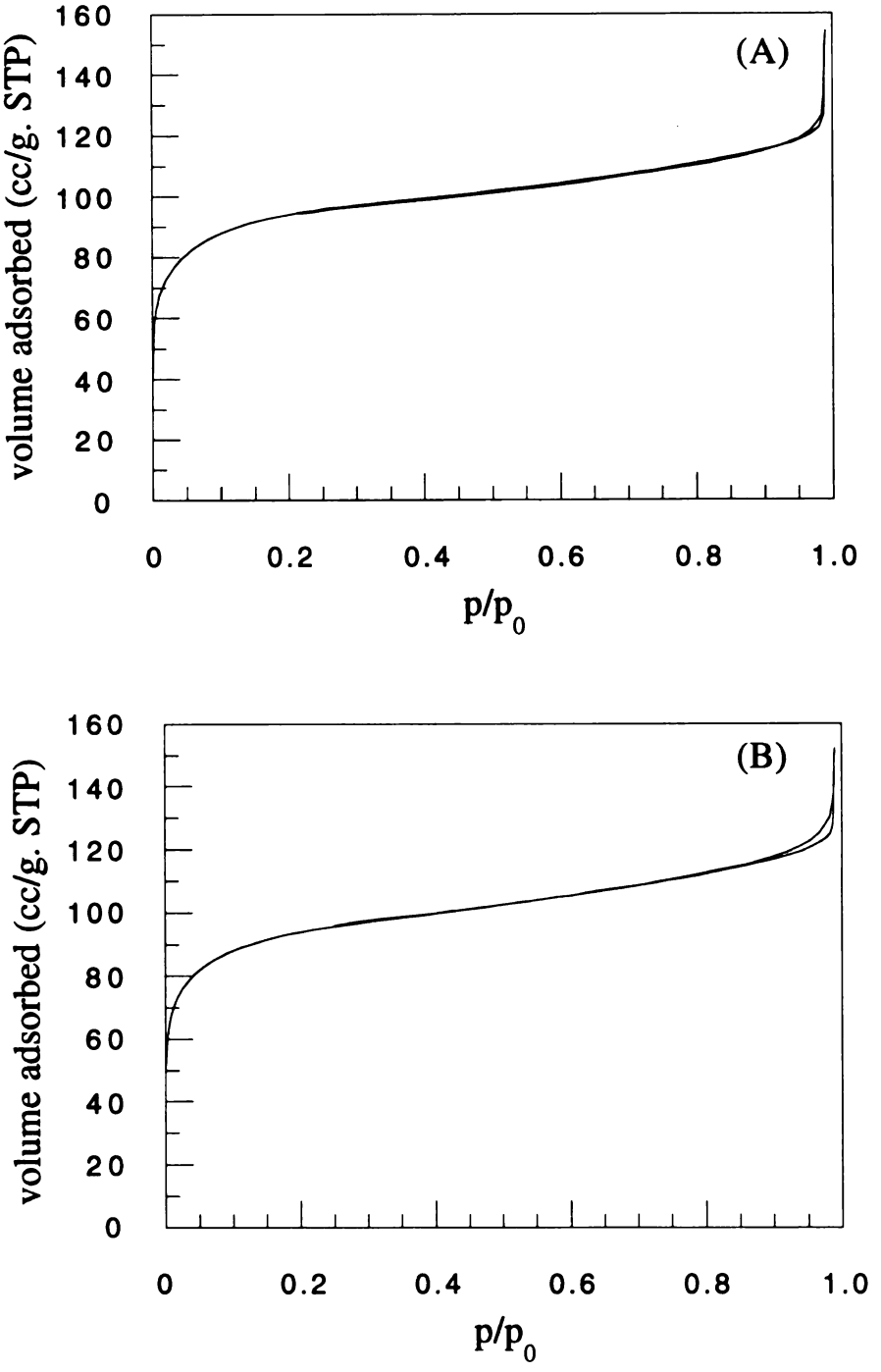

Figure 5.5 The adsorption/desorption isotherms of imogolite degassed under vacuum at (A) 150 °C; (B) 275 °C.

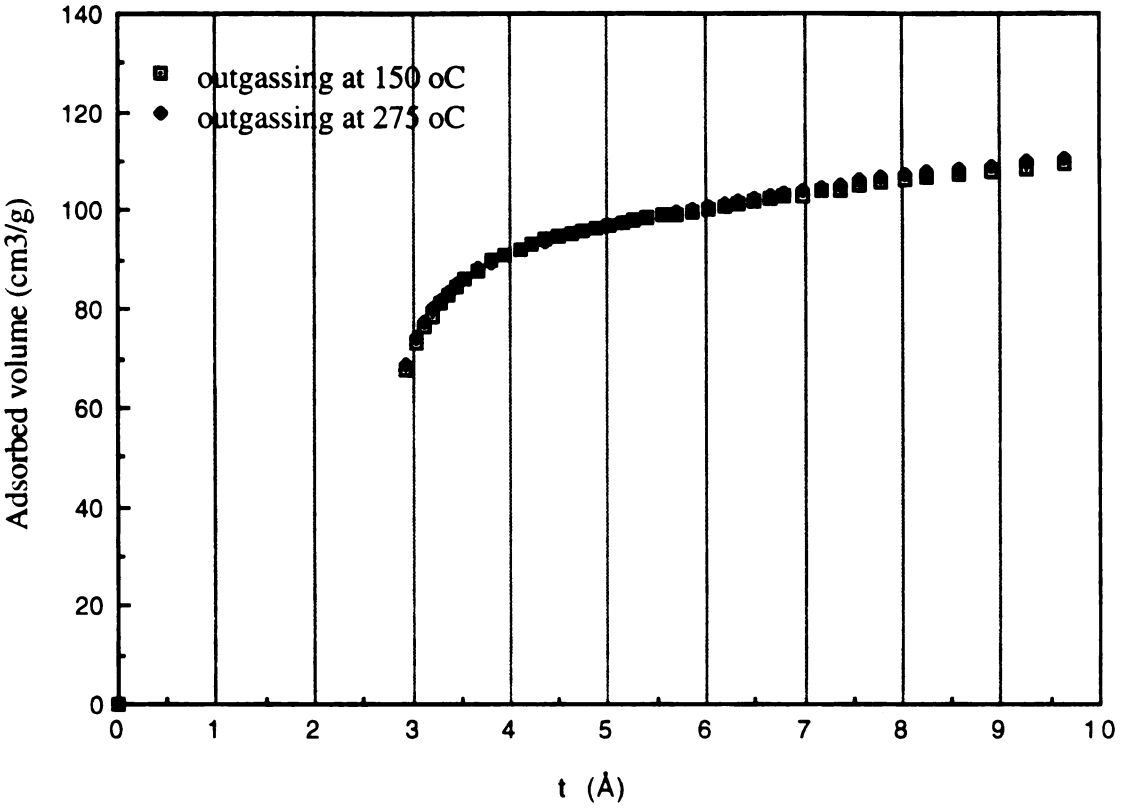

Figure 5.6 t-plot of imogolite degassed at 150 °C and 275 °C.

2. Characterization of Imogolite Pillared Beidellite

1) Structures

A 1 wt% suspension of beidellite was pillared by reaction once with a two-fold volume of imogolite (30 mM Al). The structures of pillared beidellite are examined first, and the results are then compared with the analogous product prepared by reaction twice with excess imogolite ("twice-pillared product).

X-ray diffraction patterns of film samples of imogolite and one time pillared beidellite products are illustrated in Figure 5.7. The broad peak at 23 Å for imogolite is attributed to the stacking of imogolite tubes with a diameter of 23 Å. The patterns in Figure 5.7 (A) compare of stacking order along the c-axis for the product before and after 5 times washing. A quite broad reflection corresponding to 47 Å to 30 Å appears upon washing. The corresponding product dried at 100 ^{o}C exhibits a sharper peaks at 44 Å, as shown in Figure 5.7 (B). The sharper 44 Å reflection is due to the more regular array of layers, which is agreement with the basal spacing reported for the imogolite pillared montmorillonite complex.[10] In addition to the broad reflection at 44 Å, there is a peak at 12.5 - 12.7 Å in each pattern. This relatively sharp and strong peak coincides with the d-spacing of unpillared Na^{+}-beidellite.

The presence of a two-phase model is supported by TEM. As shown in Figure 5.8, two kinds of layer structures are observed. In one groups of layers, the d-spacing is around 35-45 Å. The smaller d-spacings (< 20 Å) are observed for other groups of stacked layers. In comparison with conventional pillared clays, for example $Al_{13}O_4(OH)_{24}(H_2O)_{12}^{7+}$ pillared

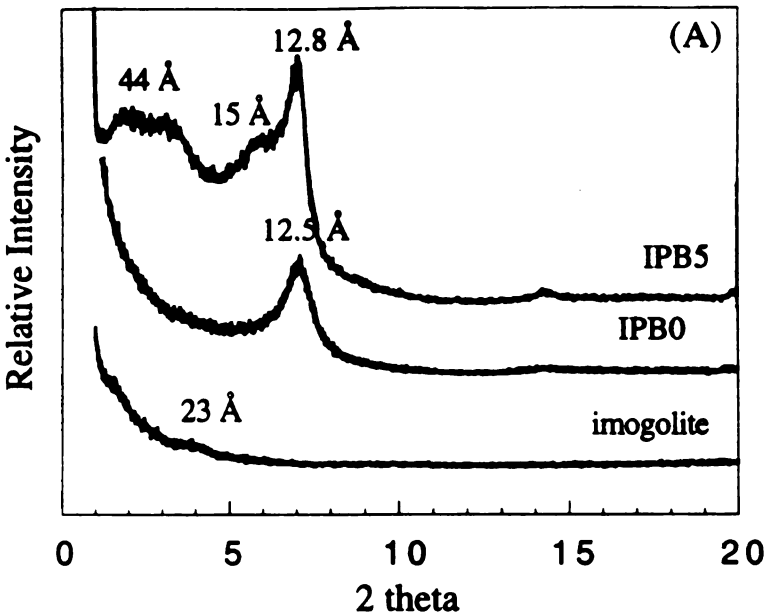

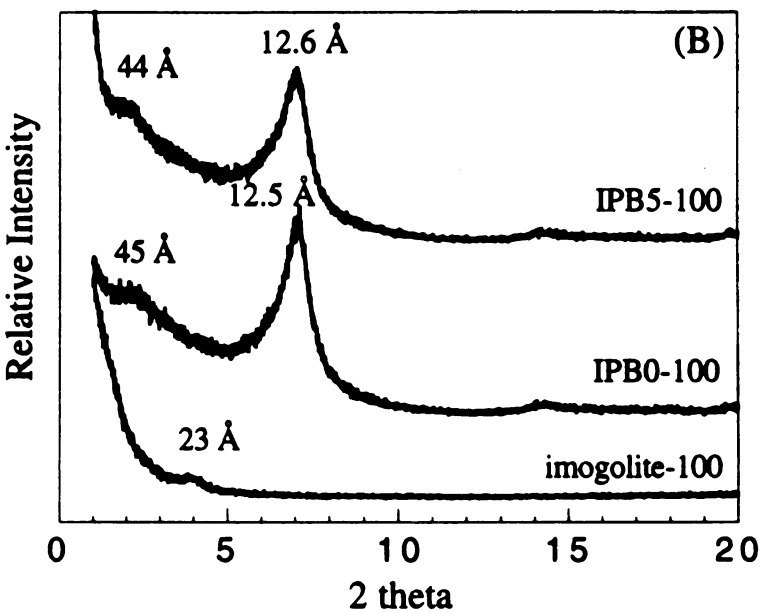

Figure 5.7 X-ray diffraction patterns of imogolite pillared beidellites without washing (IPB0) and after 5 times washing (IPB5) for (A) air-dried sample; (B) heating at 100 °C.

Figure 5.8 TEM image of imogolite pillared beidellite.


250 Å

smectites,[11] the distribution of the clay layer is less regular. It is likely that there are more meso or macro-pores in the imogolite-pillared beidellite.

As determined from the t-plots of the N_2 isotherms, there is quite a higher fraction of mesopores in the pillared products, e.g. more than 50 % of total surface area is derived from mesopores. The total surface areas and corresponding microporous areas, listed in Table 5.1, are lower than those for pure imogolite.

Table 5.1. N_2 BET Surface Areas (S_{BET}), Total Surface Areas (S_{total}) and Microporous Surface Areas (S_{micro}) for Imogolite and Once-Pillared Beidellite

sample[1]		imogolite	IPB3	IPB4	IPB5
washing times		----	3	4	5
S_{BET}, m^2/g		356	283	238	238
t-plot	S_{total}, m^2/g	375	293	229	230
	S_{micro}, m^2/g	350	139	105	109
	% micro	95	48	44	44

[1]All the samples were degassed at 150 °C for 12 h before the measurement.

Micropore size distributions were determined from the N_2 adsorption data using the parallel plate model of Horvatha-Kawazoe. Figure 5.9 is the plot of dv/dr (differential pore volume) versus r (pore diameter). Imogolite showed a quite uniform arrangement of pores with a maximum of around 6.0 Å. Most of micropores were below 10 Å, which would include both intra- and inter-tube pores. The pore distributions for the pillared beidellites show

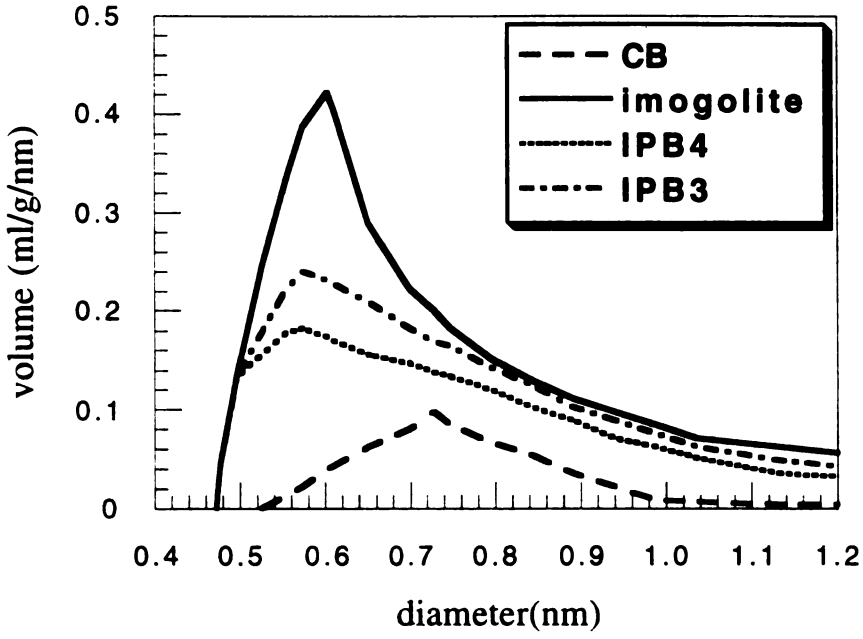

Figure 5.9 Horvath-Kawazoe pore distributions for parent beidellite (CB), imogolite, and imogolite pillared beidellites after 3 times washing (IPB3) and 4 times washing (IPB4).

lower pore volumes but the about same pore size of maximum (6.0 Å) as for the imogolite, suggesting that the micropore distributions arise mainly from intra-tube adsorption on imogolite. The micropore distribution beyond 6.0 Å is attributed to adsorption in pores between the imogolite tubes. This is also evidence in support of the model of having two types of micropores for intra and inter pillar tubes.[2]

When the once pillared beidellite was repillared one more time by imogolite, the change of structure is remarkable. In Figure 5.10 the XRD reflections for pillared stacking of layers are still broad, but stronger. Furthermore, the spacings are greatly affected by hydration and dehydration. For both unwashed and washed products, heated to 100 ^{o}C, the 001 peaks shift to the lower spacings and a reduction in the c-axis layer stacking order occurs. When the heated samples are kept in the air at 25 ^{o}C overnight, the d-spacing at 44 Å is restored. This dehydration and rehydration process is reversible, especially for a washed sample in Figure 5.10 (B). The structures are stabilized when heated at higher temperatures as shown by the patterns obtained after heating at 300 ^{o}C for 4 h. The reflections for unpillared Na^{+}-beidellite at 12.5 Å in Figure 5.10 are very weak. The reflections by imogolite pillared layers are dominant for both unwashed and washed samples.

On the bores of pore structure studies, highly microporous pillared structures are created for the twice-pillared beidellite. Data listed in Table 5.2 are the surface areas for unwashed, 3-, 4-, and 5-times washed samples. All the samples have BET surface areas or total surface areas near 420 m^2/g, higher than the pure imogolite. Also, 90% of the surface areas arise from micropores. Alumina pillared beidellites give about 70% microporous surface areas (Table 4.2).

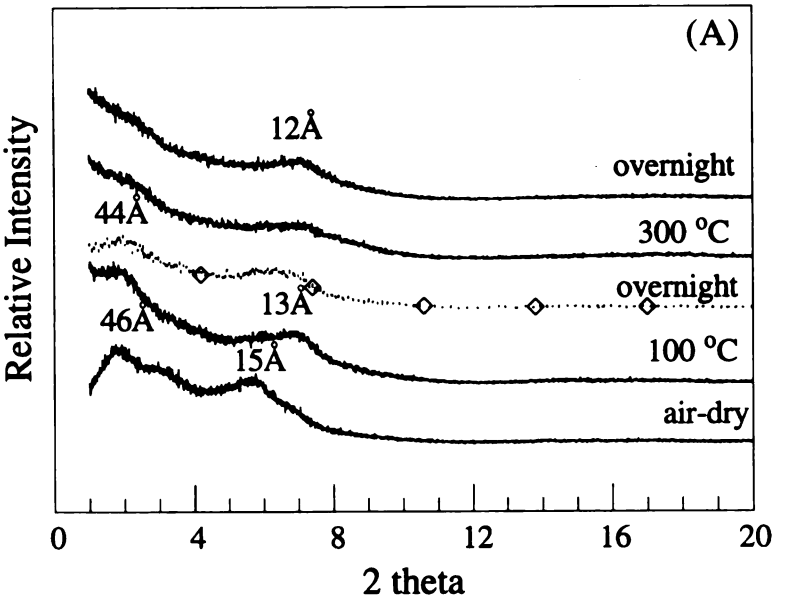

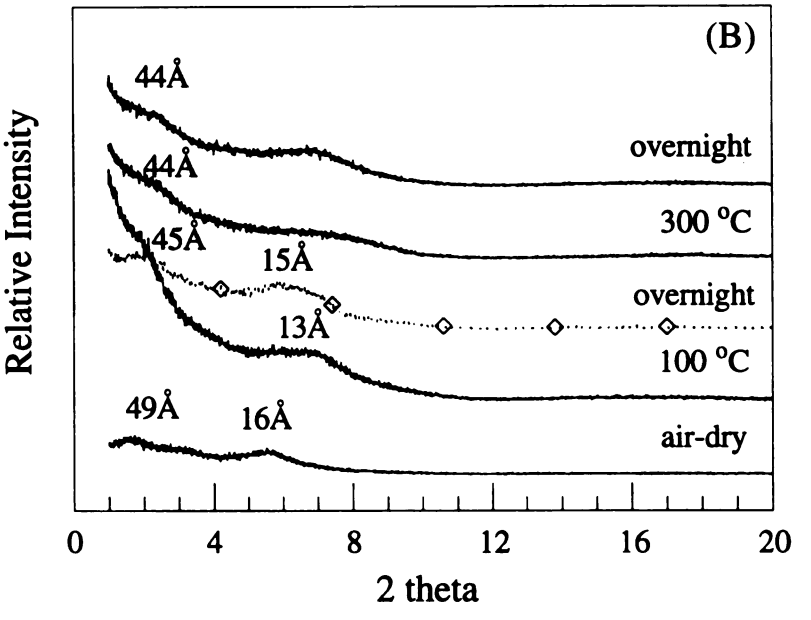

Figure 5.10 X-ray diffraction patterns (film samples) of twice imogolite pillared beidellite: (A) unwashed samples (IPB20); (B) samples prepared by washing with water 5 times before drying (IPB25).

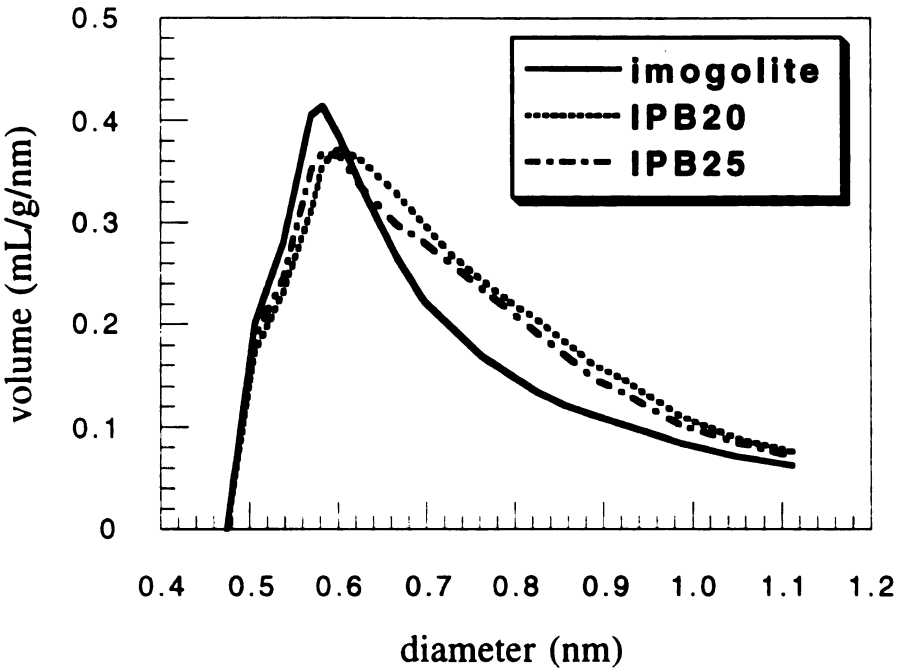

Figure 5.11 Horvath-Kawazoe pore distributions for twice imogolite pillared beidellites without washing (IPB20) and with 5 times washing (IPB25).

Table 5.2. N_2 BET Surface Areas (S_{BET}), Total Surface Areas (S_{total}) and Microporous Surface Areas (S_{micro}) for Two Times Pillared Beidellite

sample[1]		IPB20	IPB23	IPB24	IPB25
washing times		0	3	4	5
S_{BET}, m^2/g		417	412	418	406
t-plot	S_{total}, m^2/g	424	418	433	418
	S_{micro}, m^2/g	406	398	385	380
	% micro	96	95	89	91

a) all the samples were degassed at 150 °C for 12 h before the measurement.

Figure 5.11 is micropore distributions for two times pillared beidellite without washing and 5 times washing. In comparison with pure imogolite, the higher fraction of layer pores should be related to pores formed between intercalated imogolite tubes.

2) Catalytic Reactivity for Propene Alkylation of Biphenyl

Since imogolite pillared beidellites posses a highly microporous structure, the reactivity of these materials for alkylation of biphenyl by propene was investigated. Table 5.3 gives the reactivity and product distributions for alkylation reaction carried out at 250 °C. Included in the table for comparison purposes are analogous data for alumina pillared products formed from the same intrinsic clay host. Figure 5.12 gives the XRD patterns for the alumina pillared beidellites. Using the same clay host, imogolite pillared products are less active than alumina pillared beidellite, as

indicated by the fact that the conversion is lower and the monoalkyl products are prominent. The structure of imogolite suggests that most acid sites are provided by Brönsted acid sites from the imogolite tubes, whereas there are fewer Lewis acid sites from the pillars formed by alumina pillars under the reaction conditions. Also, the small fraction of the mesopores in imogolite pillared beidellite impose diffusion limitations, whereas alumina pillared beidellites with a high fraction of mesopores have less diffusion limitations.[12]

Table 5.3. Biphenyl Conversion and Product Isomer Distributions Obtained for Imogolite Pillared Beidellite and Alumina Pillared Beidellite[1]

catalyst	APB[2]	IPB1-5[3]	IPB2-5[4]
conversion %	98	44	48
% monoalkyl	11	79	76
% dialkyl	41	20	20
% trialkyl	24	4	4
% tetraalkyl	11	0	0
% pentaalkyl	13	0	0

[1]The reaction conditions were as follow: 30 g biphenyl, 0.2 g catalyst, 140 psi propene, 250 ^{o}C, 20 hours reaction time. All results were obtained with 100-200 mesh particle size catalysts.

[2]alumina pillared beidellite, air-dry.

[3]beidellite pillared once by imogolite, 5 washings, air-dry.

[4]beidellite pillared twice by imogolite, 5 washings, air-dry.

D. DISCUSSION

In this work we observed properties of imogolite pillared beidellite that are different from conventional pillared clay.

Firstly, swelling of the clay layers by imogolite pillars is reversible, as described above, which arises from the rehydration of imogolite tubes.

Secondly, the washing process plays a much less important role as in the conventional pillaring process. For the sake of comparison, Figure 5.12 show XRD patterns for $Al_{13}O_4(OH)_{24}(H_2O)_{12}^{7+}$ pillared beidellite before and after washing. Before washing, the curve (APB0) had two peaks belonging to pillared layers and Na^+-form clay respectively. If concentrated clay was used, the Na^+- form peak was even more intense.[13] The cations e. g. Na^+ and oligomers are not well-ordered. Inside the layer some cations fill pores between the pillars, because BET surface area before washing is only 30 m^2/g. The cations are adsorbed at the out surfaces and on the edges. However, in the washing process, the excess cations, mostly Na^+, are removed. A very sharp peak at 19-20 Å was observed and a surface area over 400 m^2/g was obtained. In the case of imogolite pillared beidellite, washing process only modified the structures slightly, as by XRD (Figure 5.10) and the pore structures data (Table 5.2). The total surface areas and microporous areas decrease only slightly with washing.

The imogolite structure and the interaction of imogolite and clay layer should be responsible for the unique features of imogolite pillared beidellite. The OH groups inside and outside the imogolite tubes make it very hydrophilic. Unlike the strong electrostatic interaction between highly charged gallery oligomers and negative clay layers, the interactions between the imogolite tubes and clay layer might mostly be weak hydrogen bonding,

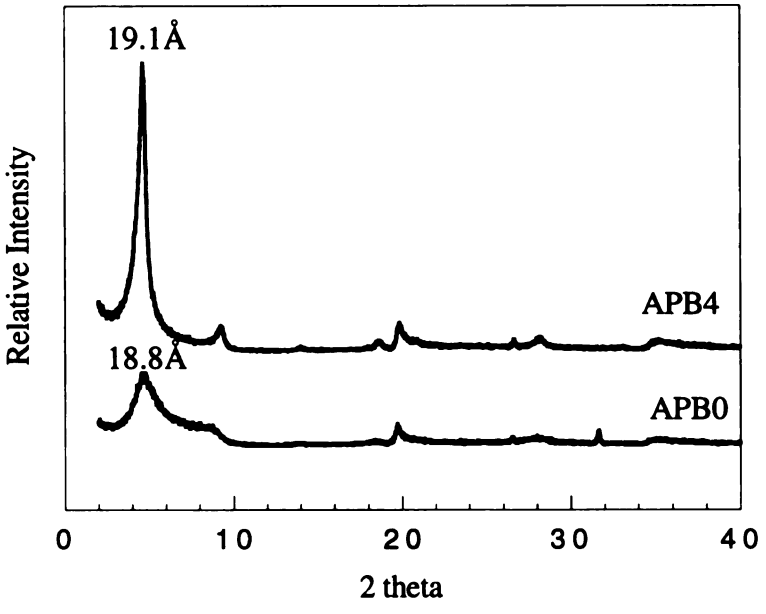

Figure 5.12 X-ray diffraction patterns for alumina pillared beidellite before and afer washing.

since imogolite tubes possess weak positive charge when pH < 9. The anion exchange capacity of imogolite is 15 meq/100g at pH 7.[14] So the pillars could rearrange in the process of dehydration and rehydration. In the pillaring steps, the equilibrium between Na^+ and imogolite controls the amount of imogolite introduced in the galleries. The washing process removes excess ions, but it does not shift the equilibrium greatly.

REFERENCE

1. Johnson, I. J.; Werpy, T. A.; Pinnavaia, T. J. J. *Am. Chem. Soc.* **1988,** *110,* 8545-8547.
2. Werpy, T. A.: Michot, L. J.; Pinnavaia, T. J. ACS symposium series, *437,* Am. Chem. Soc.:1990, pp119-128.
3. Farmer, V.C.; Adams, M. J.; Fraser, A. R.; Palmierl, F. *Clay Miner.* **1983,** *18,* 459-472.
4. De Boer, J. M.; Lippens, B. C.; Linsen, B. G.; Broekhoff, J. C. P.; Van den A. H.; Osinga, Th. *J. Coll. Interface Sci.*, **1966**, *21*, 405.
5. Horvath, G.; Kawazoe, K. G. *J. Chem. Eng. Japan*, **1983**, *16*, 470.
6. Johnson, L. M. M. S. Thesis, Michigan State University, 1988.
7. Barron, P. F.; Wilson, Campbell, A. S.; Frost, R. L. *Nature Phys. Sci.* **1982,** *299,* 616.
8. William, C. A.; Smith, D. M.; Huling, J. C.; Kim, Y. W.; Bailey, J. K.; Brinker, C. J. *Langmuir*, **1992**, *9 (4)*, 1051.
9. Brunauer, L. S. ; Deming, L. S.; Deming, W. S.; Teller, E. *J. Amer. Chem. Soc.* **1940,** *62,* 1723.
10. U. S. Patent 4,621,070, 1986.
11. Occelli, M. L. *J. Catal.* **1987,** *107,* 557-565.
12. Butruille, J. R.; Pinnavaia, T. J. *Catal. Lett.* **1992**, *12*, 187-92.
13. Molina, R. *Clay and Clay Miner.* **1992,** *40(4),* 480-482.
14. Henmi, T. and Wada, K. *Clay Miner.* **1974,** *10,* 231.

APPENDIX A

GREEN-KELLY TEST

Hofmann and Klemen (1950)[1] first indicated that the anomalous loss of expansion and cation-exchange capacity (CEC) of Li-montmorillonite after drying was due to the migration of Li^+ ions from interlayer position to vacant octahedral sites with a consequent neutralization negative charge originating in the sheet due to cationic substitution. Green-Kelly (1953, 1955)[2,3] utilized the hypothesis of Hofmann and Klemen to differentiate montmorillonite and beidellite. The irreversible collapse of an expanding mineral to 9.5 Å gave the criterion for calling the mineral montmorillonite. On the other hand, the expansion to 17.8 Å with glycerol after Li-treatment and drying was the criterion for characterizing the mineral as beidellite. Calveit and Prost (1971) confirmed that the same Li^+ ions do indeed move to octahedral sites, but that more Li^+ ions migrate to hexagonal cavities.

REFERENCE

1. Hofmann, V. U.; Klemen, R. *Z. Anorgan. Chemie*, **1950**, *262*, 95.
2. Green-Kelly, R. *Clay Mineral Bull.* **1953**, *1*, 52.
3. Green-Kelly, R. *Miner. Mag.* **1955**, *30*, 604.

APPENDIX B

POWDER DATA OF X-RAY DIFFRACTION (Cu Kα) FOR QUARTZ[1]

d	2	Î	hkl
4.26	20.8	35	100
3.343	26.6	100	101
2.458	36.6	12	110
2.282	39.4	12	102
2.237	40.3	6	111
2.128	42.5	9	200
1.980	45.5	6	201
1.817	50.2	17	112
1.672	54.9	15	202
1.541	60.0	15	211
1.382	67.7	7	212
1.375	68.1	11	203
1.372	68.9	9	301

[1] from ref. 1

REFERENCE

1. MacEwan, D.M. D.; Wilson, M. J. In "*Crystal Structures of Clay Minerals and Their x-ray Diffraction*", Brindley, G. W.; Brown, B. Eds.; London, 1980, Chapter 6.